1-1-2019

Laxity of the Hip Capsule in Natural and Posteriorly Implanted Specimens

Luke Storer
University of Denver

Laxity of the Hip Capsule in Natural and Posteriorly Implanted Specimens

Abstract

The hip capsule consists of ligament tissue that surrounds the hip joint, providing stability to ensure proper alignment, prevent dislocation, and facilitate proper joint function. The objective of this study was to characterize the torque-rotation response of the natural and posteriorly implanted hip capsule in healthy cadaveric specimens in multiple degrees-of-freedom (DOF) and under combined loading scenarios using the AMTI VIVO, a robotic joint simulator. The anterior portion of the hip capsule was stained with Methylene Blue and virtual extensometers were calculated by Digital Image Correlation (DIC) software for Finite Element Analysis (FEA) model validation. The range of motion (ROM) was evaluated at up to 3 Nm of torque applied in both internal/external rotation and abduction/adduction and varied throughout the range of flexion. The 4-dimensional (combined IE, AD/AB and Flex/Ext resistive torque) total resistive torque rotation space exhibits an 'active zone' whereby the resistive torque attempts to restore it back to the 'neutral zone' where the resistive torque is minimized. Large differences in capsular laxity between natural and implanted specimens were observed, particularly with an increased adduction torque resistance and a reduced internal rotation torque resistance in implanted specimens. Broad variability was observed across specimens highlighting the need for development of patient-specific computational models. These findings assist in characterization of capsular function, informing surgical strategies for hip arthroplasty and long term with a goal of improving patient outcomes.

Document Type

Thesis

Degree Name

M.S.

Department

Bioengineering

First Advisor

Chadd Clary, Ph.D.

Second Advisor

Pete Laz

Third Advisor

Andrew Urbaczewski

Keywords

Capsule, Digital Image Correlation, Hip, Laxity, Torque

Subject Categories

Biomedical Engineering and Bioengineering | Engineering

Laxity of the Hip Capsule in Natural and Posteriorly Implanted Specimens

_____

A Thesis

Presented to

the Faculty of the Daniel Felix Ritchie School of Engineering and Computer Science

University of Denver

_____

In Partial Fulfillment

of the Requirements for the Degree

Master of Science

_____

by

Luke Storer

June 2019

Advisor: Dr. Chadd W. Clary

Author: Luke Storer
Title: Laxity of the Hip Capsule in Natural and Posteriorly Implanted Specimens
Advisor: Dr. Chadd W. Clary
Degree Date: June 2019

ABSTRACT

The hip capsule consists of ligament tissue that surrounds the hip joint, providing stability to ensure proper alignment, prevent dislocation, and facilitate proper joint function. The objective of this study was to characterize the torque-rotation response of the natural and posteriorly implanted hip capsule in healthy cadaveric specimens in multiple degrees-of-freedom (DOF) and under combined loading scenarios using the AMTI VIVO, a robotic joint simulator. The anterior portion of the hip capsule was stained with Methylene Blue and virtual extensometers were calculated by Digital Image Correlation (DIC) software for Finite Element Analysis (FEA) model validation. The range of motion (ROM) was evaluated at up to 3 Nm of torque applied in both internal/external rotation and abduction/adduction and varied throughout the range of flexion. The 4-dimensional (combined IE, AD/AB and Flex/Ext resistive torque) total resistive torque rotation space exhibits an ‘active zone’ whereby the resistive torque attempts to restore it back to the ‘neutral zone’ where the resistive torque is minimized. Large differences in capsular laxity between natural and implanted specimens were observed, particularly with an increased adduction torque resistance and a reduced internal rotation torque resistance in implanted specimens. Broad variability was observed across specimens highlighting the need for development of patient-specific computational models. These findings assist in characterization of capsular function,

informing surgical strategies for hip arthroplasty and long term with a goal of improving patient outcomes.

ACKNOWLEDGEMENTS

First and foremost, I must thank my advisor, Dr. Chadd Clary, for his support, mentorship, patience and assistance over the past two years.

I want to thank Dr. Pete Laz and Dr. Andrew Urbaczewski for serving as members of my defense committee.

I want to thank all members of the Experimental and Computational Orthopedic Biomechanics Labs, especially Yashar Benham for his expertise and assistance with Digital Image Correlation preparation and analysis, Ahilan Krishnan for his expertise in polynomial interpolation and Hayden Wilson, Brittany Marshall and Gary Doan for their assistance in specimen preparation and running of experiments.

Finally, I would like to thank DePuy Synthes for their funding of my project and fabrication of hip fixtures and equipment, particularly Dr. Dan Huff and Dr. Brian Haas.

TABLE OF CONTENTS

LIST OF FIGURES

CHAPTER 1. INTRODUCTION

1.1 Introduction

The hip capsule consists of soft tissue that surrounds the hip joint, providing stability to ensure proper alignment, prevent dislocation, and facilitate proper joint function. With the increased prevalence of minimally invasive hip arthroplasty to treat a wide variety of hip disorders including osteoarthritis (OA), hip dysplasia and femoroactebular impingement (FAI), capsular function and management during and after surgery has received increased interest (Kuhns et al. 2016, Kraeutler et al. 2016). An increasingly multifaceted and complex understanding of the role of the hip capsule in joint stability could lead to improved surgical plans, joint replacement technology and ultimately, patient outcomes.

In vivo investigation in live patients of the hip capsule has been hard due to its invasive nature. *In vivo* studies have been limited to qualitative descriptions of capsule anatomy (Martin et al. 2008), imaging (primarily MRI) based studies on variation of capsular thickness (Kay et al. 2018) and reviews of case studies that describe capsular

resections and subsequent capsular management and effect on surgical outcomes (Weber et al. 2016, Matsuda 2016, Ekhtiari et al. 2017). As a result, prior research into hip capsular function and properties has focused on *in vitro* cadaveric studies of intact hips (Martin et al. 2008, van Arkel et al. 2015a/b, Myers et al. 2013, van Arkel et al. 2018) and Finite Element Analysis (FEA) models containing computational representations of the hip capsule (Stewart et al 2004, Elkins et al 2011, Myers et al 2019 In Review). Cadaveric studies have also included resections of the capsular ligaments to test uniaxial mechanical properties such as stiffness, strength to failure and energy absorbed for each ligament (Hewitt et al. 2002, Stewart et al. 2004, Pieroh et al. 2016), as well as the generation of torque rotation curves for internal/external rotation torques using fully preserved hips in six degrees-of-freedom robotic testing setups (Daou et al. 2018, Goldsmith et al. 2015). Digital image correlation has previously been employed to measure strain data on human tissue (Lionello et al. 2014) but has not been utilized on hip capsular tissue. A study that can compare native and resected capsular tissue as seen in a total hip arthroplasty (THA) torque-rotation curve data at increased resolution while capturing capsular strain data may be beneficial in elucidating hip capsule function.

The primary objectives of this thesis are to design an experiment capable of characterizing the torque rotation response of the hip capsule of natural and posteriorly implanted specimens, compare and evaluate the effects of posterior approach THA on hip capsular stability and laxity, and capture hip capsule strain data for natural specimens. Torque rotation curves were generated through the range of hip flexion using a 6 degrees-

of-freedom (DOF) robotic joint motion simulator, the AMTI VIVO, (Figure 1.1) (AMTI, Watertown, MA) interfaced with custom fixtures capable of mounting hip joints. The passive restraint of the hip capsule was evaluated along the abduction/adduction and internal/external rotation isolated axes as well as with the combined loading situations. A novel way of characterizing the strain map during loading of the hip capsule in natural specimens was implemented utilizing A GOM ARAMIS stereo-camera system (Figure 1.2) and analyzed using Digital Image Correlation software (GOM mbh, Braunshweig, DE). These findings could facilitate improved understanding of hip capsular function, verify 6 DOF Finite Element Analysis (FEA) models containing capsular representations and inform optimal strategies for capsular management and resection necessary during and after hip arthroplasty.

1.2 Objectives

The objectives of this thesis are to:

1) Design an experiment capable of characterizing the torque rotation response of the hip capsule of natural and posteriorly implanted specimens.
2) Compare and evaluate the effects of posterior approach THA on hip capsular stability and laxity.
3) Capture hip capsule strain data for natural specimens.

1.3 Thesis Overview

Chapter 2 provides a brief background on hip capsule anatomy, hip arthroplasty procedures and surgical approaches as well as a review of published literature on hip capsule material properties and prior *in vitro* cadaveric experiments.

Chapter 3 presents *Multi-Axis Laxity of the Natural Hip Capsule* that aims to characterize the torque rotation space of the natural hip capsule in healthy cadaveric specimens *in vitro*.

Chapter 4 compares the findings from chapter 3 with the laxity of the hip capsule in posteriorly implanted cadaveric specimens.

Chapter 5 discusses the significance of these findings and recommendations for future work.

Figure 1.1: The AMTI VIVO (AMTI, Watertown, MA) a 6 DOF joint motion simulator, interfaced with custom fixtures capable of mounting cadaveric hips.

Figure 1.2: GOM Aramis DIC Camera System (GOM mbh, Braunshweig, DE).

CHAPTER 2. BACKGROUND INFORMATION AND LITERATURE REVIEW

2.1 Hip Arthroplasty to Treat Hip Disorders

Minimally invasive hip arthroplasty has emerged as a popular surgical approach to treat a wide variety of hip disorders including osteoarthritis, femoroacetabular impingement (FAI), hip dysplasia, labral tears and other pathological hip issues (Bedi et al. 2011). Osteoarthritis, a condition caused by the loss of cartilage that results in inflammation and pain at the joint, is particularly common, with estimates of incidence for the knee and hip as high as 3.8% of people worldwide (Cross et al. 2014). As osteoarthritis of the hip progresses in severity, total hip replacement (THR), a type of hip arthroplasty, may be performed as an end-stage treatment. THR is a common procedure in the USA with an estimated prevalence for the entire U.S. population of 0.83% (Kremers et al. 2015). It has been estimated that over 2.5 million Americans have at least one THR (Kremers et al. 2015) Furthermore, due to demographic changes there is increasing demand as the prevalence of Total Hip Arthroplasty (THA) and Total Knee Arthroplasty (TKA) among adults 50 years or older is 4.4% (Maradit Kremers 2014). To meet this high and increasing demand, many THR models (Figure 2.1) have been

designed by a wide array of manufacturers in the last half century complimented by a large variety in surgical approaches combined with various rehabilitation approaches.

While THA is often seen as a 'model surgery' with increasingly high success rates (Rajee et al. 2018), there may still be complications that require revision surgery including fracture and loosening of THR component, femoroacetabular dislocation and capsular instability (Banaszkiewicz 2014b). Proper management of the hip capsule is often a critical component of successful hip replacement surgery and can prevent costly revision surgery (Bedi et al. 2011). The hip capsule consists of soft tissue that surrounds the hip joint, providing stability to keep the hip in proper alignment. As a necessity to gain access to the interior of the hip joint, hip arthroplasty procedures involve resections of the capsule. Understanding the nature of these resections, subsequent capsular management involving capsulectomies and/or capsular plication, and future effects on restoring hip function and stability may help surgeons prevent revision surgeries and ultimately improve patient outcomes.

2.2 Capsule Anatomy

The hip capsule is an integrated fibrous lining surrounding the hip joint that is composed of several discrete ligamentous structures (Bedi et al. 2011). External to the joint are the iliofemoral, ischiofemoral and pubofemoral ligaments which contain fibers that primarily run longitudinally (Pieroh et al. 2016) (Figure 2.2). Each external ligament has attachment locations on the femur and corresponding pelvic bone that gives the

ligament its name. The iliofemoral ligament comprises most of the anterior portion of the capsule and is shaped like an inverted "Y" with lateral and medial branches (also referred to as superior and inferior) that cross the joint and connect to the intertrochanteric line of the femur (Bedi et al. 2011). In contrast, the ischiofemoral ligament comprises the posterior portion of the capsule, originating at the ischial rim of the acetabulum and inserting on the posterior aspect of the femoral neck (Bedi et al. 2011). The pubofemoral ligament runs inferior to the iliofemoral ligament, originating at the obturator crest of the pubic bone while attaching distally to the femoral neck (Bedi et al. 2011). Internal to the joint is the zona orbicularis which contains longitudinal fibers that encircle the femoral neck and the ligamentum teres which contains two bands which attach interiorly from the head of the femur to the acetabulum (O'Donnell et al. 2014). The ligamentum teres is thought to play a role in dislocation resistance in addition to providing blood supply to the joint (O'Donnell et al. 2014). The ligaments combine to form the continuous hip capsular structure.

Several studies have used imaging techniques (MRI and ultrasound), intraoperative techniques and studies on cadaveric tissue to measure capsular thickness *in vivo* and *in vitro*. A review by Kay et al. of these studies which included over 1000 hips found that MRI measurements were the most consistent with the least variation (Kay et al. 2018). The mean thickness found was significantly greater in diseased hips with males having significantly thicker hip capsules than females. As expected the anterior portion of the capsule was the thickest with a mean thickness reported by MRI of between 4.4 and 4.7 mm. Several studies have demonstrated correlations between capsule thickness and

hip laxity. Devitt et al demonstrated that patients with Beighton scores (an overall joint laxity quantification method) are associated with thinner capsules (Devitt et al. 2017). Equivalently, Magerkurth et al. found that patients with pathological hip laxity defined by pre-arthroscopy hip laxity tests had considerably less thick hip capsule (Magerkurth et al. 2013). As form often follows function, understanding capsular anatomy may have implications on capsular function.

2.3 Hip Arthroplasty Surgical Approaches and Capsular Management Strategies

Hip arthroplasty procedures require resection of the hip capsule to gain access to the interior hip joint. There are several different surgical approaches as well as several different capsular management strategies post-resection. The three most common minimally invasive (which leads to a quicker recovery for the patient) surgical approaches are posterior, anterior and anterior-lateral (Bertin and Rottinger 2004, Nakamura et al. 2004, Matta et al. 2005) defined by the anatomical location in which the initial incision is made. Each approach results in arthroscopic ‘portals’ into the hip capsule for visualization by the arthroscopist. Telleria et al. utilized 8 paired cadaveric hips to look at the location of each ligament in relation to known anatomical landmarks through typical anterior, anterior-lateral, posterior arthroscopic portals. They used a clock-face reference system to describe variation in position and origin/insertion sites of the different hip capsular ligaments and the relation by which each ligament was pierced when resected through a specific surgical approach. They found that the iliofemoral ligament was pierced just inside the lateral border by the anterolateral portal, and just

inside the medial border by the anterior approach. The ischiofemoral ligament was pierced just inside the superior/lateral border using the posterior approach (Telleria et al. 2011). The authors also observed higher variation in resection relative to the corresponding ligament using the posterior approach. Limitations of the study include using only one surgeon which may have limited the quantification of variation in capsular resections made between surgeons, as well as only evaluating the portal locations at 0 and 30 degrees of flexion. The study is valuable in how it correlates typical hip arthroplasty surgical approaches to resections of different portions of the hip capsule.

There is also significant variation in hip capsular management strategies including whether to perform a capsulectomy, capsulotomy and/or capsular plication/capsulorrhaphy (tightening of the hip capsule) during hip arthroplasty (Domb et al. 2013, Ekhtiari et al. 2017). Reviews have suggested evidence for which technique leads to the best clinical outcomes is mixed and may depend on the specific case details (Domb et al. 2013, Ekhtiari et al. 2017). Domb et al. concluded that haphazard capsulotomy can reduce hip stability, but capsulotomies may be necessary in cases where the hip has overly-tight laxity. They cautiously recommend capsular plication in cases where atraumatic instability or excess capsular laxity is suspected as well as to resist dislocation post-operatively (Domb et al. 2013). In contrast, Ekhtiari et al. performed a review of 82 studies involving 4505 patients of which 55% performed an inter-portal capsulotomy while 24% performed a T-capsulotomy. 36 of those studies reported capsular management techniques with 22% of surgeons not repairing the resection, and 50% of surgeons performing a complete repair. They concluded that the evidence does

not support one specific capsular management strategy and “there is little basis on which to establish the relationship between surgical technique and post-operative instability or long-term consequences” (Ekhtiari et al. 2017). Clearly there is a need for more rigorous investigation into resection techniques and capsular management strategies.

2.4 Mechanical Testing of the Hip Capsule

Uni-axial Testing of Hip Capsule Ligaments

Mechanical testing of the hip capsule may help further elucidate both natural hip function and optimal capsular management strategies during hip arthroplasty by thoroughly quantifying passive hip stability and function. Several studies have attempted this quantification in a variety of ways from extraction of tissue to full preservation of the hip capsule *in vitro*.

Hewitt et al. (2002) was among the first to study the mechanical properties of the hip capsular ligaments by removing each ligament individually, measuring the initial length and cross-sectional area of each unloaded ligament and then mounting into a uniaxial testing setup (Hewitt et al. 2002). The ligaments were then loaded to failure at a displacement rate of .04 mm/s with displacement measured by a video analysis system. The maximal force, failure stress, stiffness and energy to failure (area under the force-displacement curve) were measured for each ligament. The authors found significant differences in maximal force to failure with both bands of the iliofemoral ligament being stronger than the other hip capsule ligaments. The energy to failure was similar for all

three extracapsular ligaments, explained by the stiffest ligament – the iliofemoral ligament – displacing the least (Hewitt et al. 2002). The authors hypothesized that lower rates of anterior dislocations were due to the stronger material properties of the iliofemoral ligament and anterior portion of the capsule.

Stewart et al. (2004) performed similar work to Hewitt et al. with the slight variation of performing a complete capsulectomy as one large piece and then excising the entire capsule into eight sectors. They performed many of the same geometrical measurements (anatomical insertion points and cross-sectional area) as well as similar uniaxial testing on the 8 sectors recording stiffness, modulus, ultimate strength and failure load analysis, obtaining measurements on par with Hewitt et al. Stewart et al., confirmed prior results that demonstrated the anterior portion of the capsule was the thickest and strongest with the posterior portion significantly thinner. One large limitation of the experimental setup is they did not use individual ligaments but instead chose different sectors of the ligamentous complex for finite element model validation purposes.

Pieroh et al. (2016) repeated prior experiments in a similar fashion and surprisingly found different results for elastic modulus (stiffness) and strain compared to the previous experiments. Pieroh et al. reported similar stiffnesses and strains for each extracapsular ligament (Pieroh et al. 2016). The authors hypothesized that small sample sizes as well as anisotropic properties, fiber orientation and direction of the test setup may explain the differing results. The iliofemoral fiber directions are largely

longitudinally oriented whereas the ischiofemoral ligament contains many perpendicular collagen fibers. Additionally, specimen dimensions differed between specimens in which Hewitt et al. contained deeper layers of the capsule not in the orientated test direction (Pieroh et al 2016). The authors conclude that a bi-axial test setup may provide a more accurate representation of the anisotropic anatomy present in extracapsular hip ligaments. The authors also found that there were no significant differences between male and female subjects, signaling that future researchers did not need to take gender into account when designing cadaveric experiments. While these studies provided strong insight into mechanical properties of individual ligaments which can be valuable for material definitions for finite element analysis (FEA) modeling purposes, they lacked bi-axial or more DOF's that may be better captured using *in vitro* cadaveric testing.

In Vitro Cadaveric Testing

While uniaxial testing of hip capsule ligaments is useful in determining mechanical properties of the hip capsule, *in vitro* cadaveric testing of intact hip capsules can often provide superior insight into capsular function. *In vitro* cadaveric testing has many advantages over fully excised-capsular measurements as it can more effectively reproduce conditions found *in vivo* and/or after hip arthroplasty. It also offers the ability to more holistically measure capsular function by careful removal of fat, muscle and other soft tissue to isolate the effects of the hip capsule. *In vitro* cadaveric testing has progressed from early measurements involving passive motion along the swing path of the hip (Martin et al. 2008) to torque-rotation curves of the hip capsule as measured in a 6

DOF robotic testing setup which has emerged as the ‘gold standard’ for *in vitro* biomechanical joint testing (Daou et al. 2018).

One of the earliest *in vitro* cadaveric studies was performed by Martin et al. which focused on characterization of internal and external rotational displacements of the hip along a neutral swing path (Martin et al. 2008). They excised the hip musculature and fat tissue to expose the hip capsule while stabilizing the pelvis and femur with mounting rods. At 4 specific flexion angles (10° extension, neutral, 15° and 30° flexion), they measured the degrees of internal and external passive rotation using a goniometer. Next, they sequentially removed ligaments and remeasured the passive rotational restraint range. With all ligaments intact, they observed a rotational displacement profile that increased as flexion increased. After sequentially excising ligaments, they were able to quantify the relative contribution of each ligament. For internal rotation, the primary restrictors were the ischiofemoral ligament and the lateral arm of the iliofemoral ligament. For external rotation, both arms of the iliofemoral ligament were the primary restrictors. Several limitations were present in this study that could be improved upon in future studies. First, the restraint of the capsule was not quantified in terms of torque resistance (it is not clear how they determined restraint in general). Furthermore, only the external/internal rotation DOF was evaluated along a relatively small range of flexion angles. When perturbing the hip capsule, they excised ligaments in the same order for each specimen, making it difficult to systemically determine the contributions of each ligament.

Myers et al. 2013 performed a similar version of Martin et al.'s 2008 experiment by quantifying the torque resistance (5 Nm) applied and measuring internal/external rotational displacement and anterior translation of the femur using biplane fluoroscopy to track injected tantalum beads. Like Martin et al., they excised the iliofemoral ligament and the labrum to see their contributions as external/internal rotator restrictors and their effect on anterior translation of the femur. They observed similar results as the iliofemoral ligament played a large role as a restrictor of external rotation and anterior translation of the femur (Myers et al. 2013). They found no significant contribution of the labrum to hip stability. Furthermore, they confirmed that flexion angle has a significant effect on the range of internal/external rotation. Han et al. performed a similar experiment to Myers et al., this time monitoring the location of the head relative to the femur with a 6-camera motion analysis system and testing femoral head translation and internal/external rotation following the incisions in the iliofemoral, pubofemoral and ischiofemoral ligaments. They found similar results such that capsular modification led to significant increases in internal and external rotations and femoral head translations (Han et al. 2018).

Recent work by van Arkel et al. improved upon many of the deficiencies of Martin et al. and Myers et al. by applying quantified torques to again measure internal and external rotational displacement at increased resolution of flexion angles. Van Arkel et al.'s testing rig consisted of a dual axis servo-hydraulic materials-testing-machine to control internal/external rotation and inferior/superior displacement equipped with weights and pulleys to apply torques at the other two rotational DOF's with the hip

allowed to translate freely in the AP and ML axes. For their experiments, van Arkel et al. increased the flexion range resolution to include 30° increments from full flexion to full extension as well as the addition of adduction/abduction loaded positions to paint a more complete picture of the passive motion envelope of the hip capsule with and without various capsular ligaments. Van Arkel et al. performed resections in a randomized order as compared to Martin et al. with the addition of the ligamentum teres and labrum which both had significant contribution to hip restraint in only a few positions (van Arkel et al. 2015a). Overall, their results agreed with Martin et al. about the role of specific capsular ligaments in low flexion/extension (van Arkel et al. 2015a) and improved upon Martin et al.'s methodology by quantifying torque resistance and randomizing excision order of the ligaments.

Van Arkel et al. also attempted to further characterize the passive restraint envelope by generating torque-rotation curves for internal/external rotation in a variety of conditions separately including neutral displacements in secondary DOF's and loaded to 5 Nm of torque at each rotational DOF (van Arkel et al. 2015b). For each torque rotation curve, they defined a 'slack' and 'stiff' region based on the change in slope of the torque rotation curves. They observed that the range of the 'slack' region varied with flexion/extension and adduction/abduction with the greatest range of the 'slack' region in 60° flexion and mid-adduction/abduction (Figure 2.3). Conversely, in positions of extreme hip ROM (high flexion/extension or high adduction/abduction), there was little to no 'slack' region with the capsule providing internal/external rotational resistance throughout the entire ROM (van Arkel et al. 2015b). These experiments helped capture

the torque-rotation space of the hip capsule in greater resolution but could be improved by adding measurements of flexion/extension, adduction/abduction torque-rotation and/or additional off-axis loading curves.

Changes in capsular ligament function after total hip arthroplasty have also been investigated. Femoral head size and neck length of THR components have been hypothesized to change the natural laxity of the hip capsule (van Arkel et al. 2018). To isolate the effects of femoral component head size and neck length, van Arkel et al. utilized the same testing setup as described above to examine internal and external ROM in 5 different THA relevant hip positions following a THA performed through the medial acetabular wall, which allowed the preservation of the entirety of the hip capsule. They found that the post-THA rotational ROM was significantly different than pre-THA ROM, of which the difference could be mitigated by neck size changes but not by head size changes. Interestingly, they found that the posterior capsule was most affected by a capsule preserving THA while the anterior portion of the capsule was largely unaffected, particularly in flexion. Similar limitations of this study existed for the other studies by van Arkel et al. including only evaluating internal/external torque curves and lack of off-axis/combined loading analysis. Additionally, they did not perform a clinically relevant THA procedure as it did not involve resection of the capsule and did not contain commercially available THA hardware such as those that would be found *in vivo.* Future studies involving post-THA capsular laxity assessments should correct these limitations by using a board approved surgeon utilizing a standard hip arthroplasty protocol and commercially available THA hardware.

Other studies have looked at the effects of capsulotomies, cam resection and capsular repair on the internal/rotational displacement envelope of the hip capsule. Ng et al. took 12 hips with cam deformities and performed a series of surgical procedures – T-capsulotomy, cam resection and capsular repair to ascertain the effects of the surgical procedures on internal/external rotation. They found that external rotation increased significantly following the capsulotomies and normal function could be restored after capsular repair (Ng et al. 2019). Significant limitations of this study include testing of pathological hips only and not natural hips as well as the focus primarily being on the effects of cam Femoroacetabular Impingement (FAI) surgery and not on the effects of THA.

Most recently, several groups have confirmed the viability of a 6 independently-controlled DOF robotic testing machine platform as the 'gold standard' for *in vitro* hip biomechanical testing (Daou et al. 2018, Goldsmith et al. 2015). While this has been available for the knee in forms such as the Kansas knee simulator (Clary et al. 2013), it has only recently been possible with the hip. These testing platforms allow for load or displacement control and have become the best way to analyze both native and implanted joints. The AMTI VIVO (AMTI, Watertown, MA) (Figure 1.1) is one of the most sophisticated robotic joint testing rigs, able to be controlled in each independent axis in position or force control as well as supporting the Grood and Suntay coordinate systems (Grood and Suntay 1983) used by major biomechanics organizations such as ASTM, ISB and ISO. Any future study should take advantage of this technology to fully test hip joint passive laxity in multiple rotational DOF's and in combined loading scenarios.

2.5 Strain Mapping of Hip Capsular Tissue *in Vitro*

While strain mapping has been performed on excised tissue such as experiments done by Stewart et al., it has been scarcely performed *in vitro* on hip capsular tissue. Several methodologies exist for measuring strain *in vitro.* Hideka et al. 2009 measured strain on the iliofemoral ligament in several different stretching positions using a displacement sensor (Hideka et al. 2009). Strains in the range of 2.1 to 4.0% were seen in the superior (lateral) and inferior (medial) arms of the iliofemoral ligament respectively. More recently, digital image correlation (DIC) technology has emerged as an alternative accurate way to map strain fields on biological soft tissue (Lionello et al. 2014). DIC is a non-contact stereo-camera system able to measure three-dimensional strain fields; providing information on both local and global strain fields at micrometer accuracy (Sutton et al. 2008). Lionello et al. have pioneered an approach to measuring biological soft tissue strain using DIC with tissue that has been stained with Methylene Blue (Figure 2.3) without damaging or significantly changing the elastic response of the soft tissue (Lionello et al. 2014). DIC has not yet been employed to measure hip capsular tissue strains but holds promising potential.

2.6 Finite Element Model Verification

Computational modeling of biological tissue using finite element analysis software is often used in tandem with *in vitro* cadaveric testing as it is often less expensive and time consuming and allows for more extensive and expansive perturbation of biomechanical systems. However, verification and validation of computational models

with experimental results is critical (Henninger et al. 2010). There have been several models that have finite element representations of the hip capsule. (Stewart et al. 2004, Elkins et al. 2011, Myers et al. 2019 in review). Stewart et al. incorporated material properties from previously obtained experimental uniaxial test data into a hyper-elastic finite element representation of 8 sectors of the hip capsule to test dislocation resistance of THA implanted hip (Stewart et al. 2004). Elkins et al. continued the work of Stewart et al. by optimizing the material properties of hip capsule by matching resulting force-displacement data from corresponding *in vitro* cadaveric testing data (Stewart et al. 2002). More recently, Myers et al. developed a probabilistic finite element hip capsule representation (Figure 2.4) and used data from van Arkel et al. to calibrate and tune the model (Myers et al. 2019 in-review). Similar work may be done in the future to match strain data of portions of the capsule to experimentally obtained strain maps and torque rotation data to verify finite element representations of the capsule are physiologically accurate and recruits the same tissue for various loading conditions as occurs *in vivo*.

2.7 Takeaways from Literature

Future studies on the role of the hip capsule on hip stability should consider prior experimental results and address their shortcomings. *In vitro* cadaveric work utilizing a 6 DOF robotic testing setup is the current gold-standard for biomechanical joint testing and should be used for future tests. Torque-rotation curves in all rotational DOF's, not just internal/external rotation, and in combined loading situations should be measured to provide a more complete picture of the torque-rotation laxity space of the hip capsule.

Furthermore, DIC technology should be utilized to measure the strain field for the hip capsule ligaments under various rotational displacements. The effect of total hip arthroplasty on hip laxity should also be investigated.

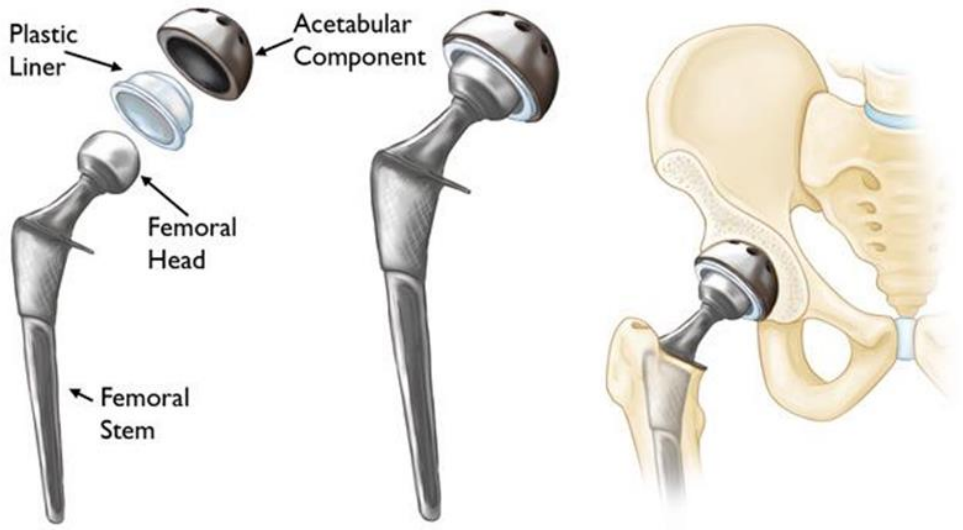

Figure 2.1: Components of a total hip replacement (orthoinfo.aaas.org)

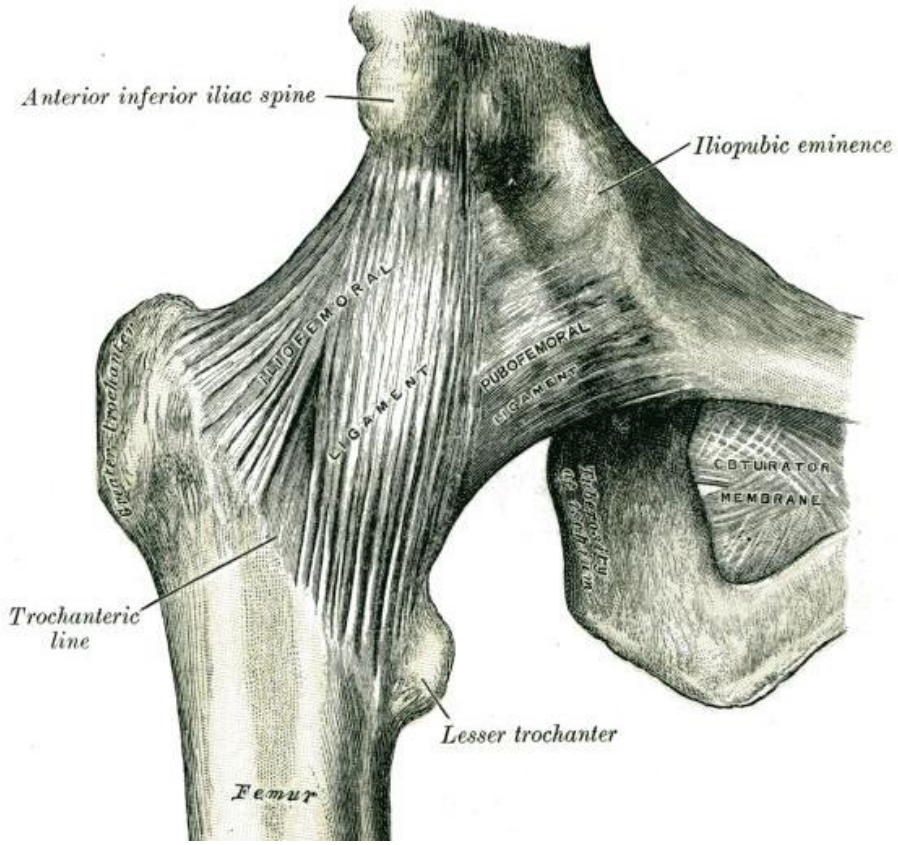

Figure 2.2: Hip capsule ligament anatomy (anterior view) (Prohealthsys.com)

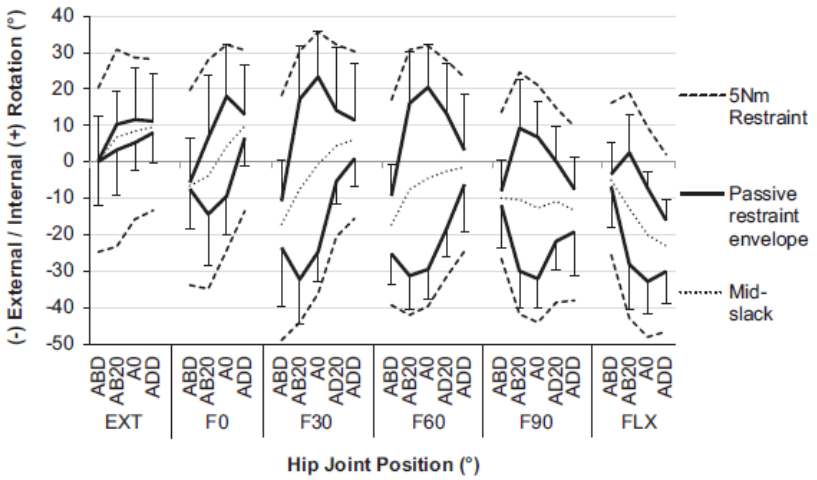

Fig. 3. The rotation passive restraint envelope (with standard deviation, $n=8$), the points of mid-slack and the 5 N m measurement boundaries across a complete hip range of motion. It can be seen that there was a greater range of un-resisted rotation (space between the solid black lines) in mid-flexion and mid-ab/adduction than when the hip was deeply flexed/extended, or highly ab/adducted. It can also be seen that the hip was more open to internal rotation in extension, and external rotation in flexion as the mid-slack points (grey dots) shifted to external rotation as hip flexion was increased. However once the ligaments had started to restrain hip rotation, the internal/extenral rotation restraint is more symmetrical (equal spacing between solid black lines and dashed grey lines at each position).

Figure 2.3: Internal/External torque rotation data from Van Arkel et al. 2015b.

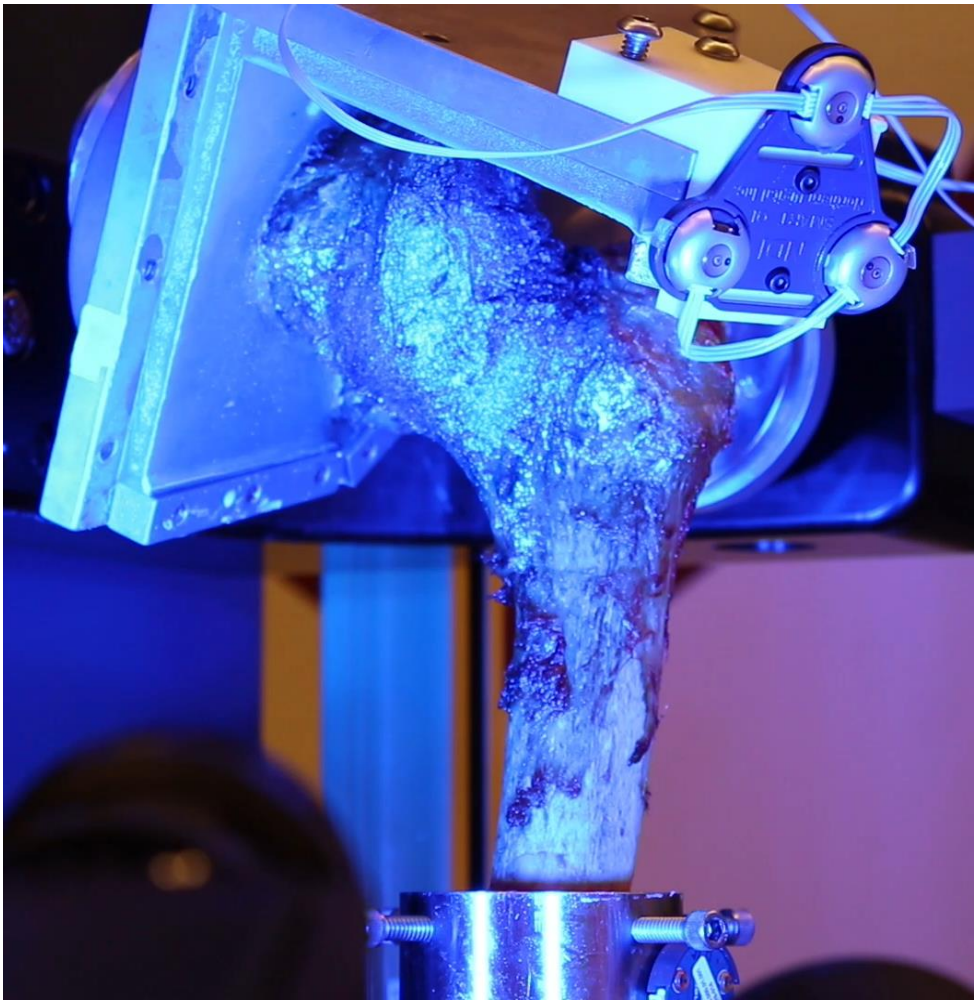

Figure 2.4: Natural hip capsule (iliofemoral ligament) stained with Methylene Blue and a stochastic speckle pattern for Digital Image Correlation (DIC) analysis.

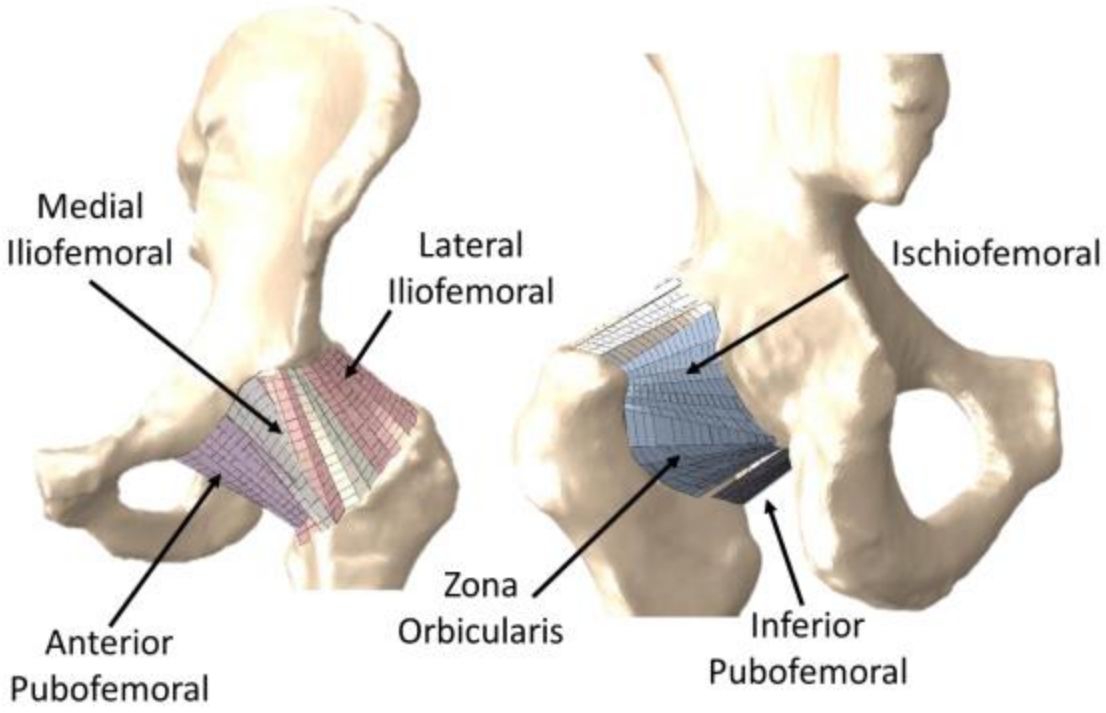

Figure 2.5: Finite Element Analysis (FEA) model representation of the hip capsule (Myers et al. 2019 in-review).

CHAPTER 3. MULTI-AXIS HIP LAXITY OF THE NATURAL HIP CAPSULE

3.1 Introduction

The hip capsule consists of soft tissue that surrounds the hip joint, providing stability to ensure proper alignment, prevent dislocation, and facilitate proper joint function. With the increased prevalence of minimally invasive hip arthroplasty to treat a wide variety of hip disorders, including Osteoarthritis (OA), hip dysplasia and Femoroactebular Impingement (FAI), capsular function and management during and after surgery has received increased interest (Kuhns 2016, Kraeutler et al. 2016). A progressively multifaceted and complex understanding of the role of the hip capsule in joint stability could lead to improved surgical plans, joint replacement technology and ultimately, patient outcomes.

Due to limitations in current technology, *in vivo* investigation of the hip capsule has been difficult due to its invasive nature. *In vivo* studies have been limited to qualitative descriptions of capsule anatomy (Martin et al. 2008), imaging (primarily magnetic resonance imaging (MRI) based studies on variation of capsular thickness (Kay et al. 2018) and reviews of case studies that describe capsular resections and subsequent

capsular management and their effect on surgical outcomes (Weber et al. 2016, Matsuda 2016, Ekhtiari et al. 2017). As a result, prior research into hip capsule function has focused on *in vitro* cadaveric studies (Martin et al. 2008, Myers et al 2011, van Arkel et al. 2015a/b, van Arkel 2018) and the analysis of FEA models containing computational representations of the hip capsule (Elkins et al. 2011, Myers et al. 2019 in-review). Cadaveric studies have also included resections of the capsular ligaments to test uniaxial mechanical properties such as stiffness, strength to failure and energy absorbed of each ligament (Hewitt et al. 2002, Stewart et al. 2004, Pieroh et al. 2016), as well as the generation of internal/external torque rotation curves using fully preserved hips in 6 degrees-of-freedom (DOF) robotic testing setups (Daou et al. 2018, Goldsmith et al. 2015). Digital Image Correlation (DIC) software has previously been employed to measure strain data on human tissue (Lionello et al. 2014) but has not been utilized on hip capsular tissue. A study that can characterize native torque rotation behavior of the hip capsule at increased resolution for multiple rotational DOF, while capturing capsular strain data *in vitro*, may be beneficial in elucidating hip capsule function.

The primary focus of this study was to experimentally characterize the laxity of the hip capsule of healthy cadaveric specimens *in vitro*. Torque rotation curves were generated through the range of hip flexion from 0° to 105° using a 6 DOF joint motion simulator, the AMTI VIVO, (Figure 3.2) (AMTI, Watertown, MA) customized with fixtures capable of mounting hip joints. The passive restraint of the hip capsule was evaluated along the abduction/adduction and internal/external rotation isolated axes as well as with the combined loading situations. A novel way of characterizing the strain

map during loading of the hip capsule was implemented utilizing a GOM ARAMIS stereo-camera system and DIC software (GOM mbh, Braunshweig, DE). These findings could facilitate improved understanding of hip capsular function, verify 6 DOF finite element models containing capsular representations and help inform optimal strategies for capsular management and resection necessary during and after hip arthroplasty.

3.2 Methods

Specimen Preparation and Management

Computed tomography (CT) scans were obtained for 10 cadaveric pelvises (mean age 71 years old, range 26 years, STD 11.6 years). Femur and pelvis bones were segmented using ScanIP (Simpleware, Mountain View, CA). After bone segmentation, pelvises and femurs were virtually aligned according to the International Society of Biomechanics (ISB) hip Joint Coordinate System (JCS) recommendations (Wu et al. 2002). Prior to testing, the cadaveric specimens were thawed at room temperature for 48 hours. Skin, muscle and fat tissue surrounding the capsule were removed, exposing the iliac crest and distal portion of the femur. Custom 3D printed cutting guides based on the specimen's geometry obtained from the CT scans were printed to ensure the center of the femoral head/acetabulum was at the center of rotation for the flexion/extension, adduction/abduction and internal/external rotational axes of the testing rig (Figure 3.1) and ensure proper bone resection for mounting into the fixtures. For each specimen, all laxity tests were performed at room temperature on the same day without removing the

specimen from the testing rig. The specimens were kept moist using regular saline solution sprayed on capsular tissue.

Mechanical Testing

The testing rig consisted of custom fixtures able to mount pelvises and femurs using bone cement and adapted to fit into the AMTI VIVO, (Figure 3.2) (AMTI, Watertown, MA), a 6 DOF joint motion simulator able to operate in both load and displacement control. The testing rig's flexion/extension axis was outfitted with an auxiliary axis that allowed the pelvis to be offset in 15° flexion increments at which each laxity test was performed from 0° to 105° of flexion. In order to map the torque rotation space limits, a 110 N compressive load (chosen based on prior research by Myers et al (2011) and van Arkel et al. (2015b) was applied through the superior/inferior axis of the femur at each flexion/extension increment, while each rotational axis (flexion/extension, adduction/abduction and internal/external rotation) was set in displacement control and the alternate translational axes (anterior/posterior and medial/lateral) were set to a load of zero. A total of 6 torque rotation laxity mappings (Figures 3.3-3.5) were performed at each flexion increment: 1) Isolated adduction/abduction laxity at neutral internal/external rotation, 2) Isolated internal/external rotation laxity at neutral adduction/abduction 3) Isolated adduction/abduction laxity at maximal internal rotation, 4) Isolated adduction/abduction laxity at maximal external rotation, 5) Isolated internal/external rotation laxity at maximal abduction, and 6) Isolated internal/external rotation laxity at maximal adduction. A target torque of 5 Nm was chosen as the limit for each torque

rotation curve. The isolated rotational axis was run in displacement control using a trapezoidal waveform input (Figure 3.6) over a period of 20 seconds, while the other rotational axes were kept at constant values as determined during the mapping phase. The load cell located at the femoral base fixture sampled associated torques, translational forces and displacements for all 6 DOF at 100 Hz.

Digital Image Correlation Specimen Preparation

In one specimen, the iliofemoral ligament was stained with Methyl Blue and a stochastic speckle pattern was applied using white acrylic paint and air brush according to a protocol developed by Lionello et al. (2014) Digital images were sampled at a frame rate of 1 Hz. Virtual extensometers were created and orientated axially in series along the medial and lateral arms of the iliofemoral ligament (Figure 3.7) to measure strains and elongation patterns throughout the neutral to full adduction laxity assessment at neutral internal/external rotation at 15° of flexion using a GOM ARAMIS stereo-camera system and Digital Image Correlation System.

Data Analysis

Torque and rotation VIVO feedback for each assessment was analyzed using custom Matlab scripts (MathWorks; Natick, MA). First, raw torque output data was smoothed using a moving average filter (Figure 6). Next, positive and negative loading curves along with torque values from -6 to 6 Nm at 0.1 Nm increments were extracted along the primary axis of rotation with displacement/torque values from all additional

axes interpolated at the same time points. Mean and standard deviations of the primary axis data were compiled at 3 Nm of torque and plotted for each torque rotation curve condition (internal/external displacements at 3 Nm of torque) and (abduction/adduction displacements at 3 Nm of torque) as this represented a value where the slope of the laxity curve changed substantially. The rotational range for each laxity assessment was taken by subtracting the mean positive displacement at 3 Nm torque from the mean negative displacement at 3 Nm torque. The slack to stiff transition points were found by fitting a 4^{th} degree polynomial to the loading curve, taking the derivative of the resulting polynomial and evaluating where the slope of the loading curve was equal to .03 Nm/degree, as established by prior data (van Arkel et al. 2015b). The total resistive torque was calculated as the sum of the squares of each axis of rotation (flexion/extension, abduction/adduction, and internal/external rotation) and was plotted for one specimen at a range of flexion values. Each total resistive torque rotation curve was fit with a second order polynomial and the total resistive torque rotation surface was interpolated using a nonlinear least squares method. In one specimen, for the neutral to full adduction loading curve at neutral internal/external rotation at 15° of flexion, Digital Image Correlation software (GOM mbh, Braunshweig, DE) was used to create 3 bundles of virtual extensometers in series along the longitudinal axis of the medial and lateral arms of the iliofemoral ligament. Percent change in length (engineering strain) was calculated and averaged for each extensometer group from proximal to the pelvis to distal to the pelvis and temporally at 5 evenly spaced intervals during the duration of the loading curve from neutral to full adduction.

3.3 Results

Laxity of Internal/External Rotation & Adduction/Abduction at Neutral Secondary Displacements

The internal/external laxity at neutral adduction/abduction of the hip capsule at 3 Nm of IE torque is shown in Figure 3.8. At 0° of flexion, the mean rotational displacement for internal rotation was approximately 27° ± 9° while the mean displacement for external rotation was 27°± 7° for a total range of motion of (ROM) of approximately 54° ± 11° (Figure 3.10). As the hip proceeds through the range of flexion the, ROM at 3 Nm of torque increases to a maximum of 63° ± 7° at 45° of flexion. At 105° of flexion, the mean rotational displacement for both internal and external rotation decreases to 21° ± 10° and 34° ± 5° respectively for a total ROM of 55° ± 11°. There is a noticeable shift in the internal/external range of motion near terminal extension with both internal and external rotational limits shifting towards increased external rotation.

Abduction/Adduction laxity at neutral internal/external rotation showed a similar trend with the mean rotational displacements at 3 Nm of torque increasing up to 45° flexion but decreasing as the hip approached full flexion. At 0° of flexion, the mean rotation was 9° ± 6° (Figure 3.9) for adduction and was 34° ± 6° resulting in a total ROM of 43° ± 6° for abduction (Figure 3.11). The abduction/adduction ROM increased in mid flexion at 60° to a ROM of at least 63° (the adduction limit was outside the VIVO actuator displacement limits). Similar to the internal/external rotational laxity profile, at 105° of flexion, the mean displacement for both adduction and abduction rotation

decreased to 13° ± 6° and at least 55° (the abduction limit was outside the VIVO actuator displacement limits) respectively for a total ROM of at least 70°.

Laxity of Internal/External Rotation & Adduction/Abduction at Maximal Secondary Rotations

The laxity of both rotational axes at maximal secondary axis rotations generally displayed similar behavior to that of neutral secondary axis displacements with the ROM of 3 Nm of torque starting out smaller at low flexion ranges, increasing through mid-flexion ranges and decreasing as the hip proceeds towards full flexion. At lower flexion angles, between 0° and 30°, the abduction/adduction displacements at maximal internal rotation demonstrate a shift towards adduction from abduction from 0° to 15° and back towards abduction from 15° to 30°. Additionally, the torques for several loading conditions appeared to be coupled, such as increased adduction torque coupled with an increased internal rotation torque response. This coupling behavior is particularly noticeable at higher flexion angles as the abduction/adduction laxity ROM decreases the internal/external rotational ROM decreases at maximum adduction decreases. Overall, the variability was significantly higher for combined loading scenarios (e.g. adduction/abduction torque at maximal internal rotation) than for neutral laxity assessments conditions most likely due to variation in where the secondary rotational limits were chosen.

Slack to Stiff Transition

The slack to stiff transition points results generally agree with the torque displacement limits found at 3 Nm with the average slack to stiff points occurring approximately 5 degrees before the torque limits as demonstrated in Figures 3.9 and 3.11 for internal/external rotation at neutral adduction/abduction and abduction/adduction at neutral internal/external rotation respectively.

4-Dimensional Torque Response

The total resistive torque response for one specimen at a range of flexion angles is shown in Figure 3.12 with the interpolated total resistive torque response shown in Figure 3.13. The resulting surface resembles a paraboloid with the total resistive torque increasing as it approaches the combined loading displacement limits. Additionally, as the flexion angle increases from 0° to mid-flexion (30° and 60°), the 'neutral zone', i.e. where the passive total resistive torque is minimal, increases in size and then decreases again as it approaches full flexion. As noted above, similar to the migration of the internal/external rotation laxity envelope, the neutral zone appears to shift along the internal/external rotation/abduction/adduction plane, trending towards increased external rotation/abduction.

Digital Image Correlation

The results of the virtual extensometers captured by a GOM ARAMIS stereo-camera system and analyzed by Digital Image Correlation (DIC) showing percent

engineering strain ($\Delta L/L_0$) over a range from neutral abduction/adduction to full adduction (21.5 degrees adduction) are shown in Figure 3.14, while the loading curve with each temporal interval corresponding to the DIC measurements are shown in Figure 3.15. Overall, the lateral arm of the iliofemoral ligament demonstrated significantly increased strain over the duration of the loading curve compared to the medial arm. The greatest change in strain temporally (approximately 20%) occurred at the same time as the loading curve transitioned from a minimal torque response to a significant torque response, demonstrating the unfolding and subsequent tightening of the lateral arm ligament tissue as the hip transitions into full adduction. The strains also varied directionally as both arms demonstrated increased strains in the distal to the pelvis portion of the ligaments compared to the proximal portions.

3.4. Discussion

In this study, we have characterized the torque rotation response of the natural hip capsule in healthy cadaveric specimens. We have built upon the work of other *in vitro* hip capsule studies (Martin et al. 2008, van Arkel et al. 2015a/b, Myers et al. 2011, van Arkel et al. 2018) by utilizing a robotic joint simulator capable of measuring torques and displacements in all 3 rotational DOF's at increased flexion range resolution. We have also presented a novel method of capturing strain data in native hip ligament tissue for various loading conditions by using Digital Image Correlation software. We intend to use the 3-dimensional torque profile along with the virtual strain data to optimize and refine

existing Finite Element Analysis (FEA) models of the hip capsule (Myers et al. 2019 in review) to match our experimental data.

The most significant finding of this study is the confirmation of a 'neutral zone' where the combined resistive torque is minimal and at the boundaries of the neutral zone, an 'active zone' where the resistive torque attempts to restore the native rotational displacements to the 'neutral zone' (Figure 3.12). The data presented here gives bounds on which the torque in all 3 DOF's increases to restore the hip back to its neutral state. Our data largely agrees with prior characterizations of the passive restraint envelope of the hip capsule (van Arkel et al. 2015b). Comparing with the findings by van Arkel et al., (Figures 3.16-3.23) the rotational ROM for internal/external rotation changes dramatically over the flexion range, increasing to a maximum in mid-flexion and decreasing again approaching terminal flexion. In addition, comparing with van Arkel et al., the 'neutral zone' appears to shift towards increased external rotation/abduction, although we did not observe as dramatic of a shift. All 4 loading conditions compared (Figures 3.16-3.23) had similar trends but had some differences in magnitude. Differences in magnitude may be explained by the presence of a different extraction torque, 3 Nm for our study compared to 5 Nm as seen in other studies, as well as the contribution of differences in loading rates between studies. The variation seen in the study was similarly large which highlights the need for the development of patient specific models of hip capsular function and lessens the applicability to population-based implant design/surgical approaches.

Our findings correspond and match to the current understanding of hip anatomy. The three main ligaments of the hip capsule ligamentous complex, the iliofemoral, ischiofemoral and pubofemoral, work conjointly to resist rotation in all 3 rotational DOF's. Our analysis of the iliofemoral ligaments elongation patterns confirms its role in preventing adduction as the fibers elongate and tighten in adduction. The lateral arm of the iliofemoral ligament demonstrated significantly greater strains than the medial arm due to the anatomic location of each respective ligament. This behavior correlates to its anatomical location as the lateral arm is located superior to the medial arm with most of its fibers aligned more closely to an adduction rotation. While the strains observed were significantly higher than previous strain measurement studies (Hewitt et al. 2002), this is most likely due to the behavior of the loading curve as the tissue is folded and providing minimal torque restraint during the neutral rotational displacement while the tissue unfolds, elongates and subsequently tightens to provide a torque response as the hip transitions into full adduction. The virtual extensometers provide valuable insight into the recruitment of ligament fibers and can be supplemented with other studies on the role of specific ligaments in providing rotational and distraction restraint (Martin et al. 2008, Myers et al. 2011; Smith et al. 2014; van Arkel et al., 2015a/b) to further define hip capsule properties and function.

We recognize certain limitations of this study. Actuator displacement limits prohibited characterizing the complete torque rotation space and impingement with fixtures prevented defining the torque rotation profile for the hip in full flexion. Although we increased the resolution of the torque rotation space by adding multi-axis

torque/displacement measurements in neutral and combined loading situations at 15° increments, tissue degradation time constraints limited complete exploration of the torque rotation space and necessitated faster loading rates than were ideal and used in previous ligament material property studies (Hewitt et al. 2001, Bigliani et al. 1992, Bigliani et al. 1996, Ticker et al. 1996). Due to the viscoelastic properties of the hip capsule soft tissue, we observed a large amount of hysteresis due to stress relaxation. Although we have presented a novel way to capture strain data of the anterior capsule using Digital Image Correlation, we experienced difficulties characterizing the full strain field primarily due to the folding and twisting of capsular tissue as it moved through the prescribed rotations. Previous studies have recognized the importance of characterizing the full strain field due to the multi-directionality of interwoven collagen fibers present in the hip capsule (Pieroh et al. 2016, Sato et al. 2012). Furthermore, our strain analysis was limited to the iliofemoral ligament and the anterior portion of the capsule. Future analysis should include characterization of the posterior capsule as well as this will strengthen the validation of Finite Element Analysis (FEA) models of the hip capsule. A more comprehensive analysis of hip stability that can be applied to *in vivo* function should also include other soft tissue stabilizers, fat and active stabilizers such as muscle tissue.

Future studies can leverage the data provided by this study to further explore the role of the hip capsule in THA, dislocation resistance and capsule repair strategies. A more sophisticated understanding of hip capsule function could lead to more robust implant designs and improved clinical outcomes.

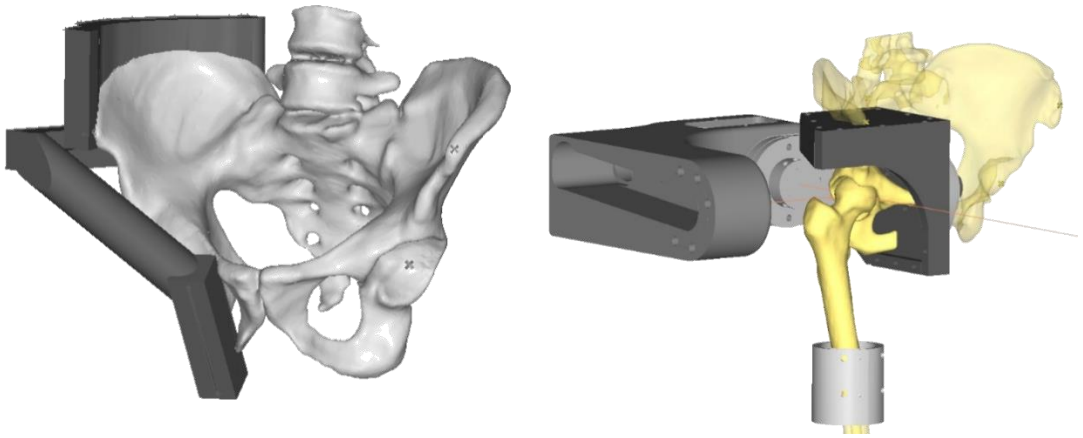

Figure 3.1: Custom resection guides (left) were 3D printed that attached to the iliac crest and pubis bone geometry and ensured the head/acetabulum centers were located at the center of rotation for all three anatomical axes in the fixtures (right).

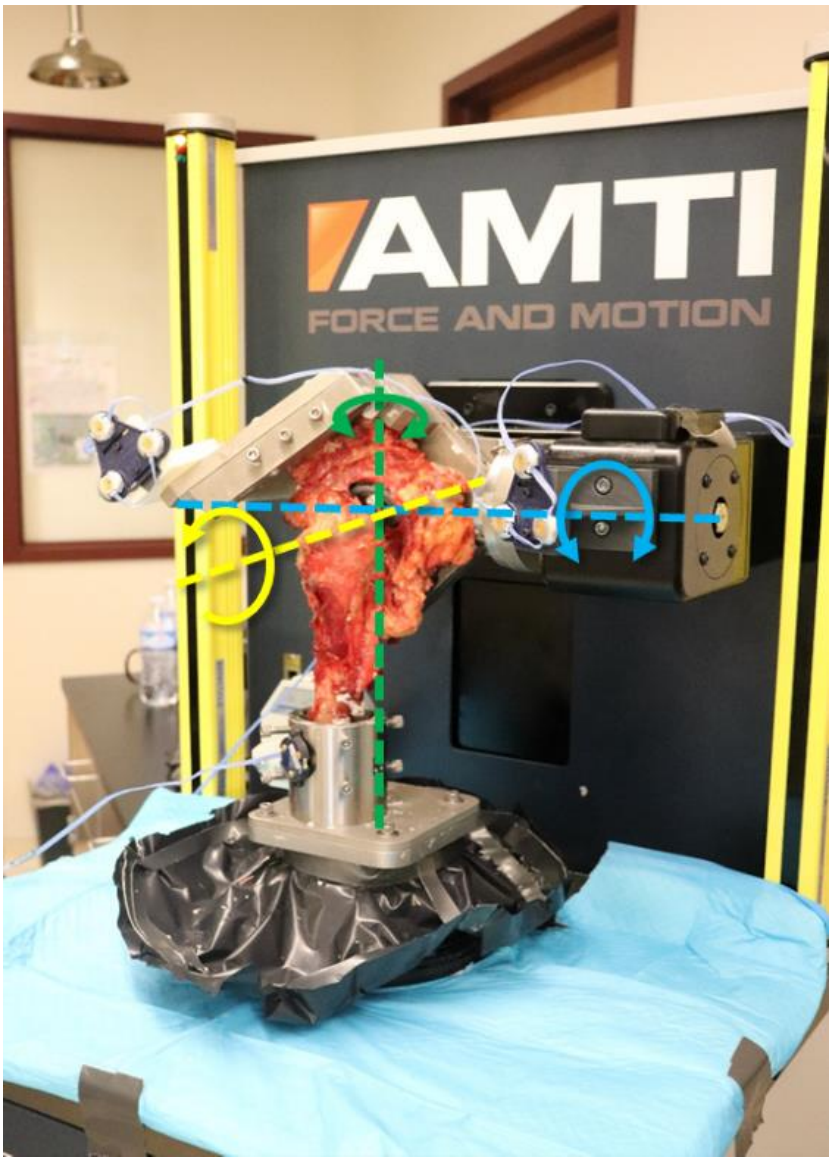

Figure 3.2: A specimen dissected down to the hip capsule cemented into custom fixtures and mounted into the VIVO joint motion simulator (AMTI, Watertown, MA). Primary axes of rotation flexion/extension (yellow), adduction/abduction (blue) and internal/external rotation (green) are labeled.

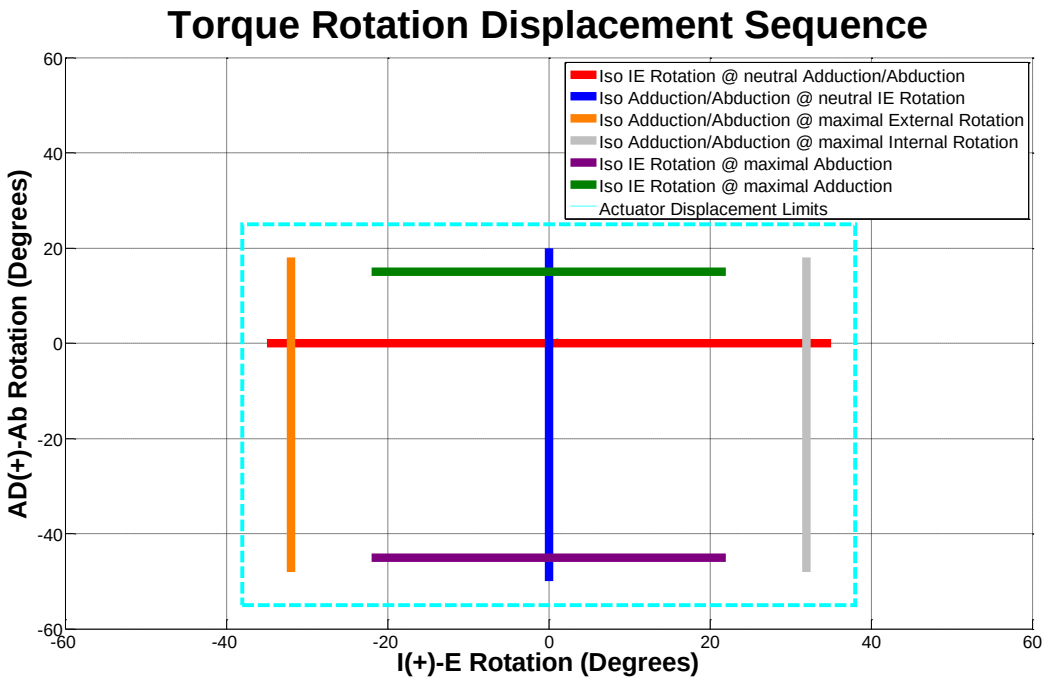

Figure 3.3: Sample laxity assessment sequence showing 1) Isolated adduction/abduction laxity at neutral internal/external rotation (blue) 2) Isolated internal/external rotation laxity at neutral adduction/abduction (red) 3) Isolated adduction/abduction laxity at maximal internal rotation (silver) 4) Isolated adduction/abduction laxity at maximal external rotation yellow) 5) Isolated internal/external rotation laxity at maximal abduction (purple) 6) Isolated internal/external rotation laxity at maximal adduction (green).

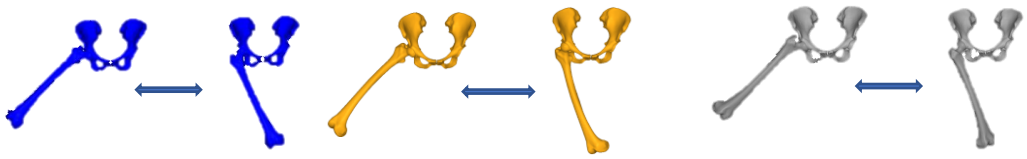

Figure 3.4: Isolated adduction/abduction laxity at neutral internal/external rotation (blue), isolated adduction/abduction laxity at maximal external rotation (orange) and isolated adduction/abduction laxity at maximal internal rotation (silver).

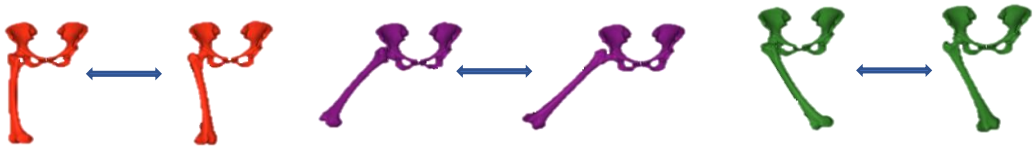

Figure 3.5: Isolated internal/external rotation laxity at neutral adduction/abduction (red), isolated internal/external rotation laxity at maximal abduction (purple), isolated internal/external rotation laxity at maximal adduction (green)

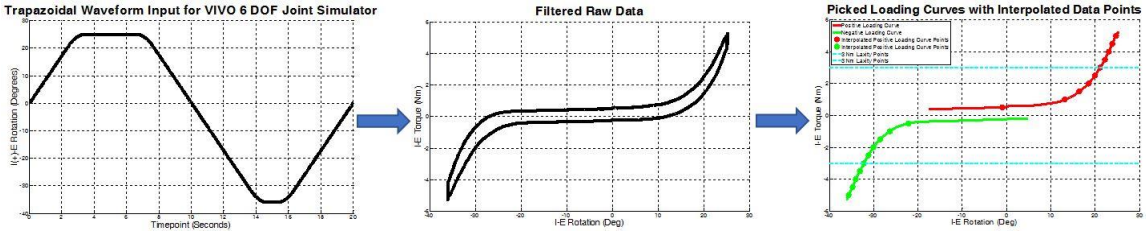

Figure 3.6: Sample trapezoidal displacement input (with constant displacement rate) into VIVO joint motion simulator for isolated axis of rotation (left), sample raw filtered data for isolated axis of rotation (middle) and positive and negative loading curves with extracted torque values (right).

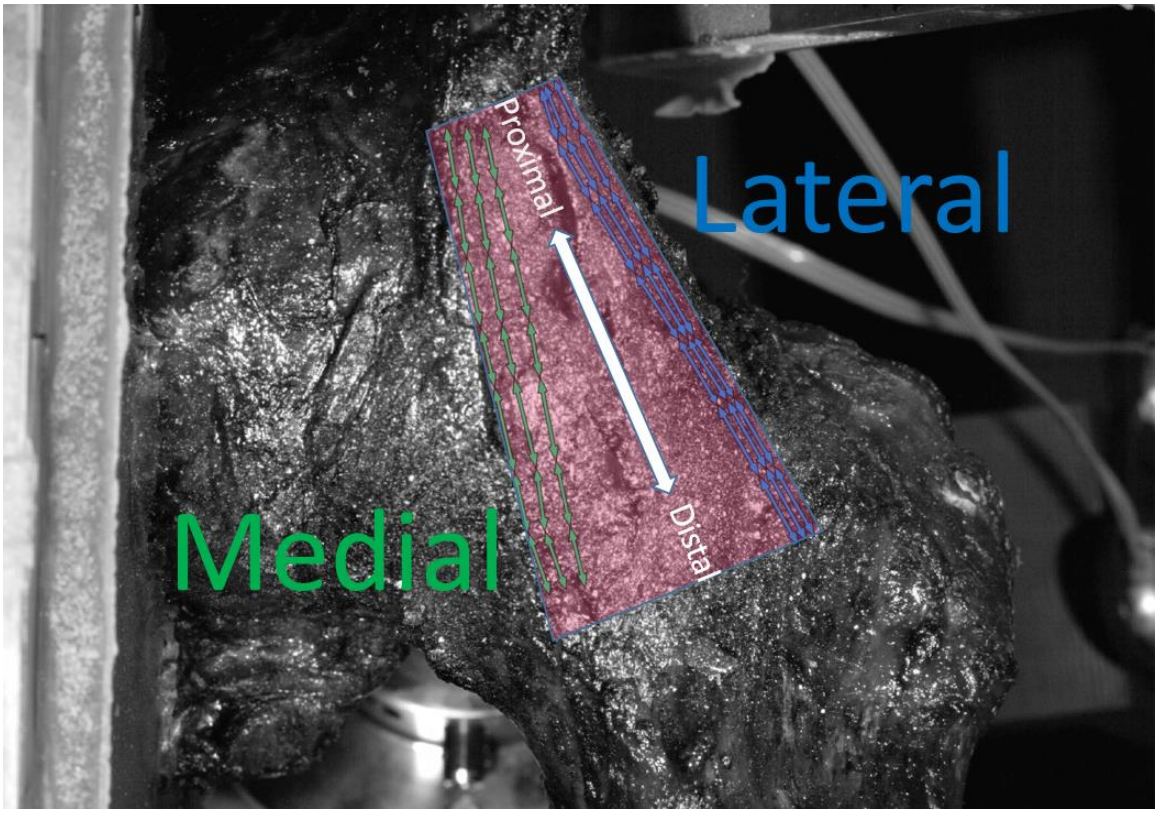

Figure 3.7: Groups of three extensometers in series oriented axially along the medial (green) and lateral (blue) arms of the iliofemoral ligament.

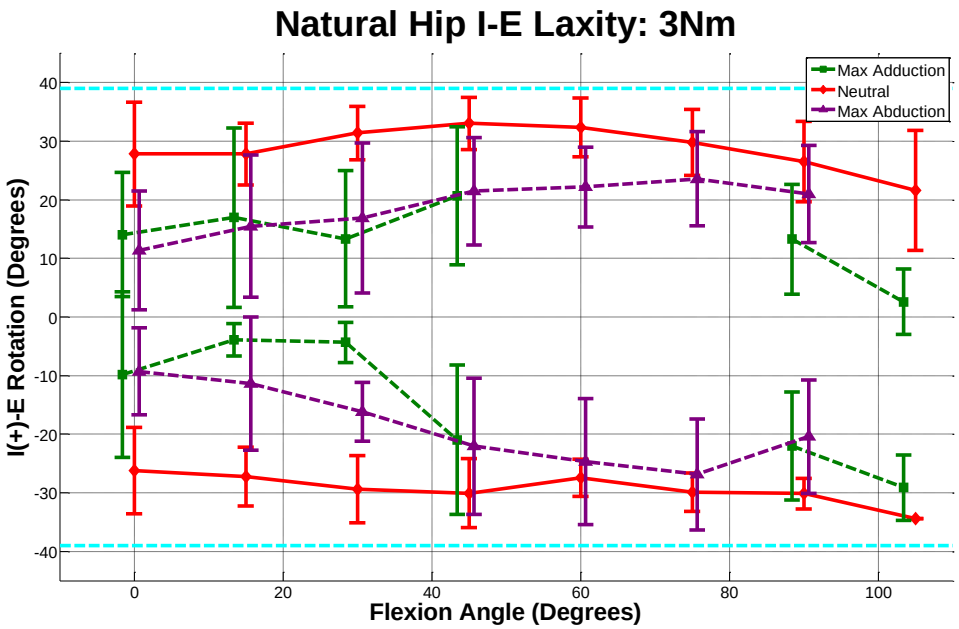

Figure 3.8: Internal/external rotation torque means and standard deviations outputs at each flexion angle for 3 Nm of isolated torque at neutral adduction/abduction (red), maximal adduction (purple), max abduction (green). Data gaps are indicative of where the displacement was outside of the VIVO actuator limits.

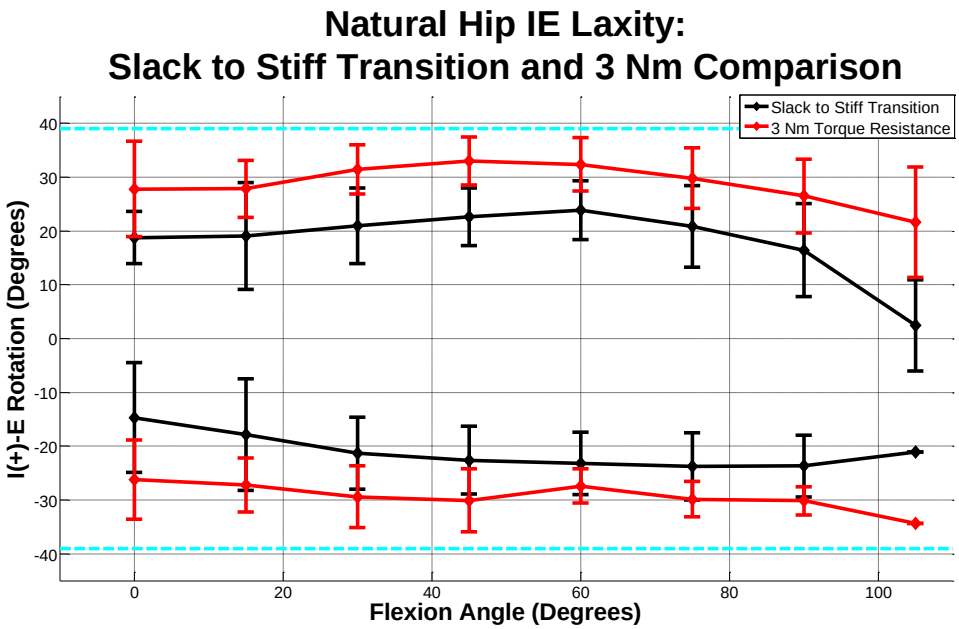

Figure 3.9: Internal/external rotation torque means and standard deviations outputs at neutral abduction/adduction each flexion angle for the slack to stiff transition points (black) and 3 Nm of torque resistance (red).

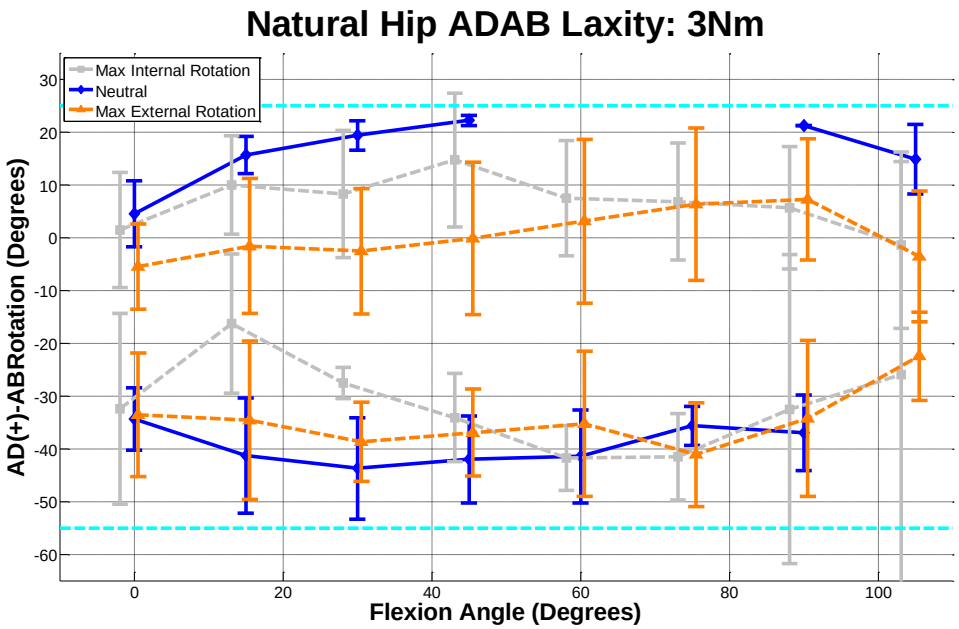

Figure 3.10: Abduction/adduction rotation torque means and standard deviations outputs at each flexion angle for 3 Nm of isolated torque at neutral internal/external rotation (blue), maximal internal rotation (silver), max external rotation (orange). Data gaps are indicative of where the displacement was outside of the VIVO actuator limits.

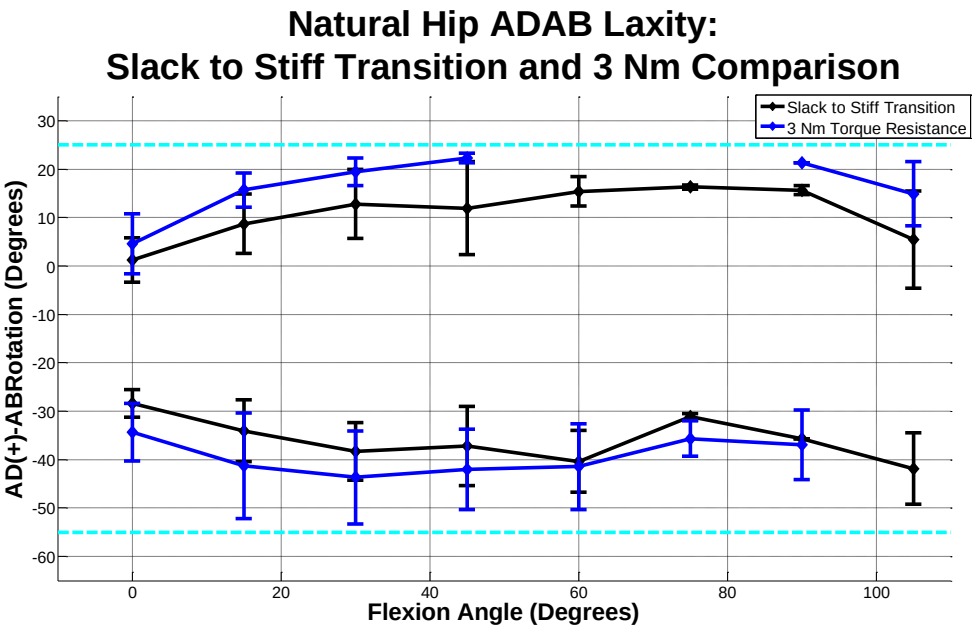

Figure 3.11: Abduction/adduction rotation torque means and standard deviations outputs at neutral internal/external rotation at each flexion angle for the slack to stiff transition points (black) and 3 Nm of torque resistance (blue).

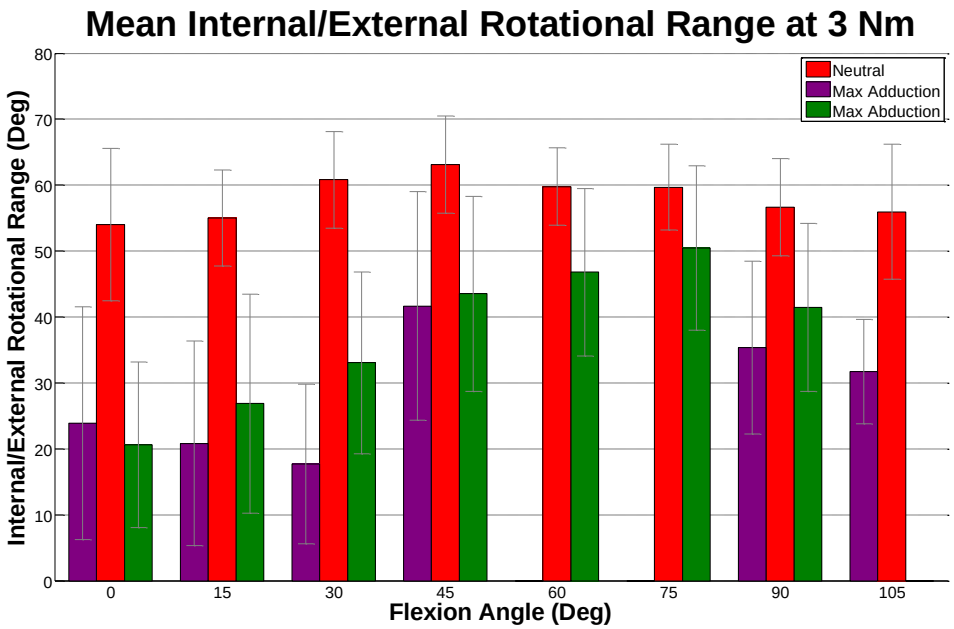

Figure 3.12: Internal/external rotational ROM at 3 Nm for each internal/external rotational laxity assessment.

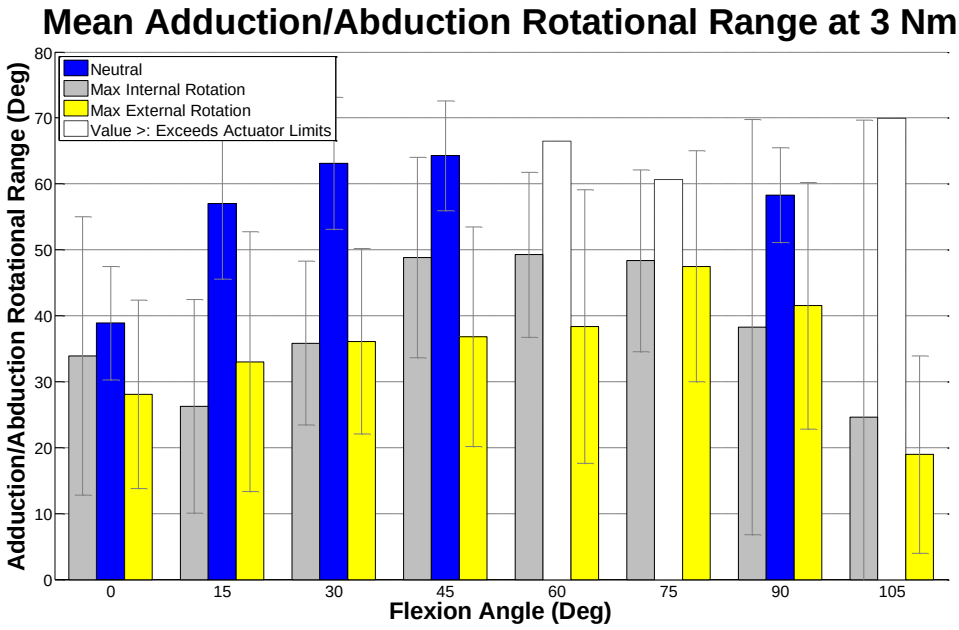

Figure 3.13: Abduction/adduction rotational ROM at 3 Nm for each abduction/adduction rotational laxity assessment.

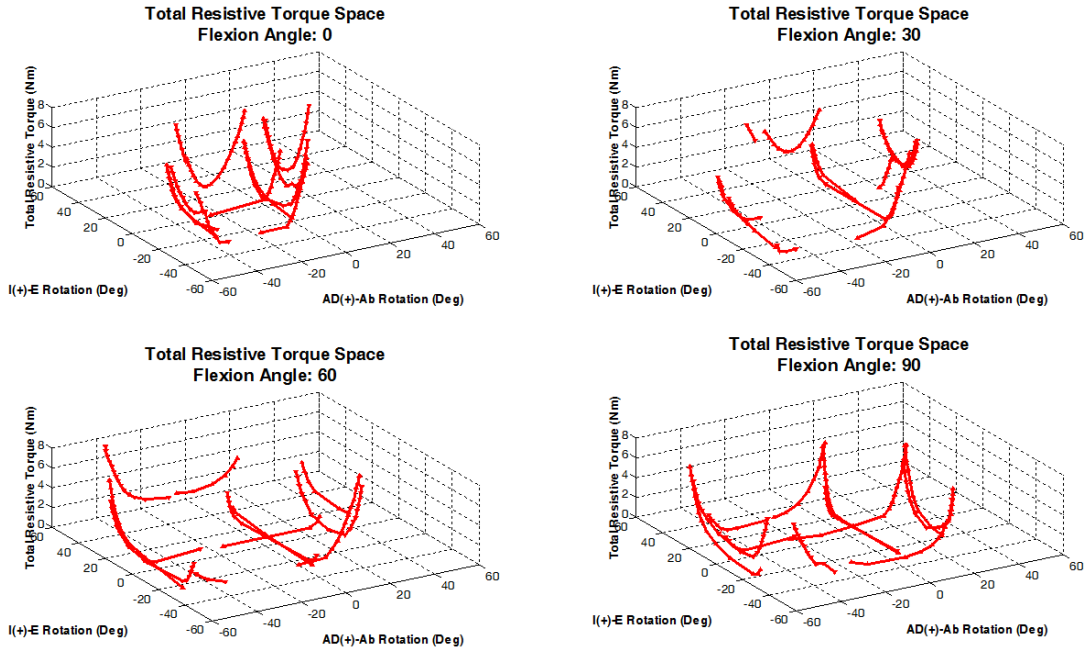

Figure 3.12: Total resistive torque space (calculated as the sum of the squares of the torque of each axis of rotation) at various flexion angles for one specimen for 0° (top right), 30° (top right), 60° (bottom left) and 90° (bottom right).

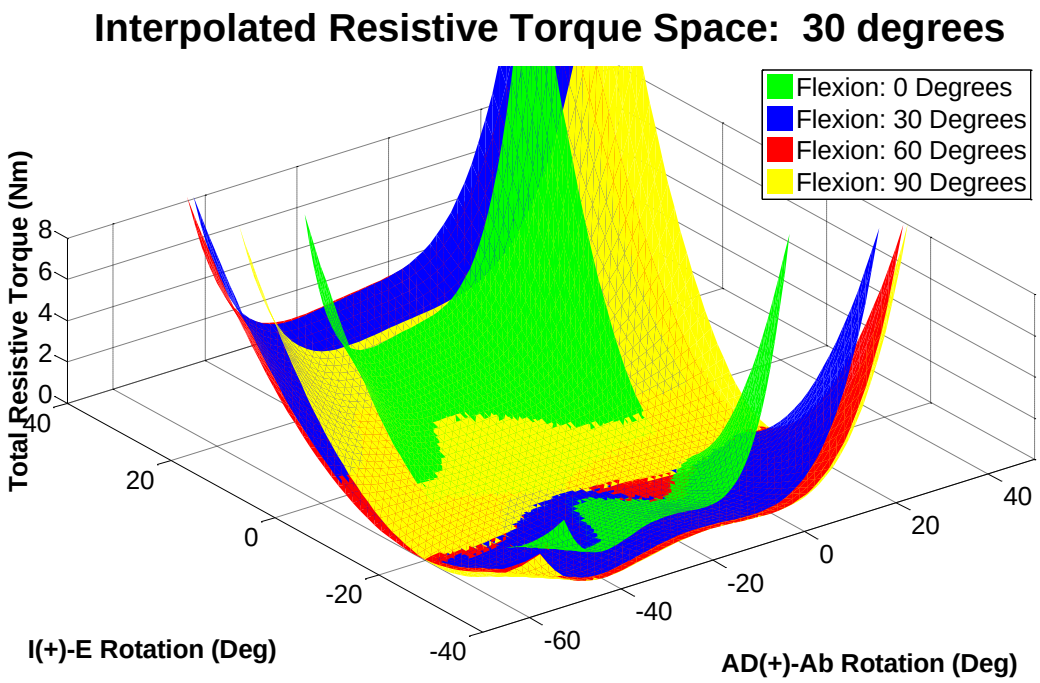

Figure 3.13: Interpolated total resistive torque space for one specimen for various flexion angles from 0° to 90°.

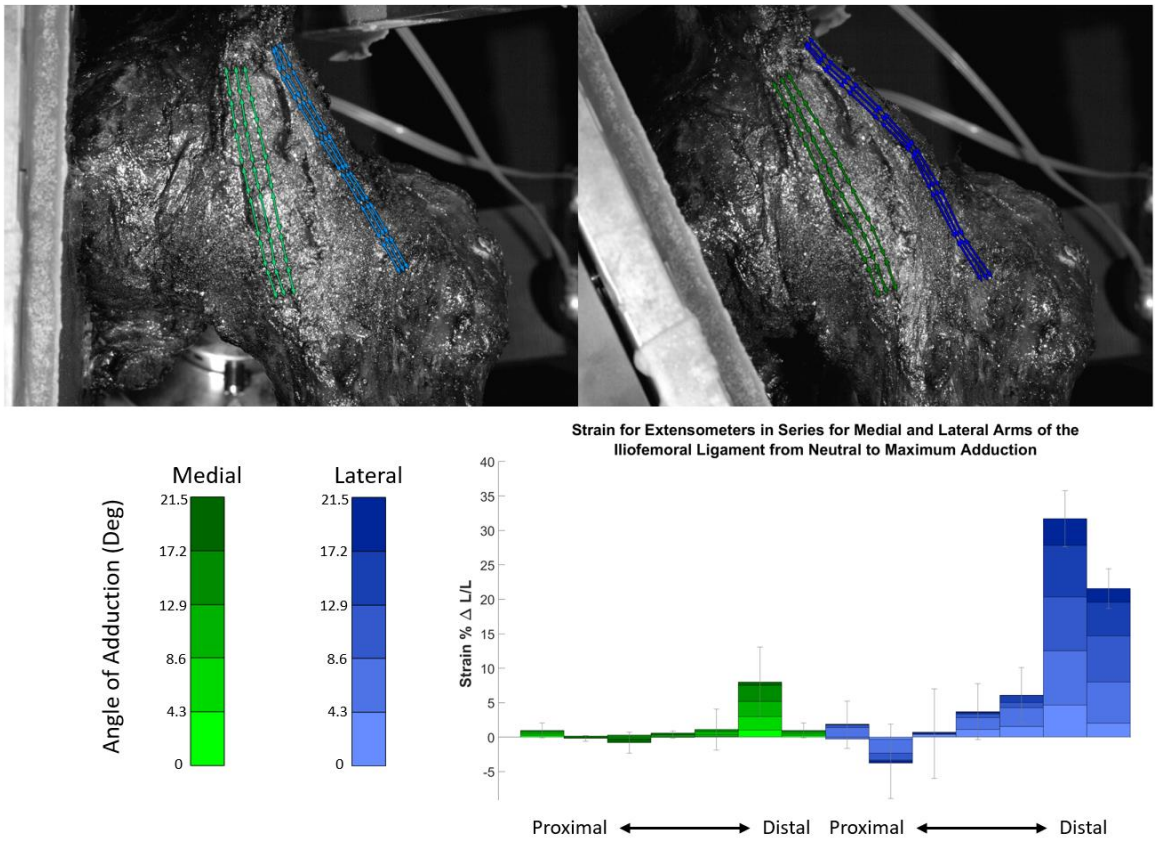

Figure 3.14: Groups of 3 virtual extensometers in series oriented axially along the fiber direction for the medial (green) and lateral (blue) arms of the iliofemoral ligaments at neutral abduction/adduction (top left) and full adduction (top right). Percent strain (Δ length/length) for each extensometer was calculated at evenly spaced intervals throughout the duration of the loading curve (bottom left). The strains for each transverse grouping of 3 extensometers from proximal to the pelvis to distal to the pelvis was averaged for each interval and is plotted above (bottom right).

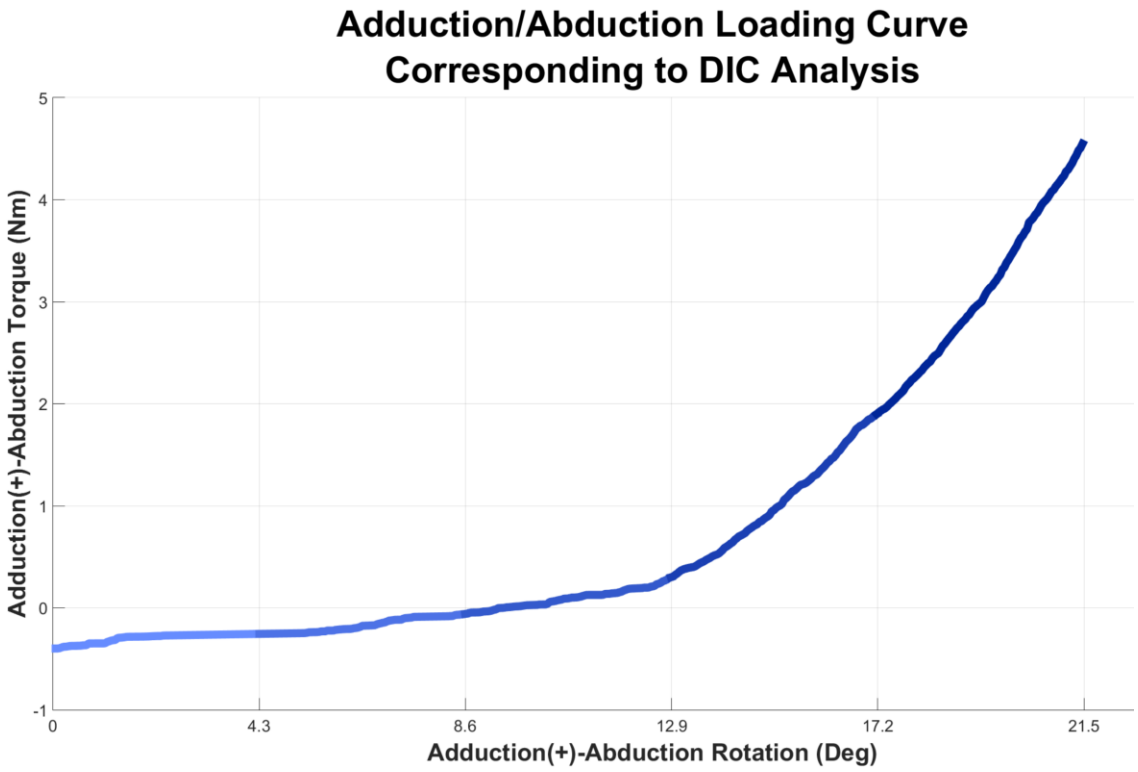

Figure 3.15: Loading curve from neutral (light blue) to full adduction (purple) with intervals shown in which strain from DIC measurements was calculated.

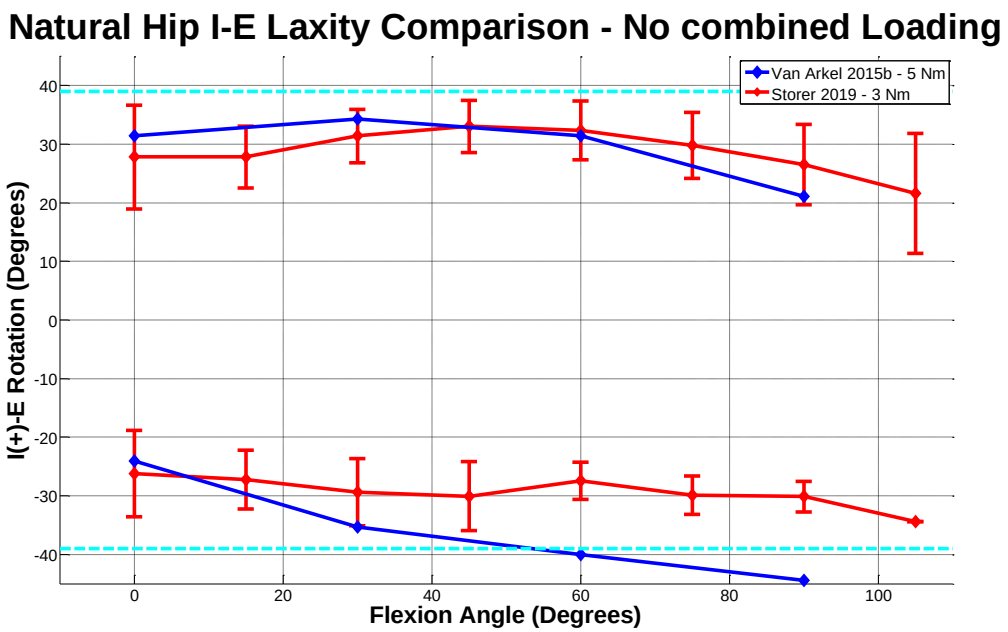

Figure 3.16: Comparison of results for internal/external rotation at neutral abduction/adduction between van Arkel et al 2015b (blue) and the results of this thesis (red).

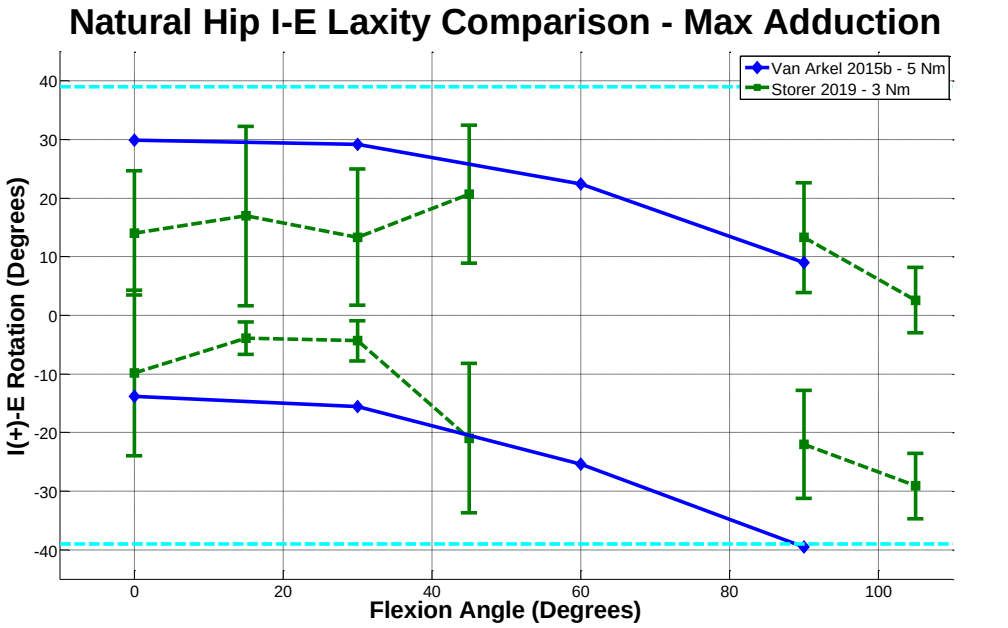

Figure 3.17: Comparison of results for internal/external rotation at maximal adduction between van Arkel et al 2015b (blue) and the results of this thesis (green).

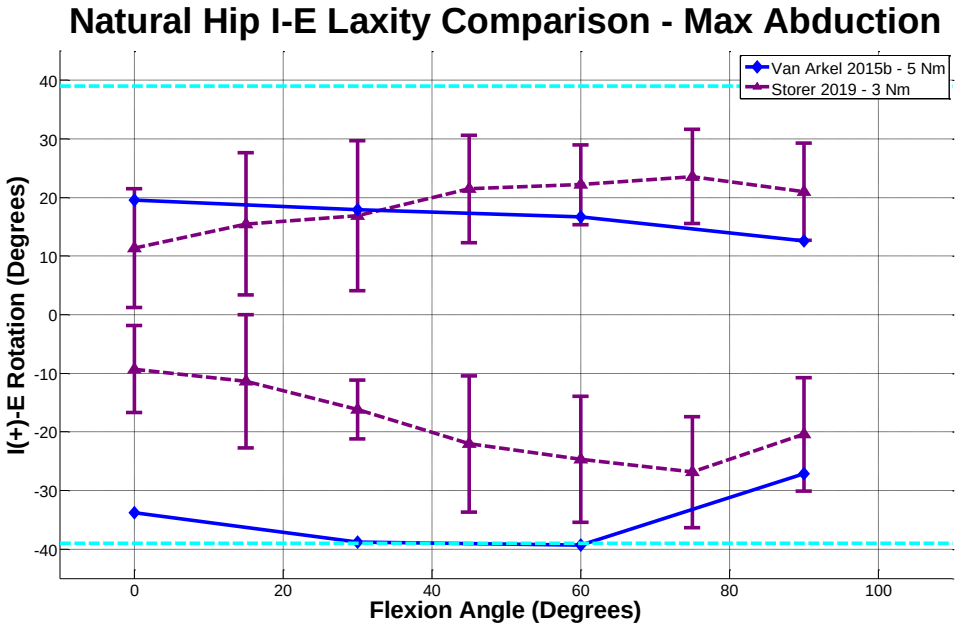

Figure 3.18: Comparison of results for internal/external rotation at maximal abduction between van Arkel et al 2015b (blue) and the results of this thesis (purple).

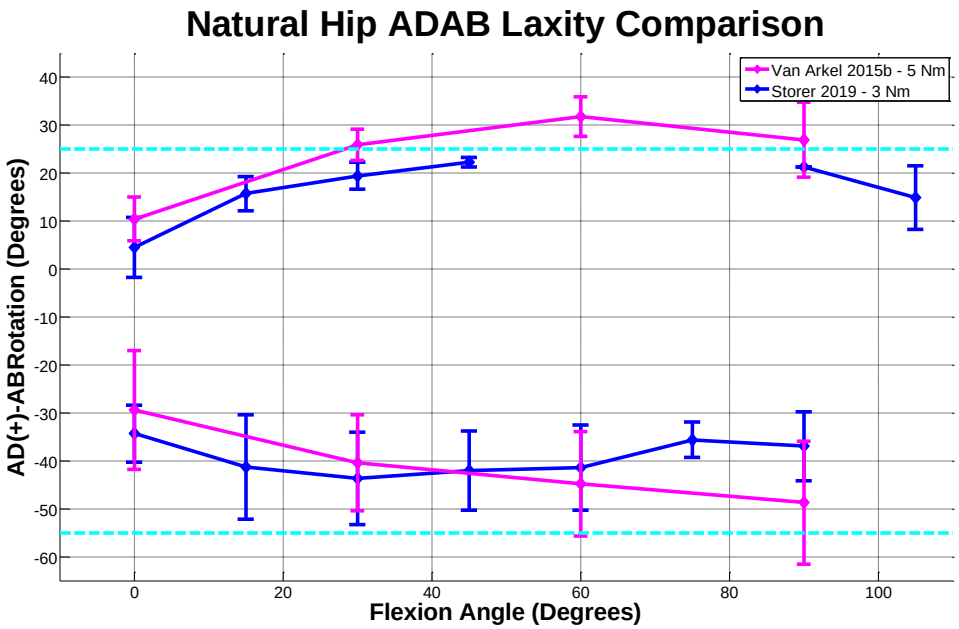

Figure 3.19: Comparison of results for adduction/abduction at neutral internal/external rotation between van Arkel et al 2015b (magenta) and the results of this thesis (blue).

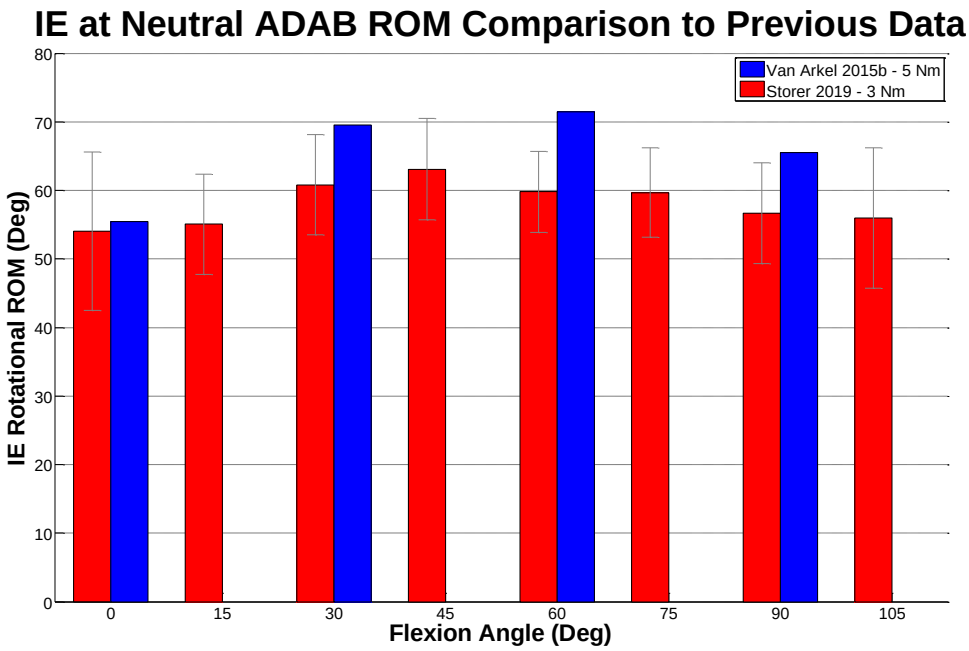

Figure 3.20: Comparison of results for internal/external rotation ROM at neutral abduction/adduction between van Arkel et al 2015b (blue) and the results of this thesis (red).

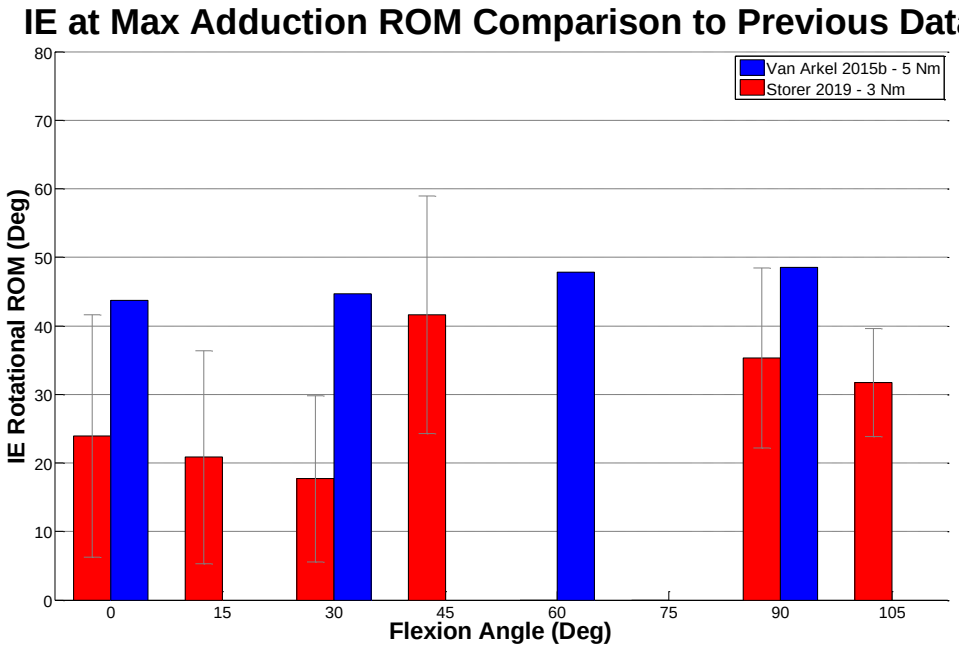

Figure 3.21: Comparison of results for internal/external rotation ROM at maximal adduction between van Arkel et al 2015b (blue) and the results of this thesis (red).

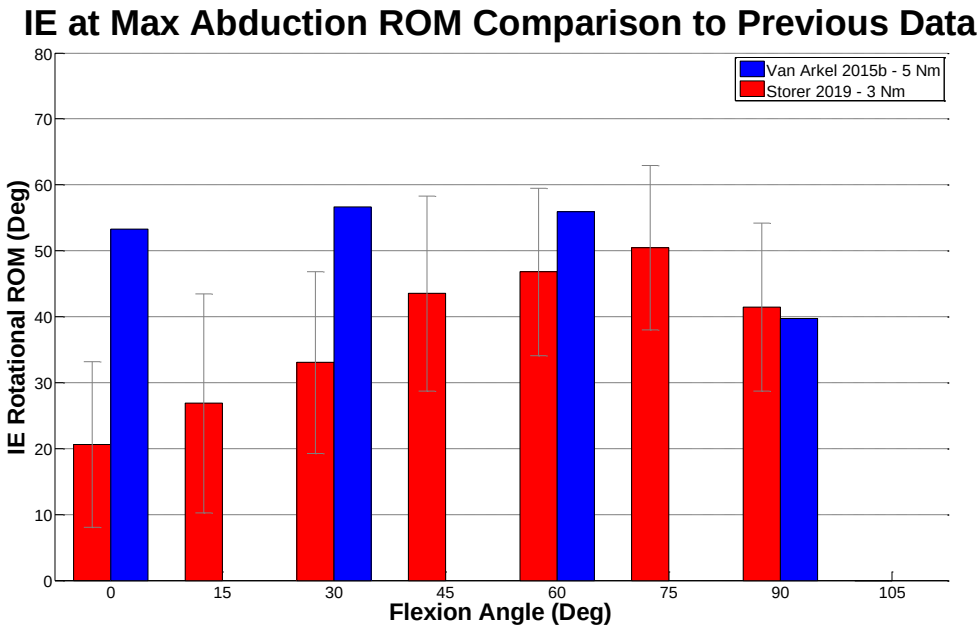

Figure 3.22: Comparison of results for internal/external rotation at maximal abduction between van Arkel et al 2015b (blue) and the results of this thesis (red).

.

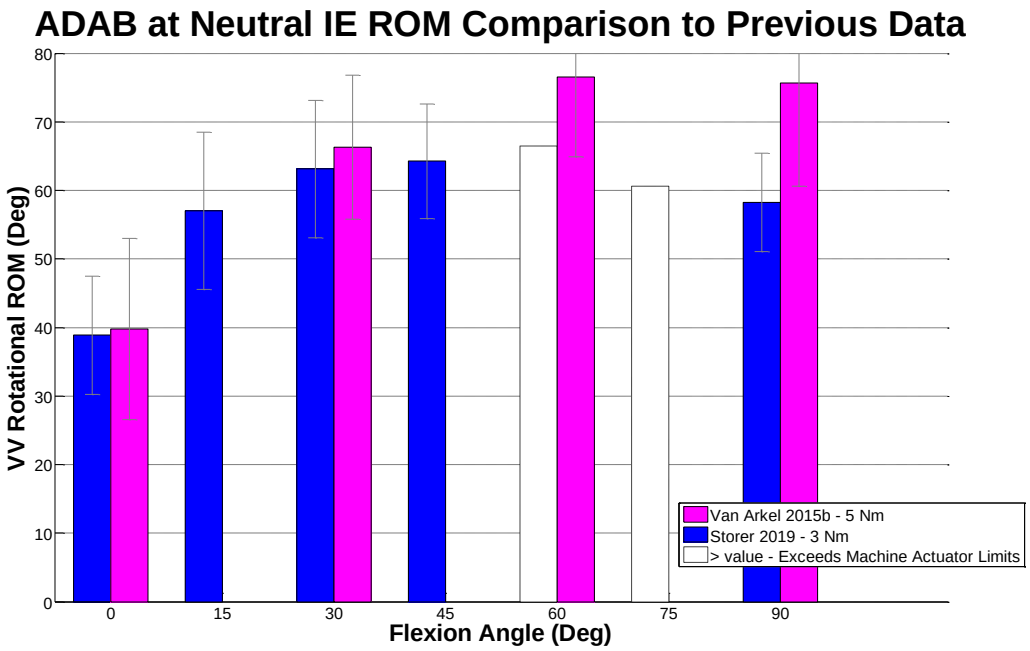

Figure 3.23: Comparison of results for adduction/abduction at neutral internal/external rotation between van Arkel et al 2015b (magenta) and the results of this thesis (blue).

CHAPTER 4. COMPARISON OF LAXITY BETWEEN NATURAL AND IMPLANTED HIPS

4.1 Introduction

The prevalence of THA in the U.S. (the percentage of the population who has received a THR) is 0.83% or 2.5 million people (Kremers 2015). Due to a rapidly aging population, this number is expected to increase substantially in the coming decades (Jafari et al. 2010). While THA has a relatively high success rate, revision procedures are sometimes necessary at an increased cost compared to primary THA which presents a huge strain on the hospitals and the healthcare system (Crowe et al. 2003) as well as patients with the second leading cause of revision surgery being instability/dislocation (Jafari et al. 2010). As THA necessitates resection of the hip capsule in order to gain access to the femoral head and acetabulum for further resection and insertion of THR components, it is unclear how various surgical approaches alter capsular laxity and thus hip stability. The purpose of this study is to compare the laxity differences between natural to posteriorly implanted hips

4.2 Methods

An experienced board approved surgeon performed a posterior approach THA on 6 specimens (Mean age 70 years old, range 19 years, STD 9.2 years) as shown in Table 4.1. The selection criteria was consistent for natural and implanted specimens and specimens chosen for implantation were selected at random. A Pinnacle cup and Summit stem (DePuy Synthes, Warsaw, IN) (Figure 4.2) were implanted. Right hips were implanted with a lipped acetabular component and left hips with a neutral acetabular component. A substantial capsulotomy with a large part of the posterior capsule removed (Figure 4.1) was performed by the surgeon as part of his preferred surgical technique. The same protocol as detailed in section 3.2 was followed for specimen preparation and mounting into the VIVO 6 DOF joint motion simulator for testing. All 6 laxity assessments and data analysis (except for DIC) as described in section 3.2 were performed. Because the flexion/extension laxity profile was dramatically different as compared to the natural specimens, only a subset of flexion increments (varied across specimens, at most 30° to 105°, at least 60° to 90°) was able to be completed. ROM at 3 Nm as well as percent difference was compared for each laxity assessment between natural and implanted specimens.

4.3 Results

Substantial differences in the flexion/extension range of motion between implanted and natural specimens was observed. There was a dramatic shift toward flexion in the angle of full extension in the implanted hips, as large as 60° in some

specimens. The isolated internal/external rotation and isolated abduction/adduction for each assessment condition for implanted specimens are shown in Figures 4.3 and 4.4. External rotation for implanted specimens matched up well with natural data. In contrast, in mid-flexion none of the implanted specimens reached the internal rotation 3 Nm torque limit at neutral abduction/adduction prior to exceeding the rotational limits of the simulator, demonstrating a dramatic increase in internal rotational laxity. The mean abduction/adduction laxity ROM at neutral internal/external rotation appeared to be reduced compared to natural specimens, although not to a statistically significant degree. The combined loading conditions also reflected a significantly altered laxity profile as the adduction/abduction ROM at maximum internal rotation was increased (as much as 65%) in implanted specimens compared to natural. Internal/external rotation ROM at maximum abduction was decreased in implanted specimens reflecting the effect of a decreased abduction/adduction ROM. In addition, the stability of the implanted specimens was noticeably compromised as we observed several inadvertent dislocations throughout the testing process. There was no statistically significant difference observed between the lipped and neutral acetabular components. Overall variability in the implanted specimens was extremely large making robust comparisons difficult.

4.4 Discussion

The most significant findings from this study were the altered flexion/extension range of motion, the lack of internal rotation torque resistance and decreased abduction/adduction ROM in the implanted hips, although we urge caution when making

conclusions from this study due to the large variability of the results and the flexion laxity changes present after THA. The lack of internal torque resistance fits in well with a current understanding of capsular anatomy and function. The posterior approach chosen by the surgeon resulted in a capsulectomy which involved an excision of a large portion of the posterior capsule which primarily consists of the ischiofemoral ligament (Bedi et al. 2011). Prior research has indicated the importance of the iliofemoral ligament in preventing excessive internal rotation (Martin et al. 2008, van Arkel et al. 2015a) which we observed as well. Furthermore, the posterior approach preserves the iliofemoral ligament which has been observed to be one of the main restrictors of external rotation (Martin et al. 2008, Myers et al. 2011). The external rotation displacement limits in posterior specimens were consistent with those of natural specimens confirming prior findings.

The causes of stability and capsular laxity changes following THA are complex and due to many factors including surgical approach, technique and capsular management (Domb et al. 2013, Ekhtiari et al. 2017), orientation and placement of THA components (Barrack 2003), and component size and design such as femoral neck length and head size (van Arkel et al. 2018). As a result, it is difficult to make strong conclusions on the precise cause of the large differences observed in this study. Further exploration to control for the large number of variables affecting capsular laxity changes are needed. In addition, in a THR patient, other soft tissue stabilizers such as skin and fat and active stabilizers such as muscle contribute to hip joint stability. Future studies can build upon this work by investigating the role of surgical technique and training, anatomical

approach, THR component design and capsular repair and management, as well as inter-subject variability. The current study is a strong and useful pilot study that points to the benefit of further research into the aforementioned areas.

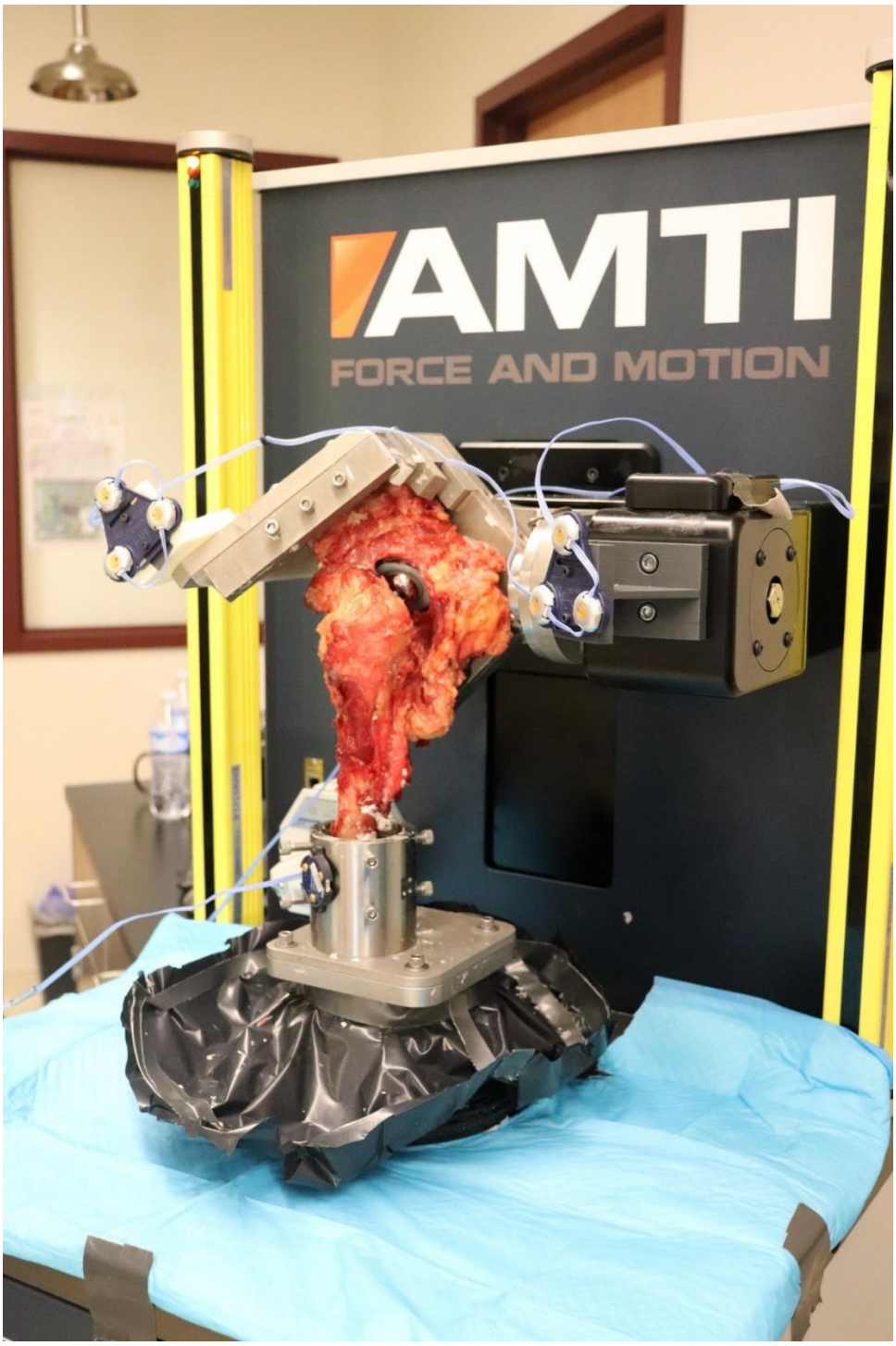

Figure 4.1: A posteriorly-approach implanted Total Hip Replacement (THR) with a pinnacle cup and summit stem mounted into the AMTI VIVO (DePuy Synthes, Warsaw, IN).

Figure 4.2: A summit stem (top left) (DePuy Synthes, Warsaw, IN). A summit stem with a pinnacle cup (top right) (DePuy Synthes, Warsaw, IN). A cementless pinnacle cup (bottom) (DePuy Synthes, Warsaw, IN)

Natural Specimens	Implanted Specimens – Lipped Acetabulum	Implanted Specimens – Neutral Acetabulum
S171645 (Right and Left)	S171455 (Right)	S171455 (Left)
S171562 (Right and Left)	S171613 (Right)	S171613 (Left)
S171618 (Right and Left)	S171624 (Right)	S171624 (Left)
S182484 (Right and Left)	N/A	N/A
S182590 (Right and Left)	N/A	N/A

Table 4.1: Cadaveric specimens tested in the study.

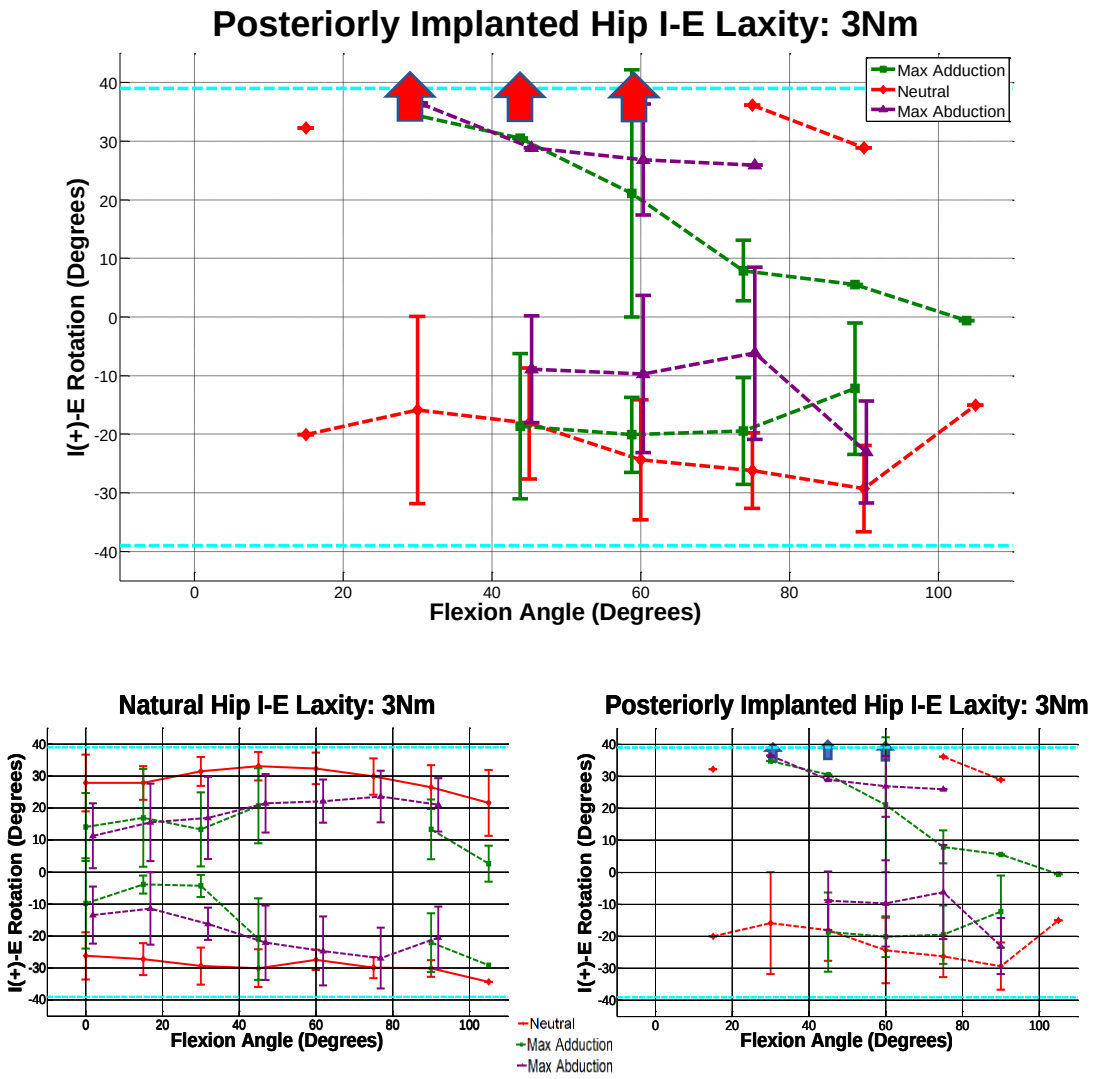

Figure 4.3: Internal/external rotation torque means and standard deviations outputs at each flexion angle for neutral adduction/abduction (red), maximal adduction (purple), max abduction (green) for implanted specimen (top). Comparison between natural and implanted specimens (bottom).

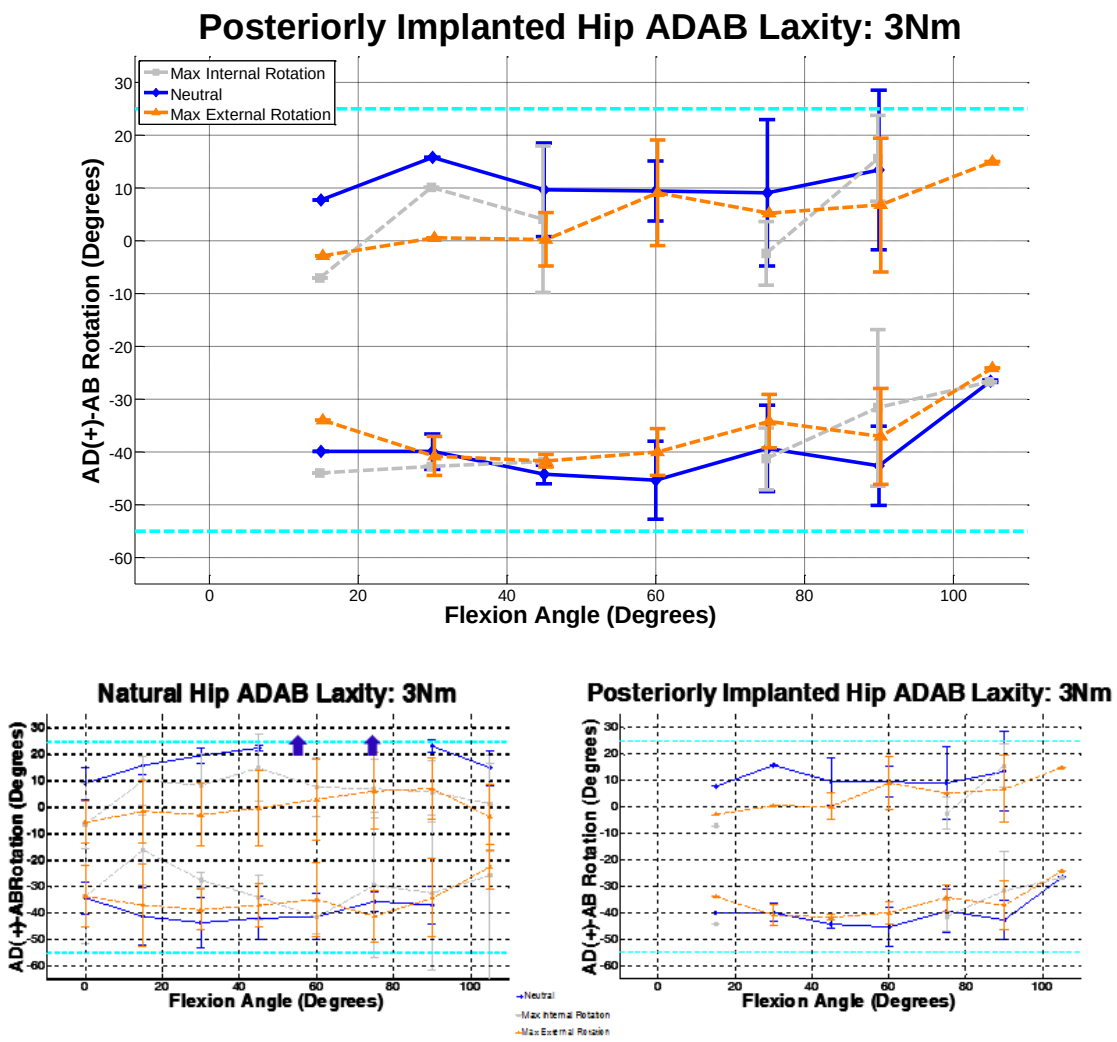

Figure 4.4: Abduction/adduction rotation torque means and standard deviations outputs at each flexion angle for neutral internal/external rotation (blue), maximal internal rotation (silver), max external rotation (yellow) (top). Comparison between natural and implanted specimens (bottom)

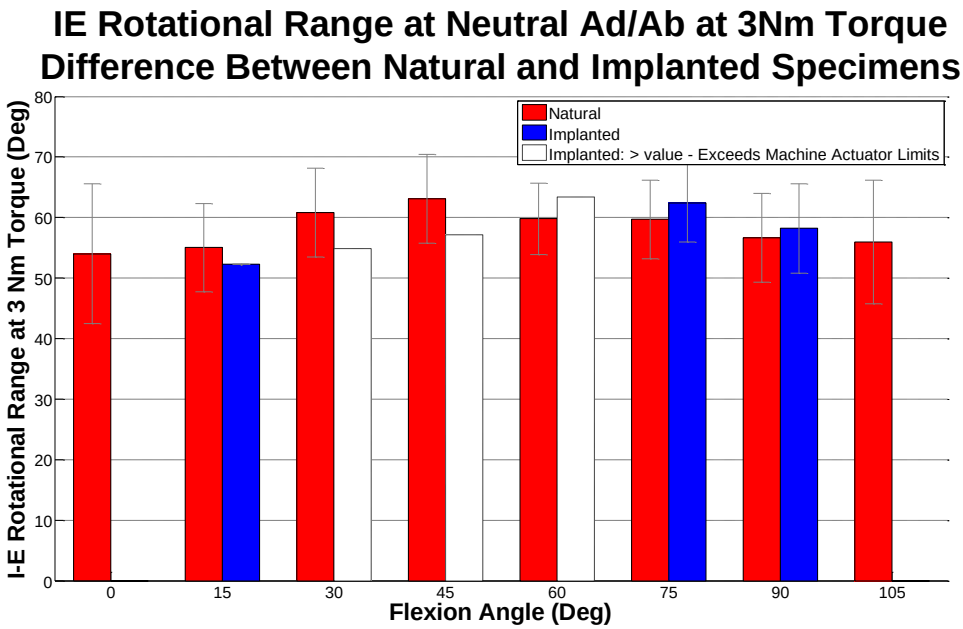

Figure 4.5: Internal/external rotational range (ROM) at neutral adduction/abduction at 3 Nm for natural (red) and posteriorly implanted (blue) specimens.

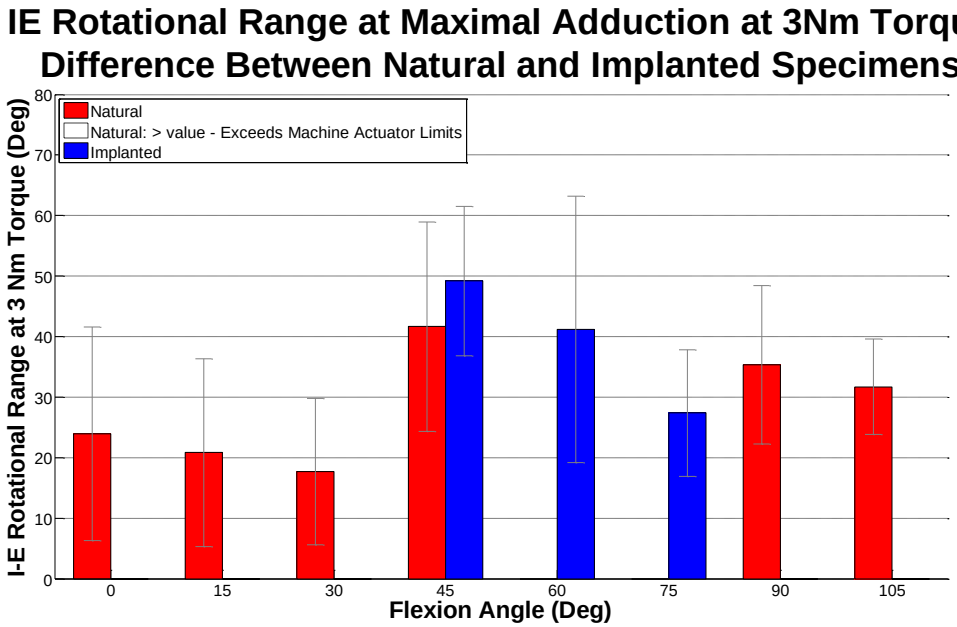

Figure 4.6: Internal/external rotational range (ROM) at maximal adduction at 3 Nm for natural (red) and posteriorly implanted (blue) specimens.

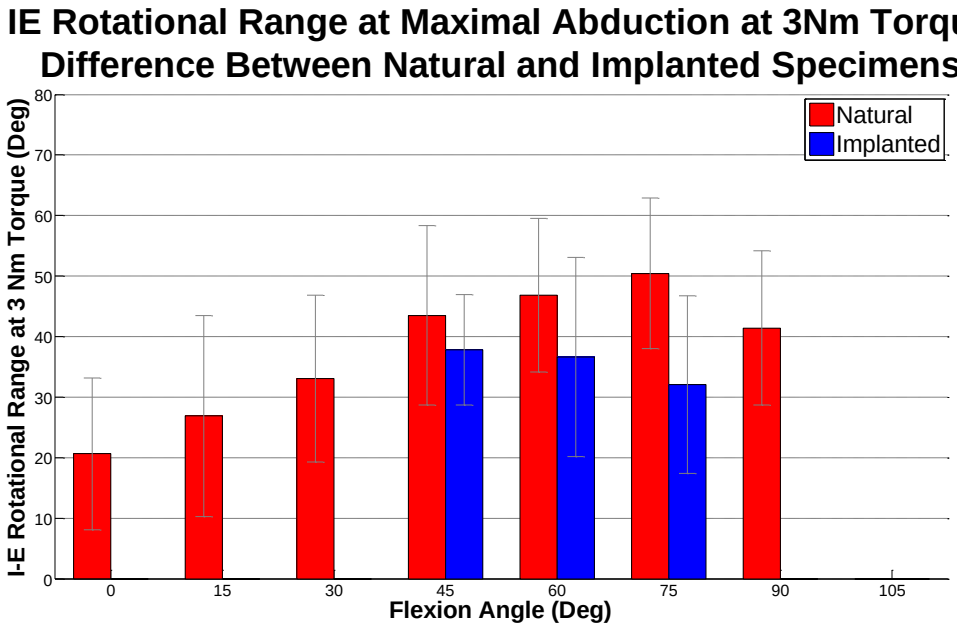

Figure 4.7: Internal/external rotational range (ROM) at maximal abduction at 3 Nm for natural (red) and posteriorly (blue) implanted specimens.

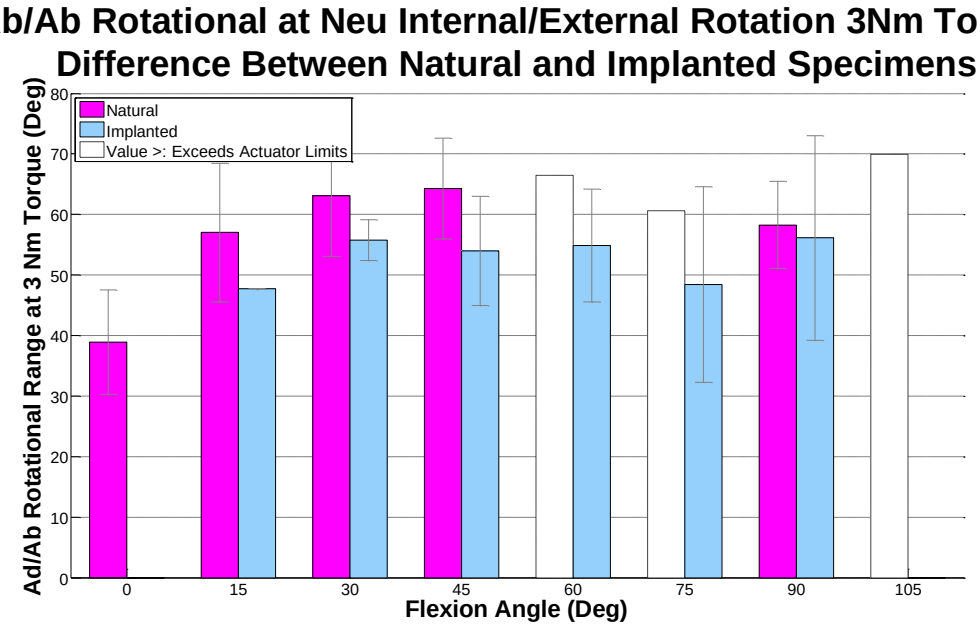

Figure 4.8: Adduction/abduction rotational range (ROM) at neutral internal/external rotation at 3 Nm for natural (pink) and posteriorly (blue) implanted specimens.

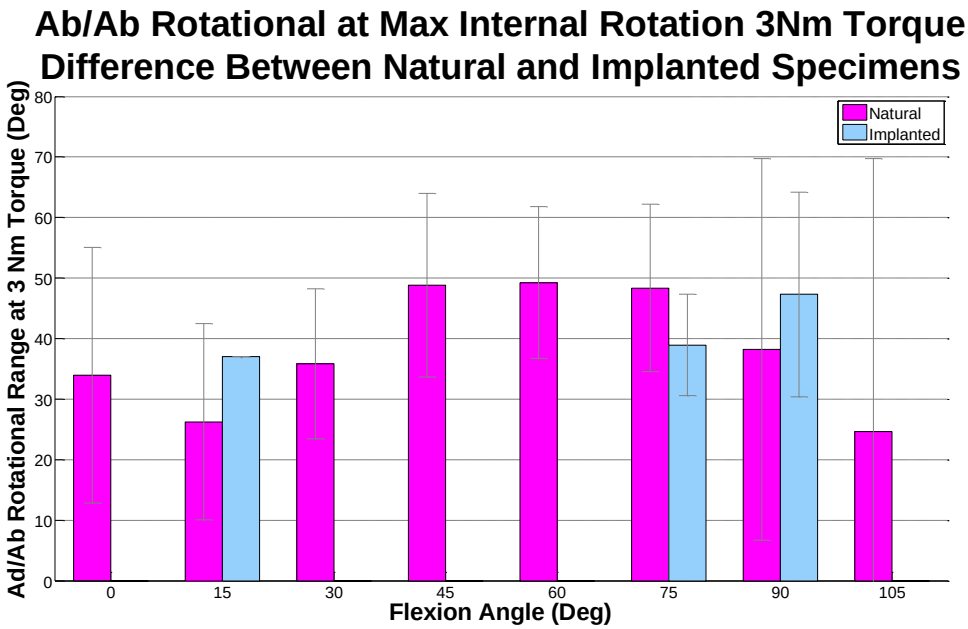

Figure 4.9: Adduction/abduction rotational range (ROM) at maximal internal rotation at 3 Nm for natural (pink) and posteriorly implanted (blue) specimens.

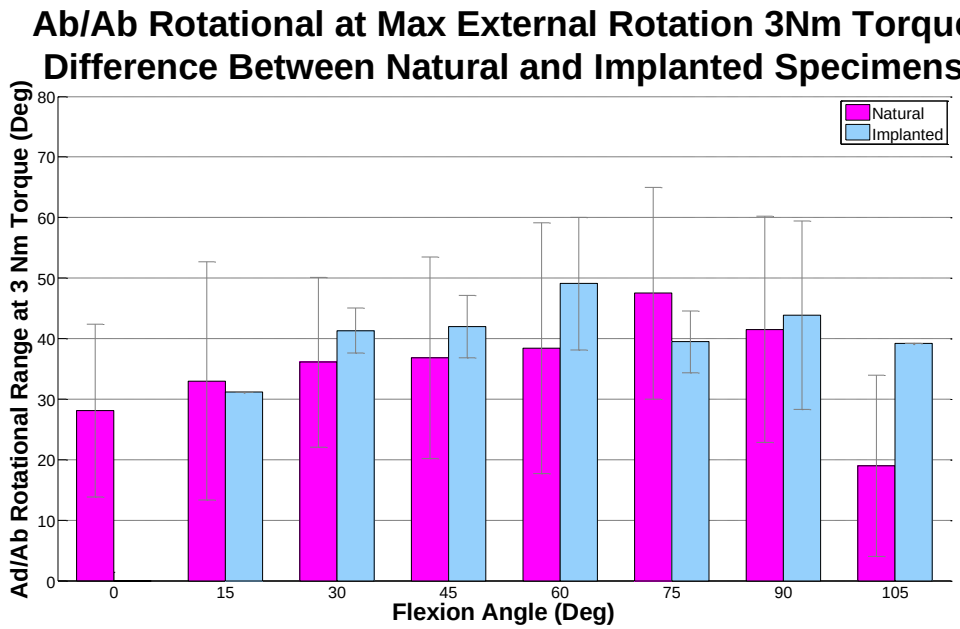

Figure 4.10: Adduction/abduction rotational range (ROM) at maximal external rotation at 3 Nm for natural (pink) and posteriorly implanted (blue) specimens.

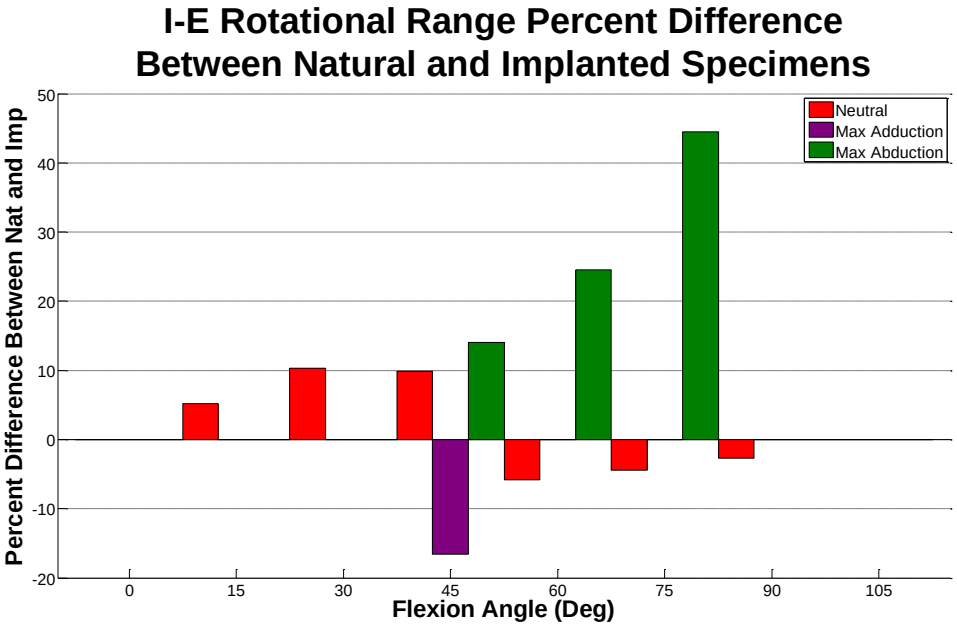

Figure 4.11: Internal/external rotational ROM Percent difference between natural and implanted specimens at neutral adduction/abduction (red), maximal adduction (purple) and maximal abduction (green).

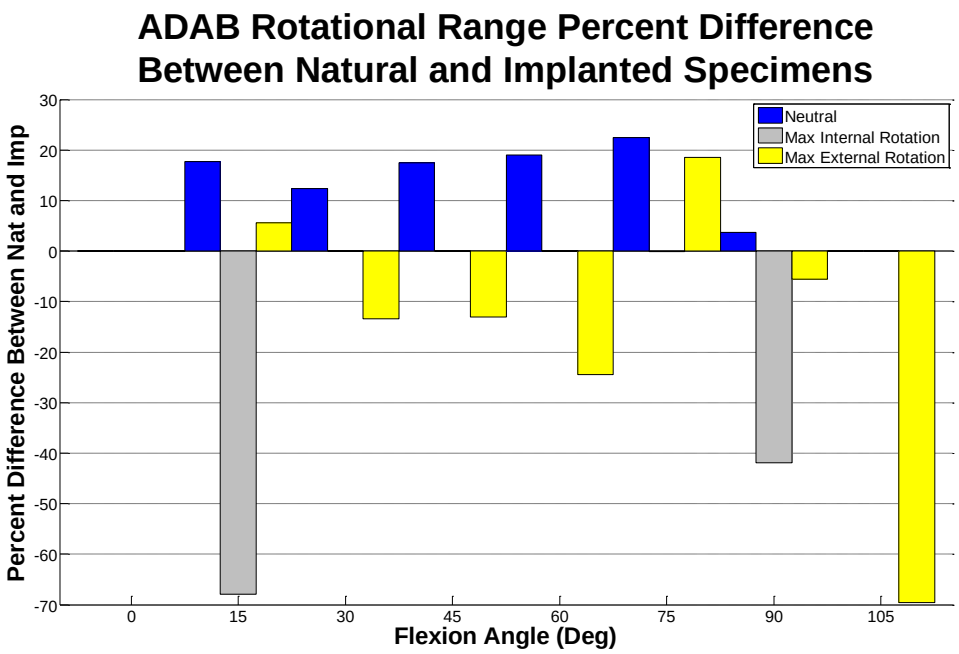

Figure 4.12: Abduction/adduction rotational ROM Percent difference between natural and implanted specimens at neutral internal/external rotation (blue), maximal internal rotation (silver) and maximal external rotation (yellow).

CHAPTER 5. CONCLUSIONS AND RECOMMENDATIONS

5.1 Key Findings

The work presented in this thesis adds to the base of knowledge in orthopedics research by characterizing and quantifying capsular laxity and restraint *in vitro*. As hip arthroplasty procedures become more common, understanding hip capsule properties is important in optimizing the efficacy of surgical procedures and implant designs in order to improve patient outcomes.

As delineated in chapter 2, previous investigations into hip capsular properties and laxity *in vitro* have resulted in increased understanding of hip capsule material properties, internal/external rotation capsular restrain boundaries and ligament function. Early experimental methods were hampered by limited DOF and lack of tissue strain measurement capabilities as well as a lack of exploration into the effects of hip arthroplasty. This thesis addresses those shortcomings by utilizing the current 'gold standard' for joint research, a 6 DOF robotic testing rig capable of displacement and load control, state-of-the-art imaging analysis software to measure tissue deformation as demonstrated in chapter 3 and a comparison between natural and implanted specimens as

explained in chapter 4. The most interesting results included the large amount of unfolding of tissue indicating large strain as seen in digital image correlation results in chapter 3 and the large differences in laxity between natural and implanted specimens in chapter 4. Work is currently underway utilizing these test methods and improved fixtures to quantify hip dislocation parameters for a modular dual-mobility THR and the effect of capsular repair using various types of sutures on capsular stability.

5.2 Limitations and Future Work

This study had several limitations that can be addressed in future studies. Impingement of tissue and actuator displacement limits prohibited full characterization of the torque rotation space, primarily in natural specimens. Loading rates were not optimized and as a result large amounts of hysteresis were observed. There were also difficulties with strain field quantification by Digital Image Correlation and the complexity of capsule anatomy and ancillary soft tissue/fat made method consistency challenging. The use of cadaveric tissue also presents problems when applying results to make *in vivo* conclusions about hip stability and function as tissue properties may change due to death and exposure as well as the lack of active stabilizers such as muscles.

There are many routes future work could go to expand upon and improve experimental results to obtain more clinically meaningful data. The large variability in data necessitates the use of patient-specific computational models. The authors recommendation for future experiments is to control for the large number of variables present in THA including surgical technique and approach (which can vary dramatically

between surgeons), device design and implantation and to verify existing FEA models using the obtained experimental design. Hopefully this leads to improved implant designs by load analysis taken by the capsule that can be offset by component design, improved surgical plans that can allow doctors to make the optimal capsule resections, and improved patient satisfaction by allowing them to return to pain-free living as soon as possible.

BIBLIOGRAPHY

Barrack, R. L. (2003). Dislocation after total hip arthroplasty: implant design and orientation. JAAOS-Journal of the American Academy of Orthopaedic Surgeons, 11(2), 89-99.

Banaszkiewicz, P. A. (2014). Dislocations After Total Hip-Replacement Arthroplasties. In Classic Papers in Orthopaedics (pp. 113-115). Springer, London.

Banaszkiewicz, P. A. (2014). Porous-coated hip replacement. The factors governing bone ingrowth, stress shielding, and clinical results. In Classic papers in orthopaedics (pp. 51-55). Springer, London.

Bedi, A., Galano, G., Walsh, C., & Kelly, B. T. (2011). Capsular management during hip arthroscopy: from femoroacetabular impingement to instability. Arthroscopy: The Journal of Arthroscopic & Related Surgery, 27(12), 1720-1731.

Bertin, K. C., & Röttinger, H. (2004). Anterolateral mini-incision hip replacement surgery: a modified Watson-Jones approach. Clinical Orthopaedics and Related Research®, 429, 248-255.

Bigliani, L. U., Pollock, R. G., Soslowsky, L. J., Flatow, E. L., Pawluk, R. J., & Mow, V. C. (1992). Tensile properties of the inferior glenohumeral ligament. Journal of Orthopaedic Research, 10(2), 187-197.

Bigliani, L. U., Kelkar, R., Flatow, E. L., Pollock, R. G., & Mow, V. C. (1996). Glenohumeral Stability: Biomechanical Properties of Passive and Active Stabilizers. Clinical Orthopaedics and Related Research (1976-2007), 330, 13-30.

Clary, C. W., Fitzpatrick, C. K., Maletsky, L. P., & Rullkoetter, P. J. (2013). The influence of total knee arthroplasty geometry on mid-flexion stability: an experimental and finite element study. Journal of biomechanics, 46(7), 1351-1

Cross, M., Smith, E., Hoy, D., Nolte, S., Ackerman, I., Fransen, M., ... & Laslett, L. L. (2014). The global burden of hip and knee osteoarthritis: estimates from the global burden of disease 2010 study. Annals of the rheumatic diseases, 73(7), 1323-1330.

Crowe, J. F., Sculco, T. P., & Kahn, B. (2003). Revision total hip arthroplasty: hospital cost and reimbursement analysis. Clinical Orthopaedics and Related Research®, 413, 175-182.

Daou, H. E., Ng, K. G., Van Arkel, R., Jeffers, J. R., & y Baena, F. R. (2019). Robotic hip joint testing: Development and experimental protocols. Medical Engineering & Physics, 63, 57-62.

Devitt, B. M., Smith, B. N., Stapf, R., Tacey, M., & O'Donnell, J. M. (2017). Generalized joint hypermobility is predictive of hip capsular thickness. Orthopaedic Journal of Sports Medicine, 5(4), 2325967117701882.

de Palma, L., Procaccini, R., Soccetti, A., & Marinelli, M. (2012). Hospital cost of treating early dislocation following hip arthroplasty. Hip International, 22(1), 62-67.

Domb, B. G., Philippon, M. J., & Giordano, B. D. (2013). Arthroscopic capsulotomy, capsular repair, and capsular plication of the hip: relation to atraumatic instability. Arthroscopy: The Journal of Arthroscopic & Related Surgery, 29(1), 162-173.

Ekhtiari, S., Haldane, C. E., Simunovic, N., Larson, C. M., Safran, M. R., & Ayeni, O. R. (2017). Hip arthroscopic capsulotomy techniques and capsular management strategies: a systematic review. Knee Surgery, Sports Traumatology, Arthroscopy, 25(1), 9-23.

Elkins, J. M., Stroud, N. J., Rudert, M. J., Tochigi, Y., Pedersen, D. R., Ellis, B. J., ... & Brown, T. D. (2011). The capsule's contribution to total hip construct stability–A finite element analysis. Journal of Orthopaedic Research, 29(11), 1642-1648.

Grood, E. S., & Suntay, W. J. (1983). A joint coordinate system for the clinical description of three-dimensional motions: application to the knee. Journal of biomechanical engineering, 105(2), 136-144.

Goldsmith, Mary T., et al. "Validation of a six degree-of-freedom robotic system for hip in vitro biomechanical testing." Journal of Biomechanics 48.15 (2015): 4093-4100.

Han, S., Alexander, J. W., Thomas, V. S., Choi, J., Harris, J. D., Doherty, D. B., ... & Noble, P. C. (2018). Does capsular laxity lead to microinstability of the native hip?. The American journal of sports medicine, 46(6), 1315-1323.

Henninger, H. B., Reese, S. P., Anderson, A. E., & Weiss, J. A. (2010). Validation of computational models in biomechanics. Proceedings of the Institution of Mechanical Engineers, Part H: Journal of Engineering in Medicine, 224(7), 801-812.

Hewitt, J. D., Glisson, R. R., Guilak, F., & Vail, T. P. (2002). The mechanical properties of the human hip capsule ligaments. The Journal of arthroplasty, 17(1), 82-89.

Hidaka, E., Aoki, M., Muraki, T., Izumi, T., Fujii, M., & Miyamoto, S. (2009). Evaluation of stretching position by measurement of strain on the ilio-femoral ligaments: an in vitro simulation using trans-lumbar cadaver specimens. Manual therapy, 14(4), 427-432.

Jafari, S. M., Coyle, C., Mortazavi, S. J., Sharkey, P. F., & Parvizi, J. (2010). Revision hip arthroplasty: infection is the most common cause of failure. Clinical Orthopaedics and Related Research®, 468(8), 2046-2051.

Kay, J., Memon, M., Rubin, S., Simunovic, N., Nho, S. J., Belzile, E. L., & Ayeni, O. R. (2018). The dimensions of the hip capsule can be measured using magnetic resonance imaging and may have a role in arthroscopic planning. Knee Surgery, Sports Traumatology, Arthroscopy, 1-16.

Ng, K. G., El Daou, H., Bankes, M. J., Rodriguez y Baena, F., & Jeffers, J. R. (2019). Hip Joint Torsional Loading Before and After Cam Femoroacetabular Impingement Surgery. The American journal of sports medicine, 47(2), 420-430.

Kraeutler, M. J., Garabekyan, T., Pascual-Garrido, C., & Mei-Dan, O. (2016). Hip instability: a review of hip dysplasia and other contributing factors. Muscles, ligaments and tendons journal, 6(3), 343.

Kremers, H. M., Larson, D. R., Crowson, C. S., Kremers, W. K., Washington, R. E., Steiner, C. A., ... & Berry, D. J. (2015). Prevalence of total hip and knee replacement in the United States. The Journal of bone and joint surgery. American volume, 97(17), 1386.

Kuhns, B. D., Weber, A. E., Levy, D. M., Bedi, A., Mather III, R. C., Salata, M. J., & Nho, S. J. (2016). Capsular management in hip arthroscopy: an anatomic, biomechanical, and technical review. Frontiers in surgery, 3, 13.

Lie, S. A., Havelin, L. I., Furnes, O. N., Engesaeter, L. B., & Vollset, S. E. (2004). Failure rates for 4762 revision total hip arthroplasties in the Norwegian Arthroplasty Register. The Journal of bone and joint surgery. British volume, 86(4), 504-509.

Lionello, G., Sirieix, C., & Baleani, M. (2014). An effective procedure to create a speckle pattern on biological soft tissue for digital image correlation measurements. Journal of the mechanical behavior of biomedical materials, 39, 1-8.

Matta, Joel M., Cambize Shahrdar, and Tania Ferguson. "Single-incision anterior approach for total hip arthroplasty on an orthopaedic table." Clinical Orthopaedics and Related Research® 441 (2005): 115-124.

Magerkurth, O., Jacobson, J. A., Morag, Y., Caoili, E., Fessell, D., & Sekiya, J. K. (2013). Capsular laxity of the hip: findings at magnetic resonance arthrography. Arthroscopy: The Journal of Arthroscopic & Related Surgery, 29(10), 1615-1622.

Maradit Kremers H. Poster 57. Presented at: The American Academy of Orthopaedic Surgeons Annual Meeting; March 11-15, 2014; New Orleans.

Martin, H. D., Savage, A., Braly, B. A., Palmer, I. J., Beall, D. P., & Kelly, B. (2008). The function of the hip capsular ligaments: a quantitative report. Arthroscopy: The Journal of Arthroscopic & Related Surgery, 24(2), 188-195.

Matsuda, D. K. (2017). Editorial commentary: hip capsule: to repair or not?.

Myers, C. A., Register, B. C., Lertwanich, P., Ejnisman, L., Pennington, W. W., Giphart, J. E., ... & Philippon, M. J. (2011). Role of the acetabular labrum and the iliofemoral ligament in hip stability: an in vitro biplane fluoroscopy study. The American journal of sports medicine, 39(1_suppl), 85-91.

Myers CA, Fitzpatrick CK, Huff DN, Laz PJ, Rullkoetter PJ. (2019) Development and Calibration of a Probabilistic Finite Element Hip Capsule Representation. Comput Method Biomech. (in-review).

Myers, C. A., Register, B. C., Lertwanich, P., Ejnisman, L., Pennington, W. W., Giphart, J. E., ... & Philippon, M. J. (2011). Role of the acetabular labrum and the iliofemoral ligament in hip stability: an in vitro biplane fluoroscopy study. The American journal of sports medicine, 39(1_suppl), 85-91.

Nakamura, S., Matsuda, K., Arai, N., Wakimoto, N., & Matsushita, T. (2004). Mini-incision posterior approach for total hip arthroplasty. International orthopaedics, 28(4), 214-217.

Ng, K. G., El Daou, H., Bankes, M. J., Rodriguez y Baena, F., & Jeffers, J. R. (2019). Hip Joint Torsional Loading Before and After Cam Femoroacetabular Impingement Surgery. The American journal of sports medicine, 47(2), 420-430.

O'Donnell, John M., et al. "The ligamentum teres—its increasing importance." Journal of hip preservation surgery1.1 (2014): 3-11.

Pieroh, P., Schneider, S., Lingslebe, U., Sichting, F., Wolfskämpf, T., Josten, C., ... & Steinke, H. (2016). The stress-strain data of the hip capsule ligaments are gender and side independent suggesting a smaller contribution to passive stiffness. PloS one, 11(9), e0163306.

Rajaee, S. S., Campbell, J. C., Mirocha, J., & Paiement, G. D. (2018). Increasing burden of total hip arthroplasty revisions in patients between 45 and 64 years of age. JBJS, 100(6), 449-458.

Sato, K., Uchiyama, E., Katayose, M., & Fujimiya, M. (2012). Microscopic analysis of the iliofemoral and ischiofemoral ligaments in the hip joint: collagen fiber direction and crimp distribution. Anatomical science international, 87(1), 50-55.

Smith, M. V., Costic, R. S., Allaire, R., Schilling, P. L., & Sekiya, J. K. (2014). A biomechanical analysis of the soft tissue and osseous constraints of the hip joint. Knee Surgery, Sports Traumatology, Arthroscopy, 22(4), 946-952.

Stewart, K. J., Edmonds-Wilson, R. H., Brand, R. A., & Brown, T. D. (2002). Spatial distribution of hip capsule structural and material properties. Journal of biomechanics, 35(11), 1491-1498.

Stewart, K. J., Pedersen, D. R., Callaghan, J. J., & Brown, T. D. (2004). Implementing capsule representation in a total hip dislocation finite element model. The Iowa orthopaedic journal, 24, 1.

M. A. Sutton, J. H. Yan, V. Tiwari, H. W. Schreier, Jean-José Orteu. The effect of out-of-plane motion on 2D and 3D digital image correlation measurements. Optics and Lasers in Engineering, Elsevier, 2008, 46 (10), pp.746-757.

Telleria, J. J., Lindsey, D. P., Giori, N. J., & Safran, M. R. (2011). An anatomic arthroscopic description of the hip capsular ligaments for the hip arthroscopist. Arthroscopy: The Journal of Arthroscopic & Related Surgery, 27(5), 628-636.

Ticker, J. B., Bigliani, L. U., Soslowsky, L. J., Pawluk, R. J., Flatow, E. L., & Mow, V. C. (1996). Inferior glenohumeral ligament: geometric and strain-rate dependent properties. Journal of Shoulder and Elbow Surgery, 5(4), 269-279.

Weber, A. E., Kuhns, B. D., Cvetanovich, G. L., Lewis, P. B., Mather, R. C., Salata, M. J., & Nho, S. J. (2017). Does the hip capsule remain closed after hip arthroscopy with routine capsular closure for femoroacetabular impingement? A magnetic resonance imaging analysis in symptomatic postoperative patients. Arthroscopy: The Journal of Arthroscopic & Related Surgery, 33(1), 108-115.

Wu, G., Siegler, S., Allard, P., Kirtley, C., Leardini, A., Rosenbaum, D., ... & Schmid, O. (2002). ISB recommendation on definitions of joint coordinate system of various joints for the reporting of human joint motion—part I: ankle, hip, and spine. Journal of biomechanics, 35(4), 543-548.

Van Arkel, R. J., Amis, A. A., Cobb, J. P., & Jeffers, J. R. T. (2015a). The capsular ligaments provide more hip rotational restraint than the acetabular labrum and the ligamentum teres: an experimental study. The bone & joint journal, 97(4), 484-491.

van Arkel, R. J., Amis, A. A., & Jeffers, J. R. (2015b). The envelope of passive motion allowed by the capsular ligaments of the hip. Journal of Biomechanics, 48(14), 3803-3809.

van Arkel, R. J., Ng, K. G., Muirhead-Allwood, S. K., & Jeffers, J. R. (2018). Capsular Ligament Function After Total Hip Arthroplasty. JBJS, 100(14), e94.

APPENDICES

Appendix 1A: Full Primary Axis Laxity Curves for Natural Specimens

S182590L - Natural

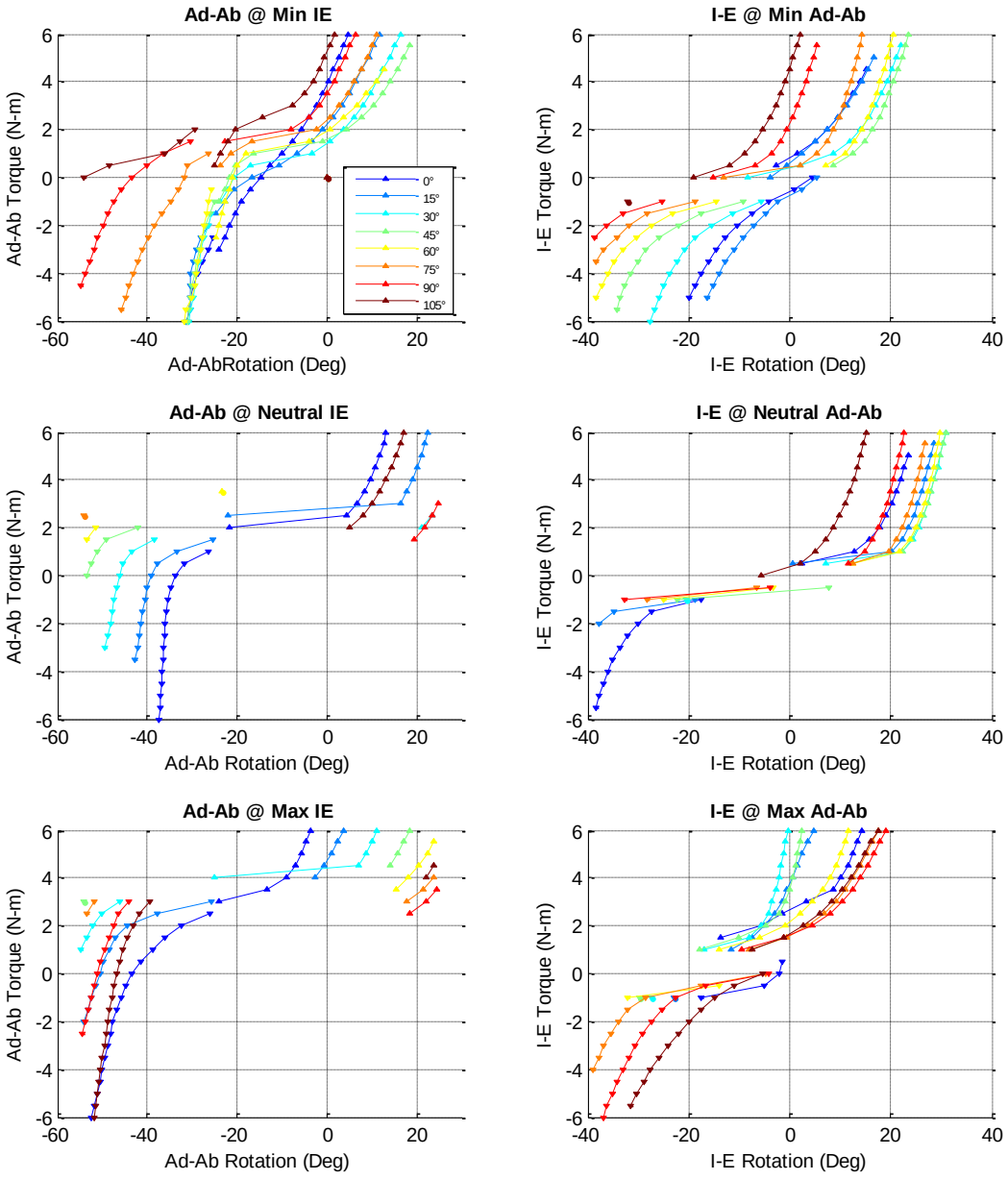

S182590R - Natural

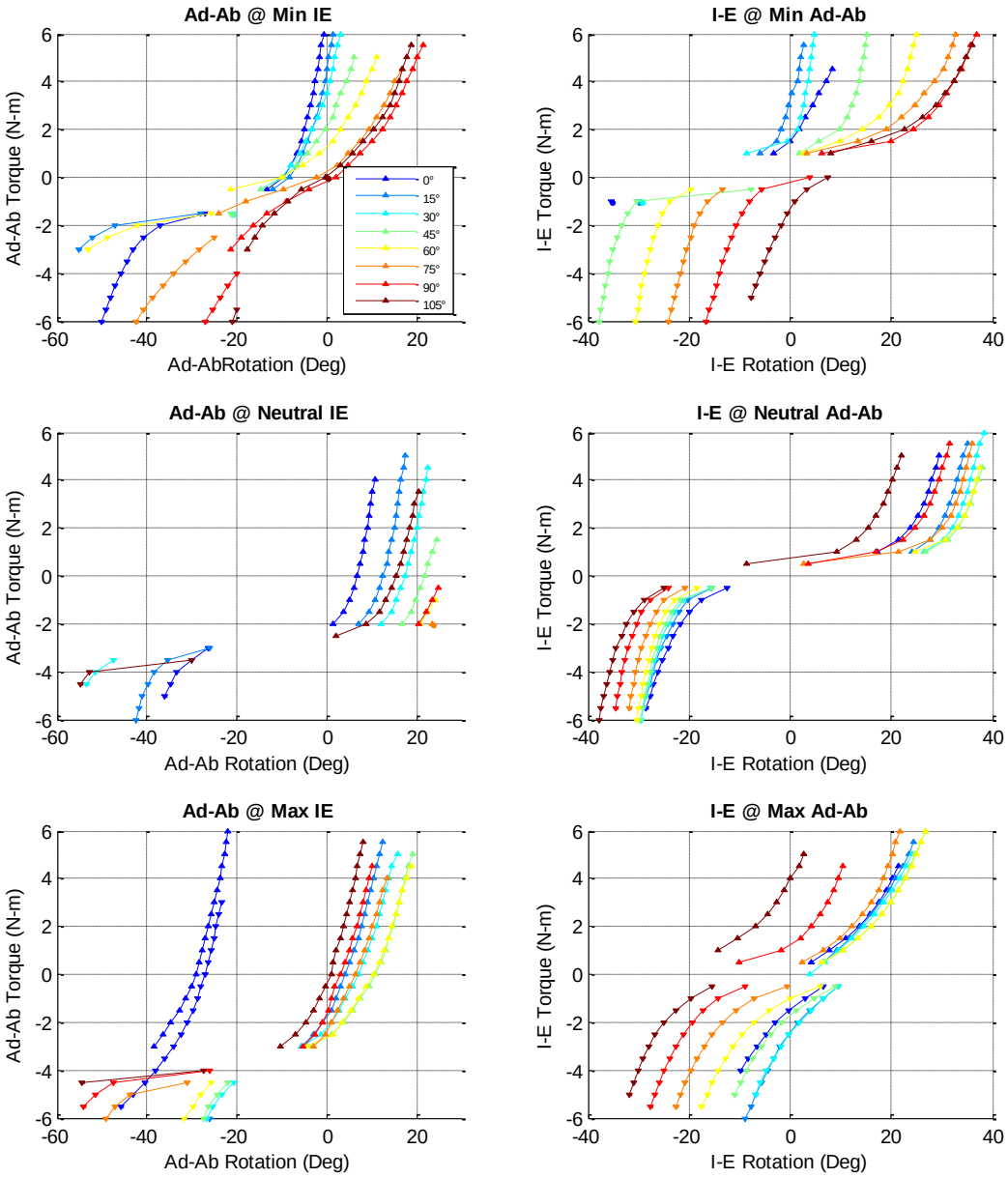

S182484L - Natural

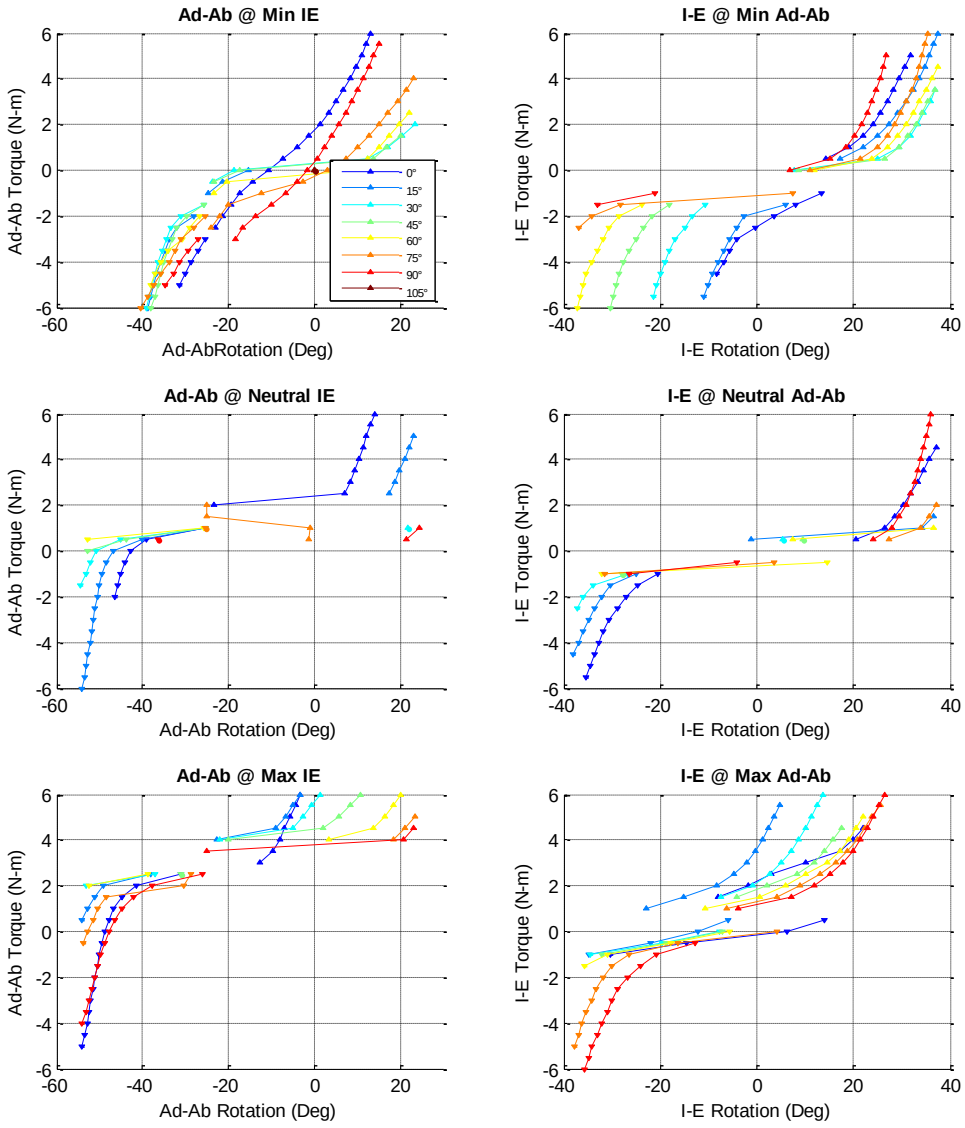

S182484R - Natural

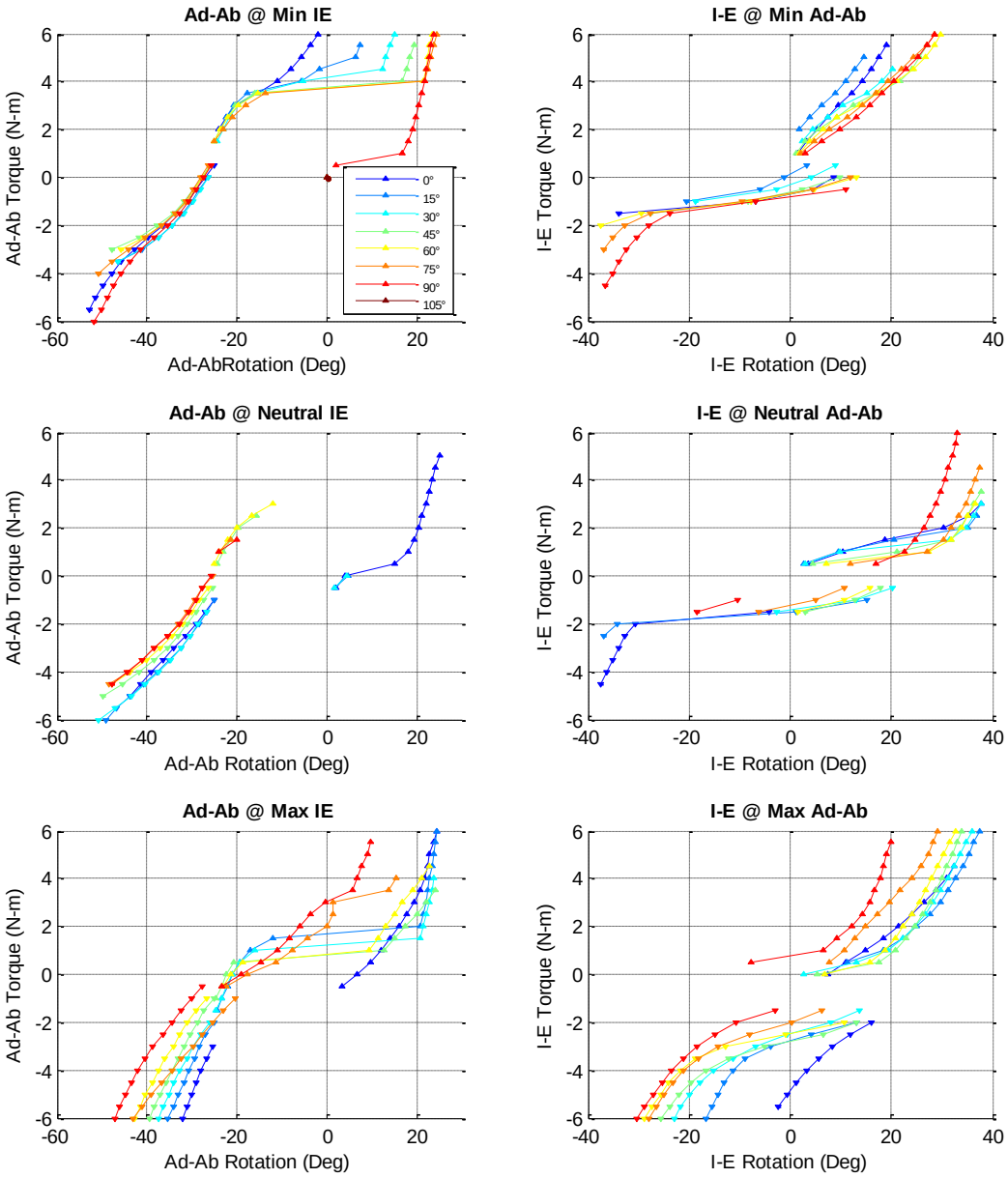

S171562L - Natural

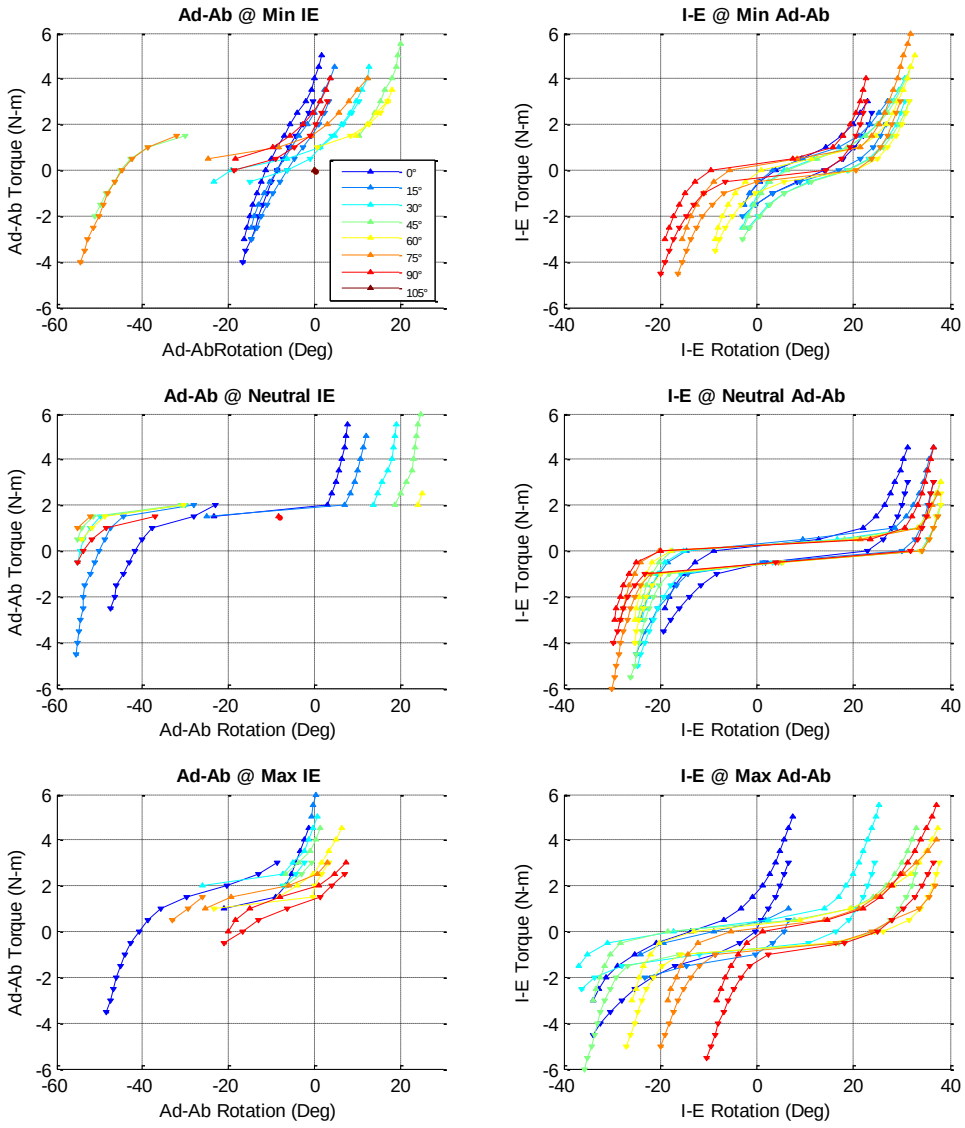

S171562R - Natural

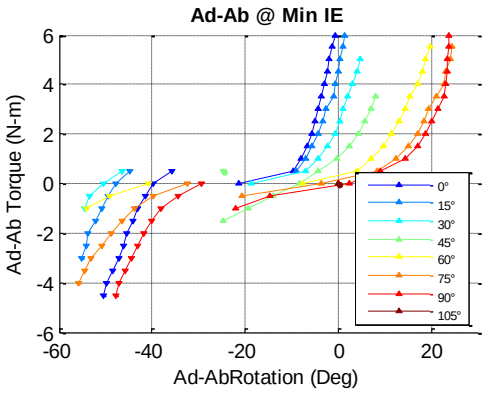

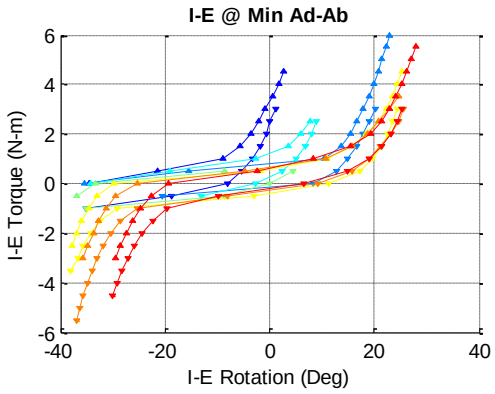

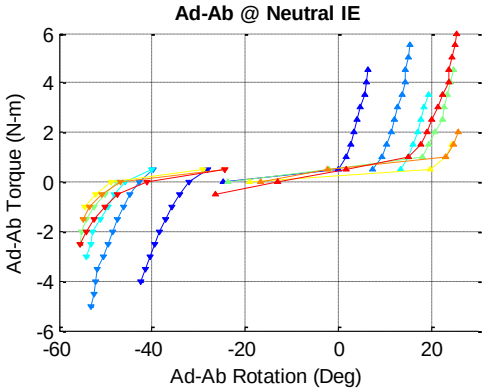

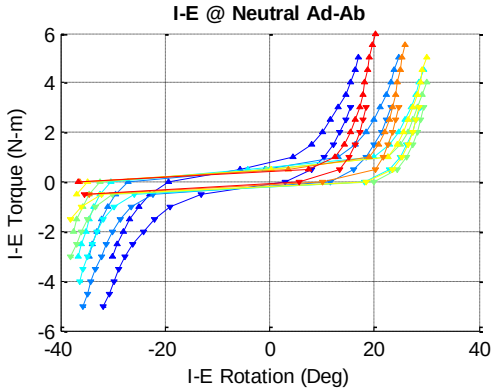

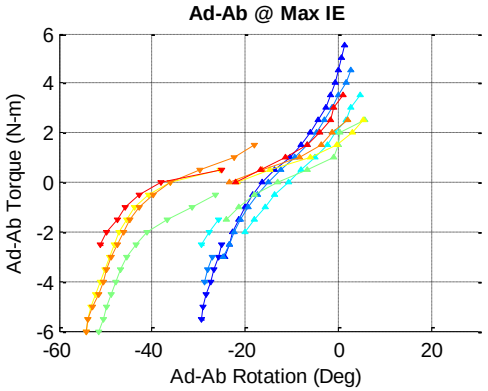

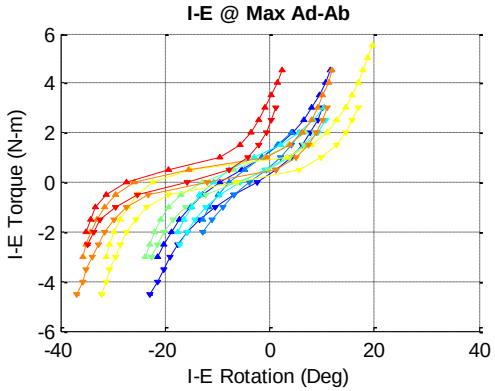

S171645L - Natural

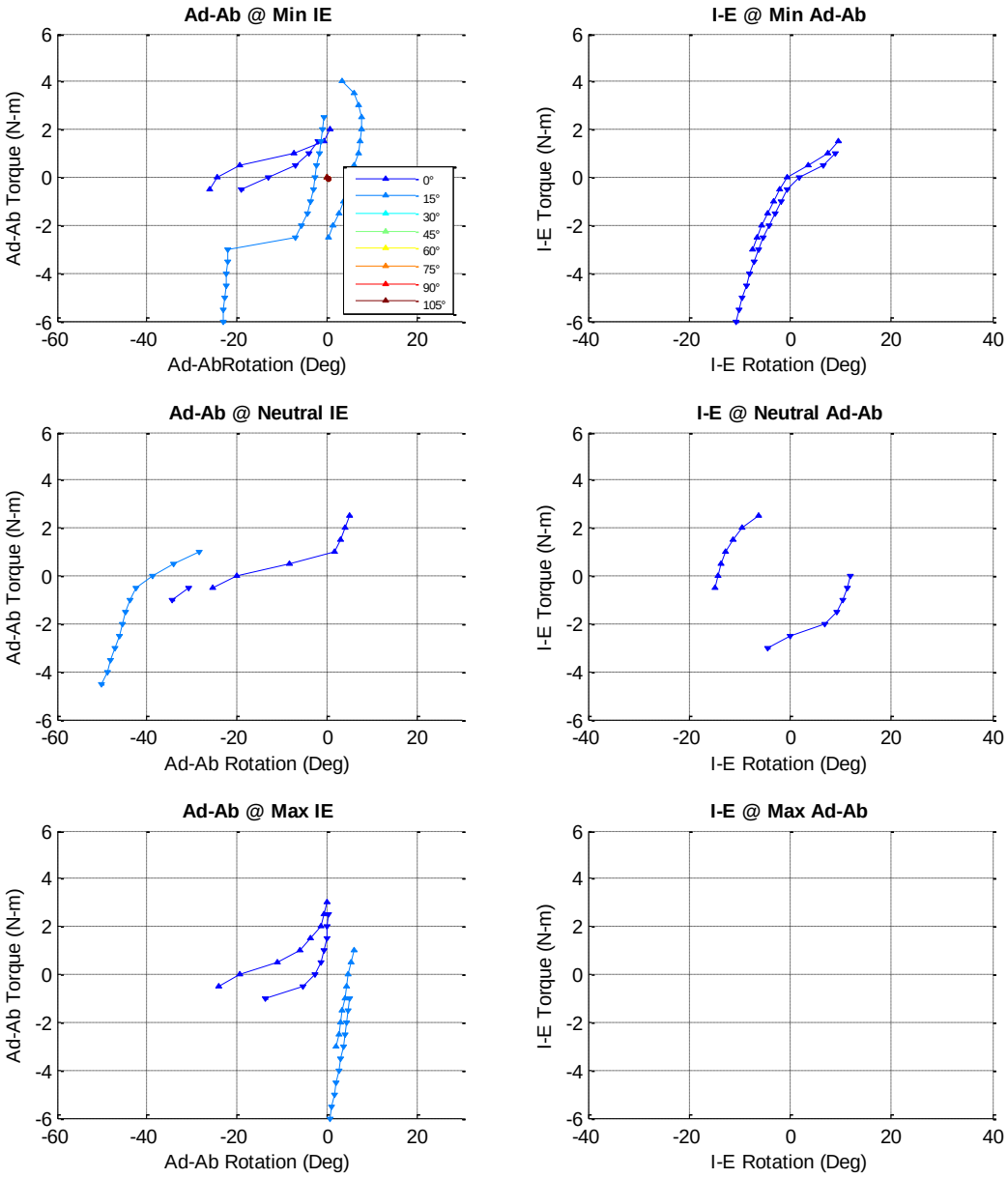

S171645R - Natural

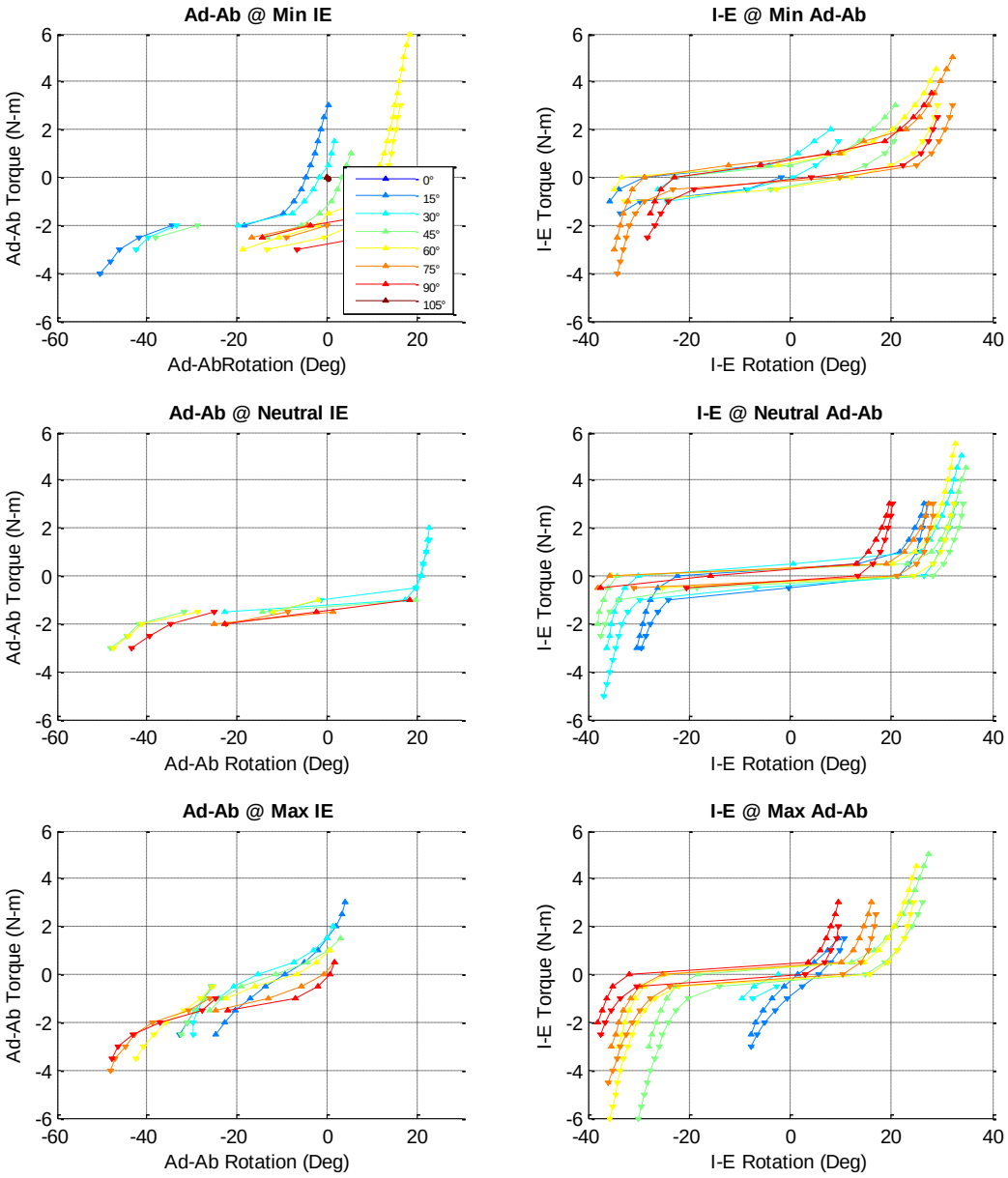

S171618L - Natural

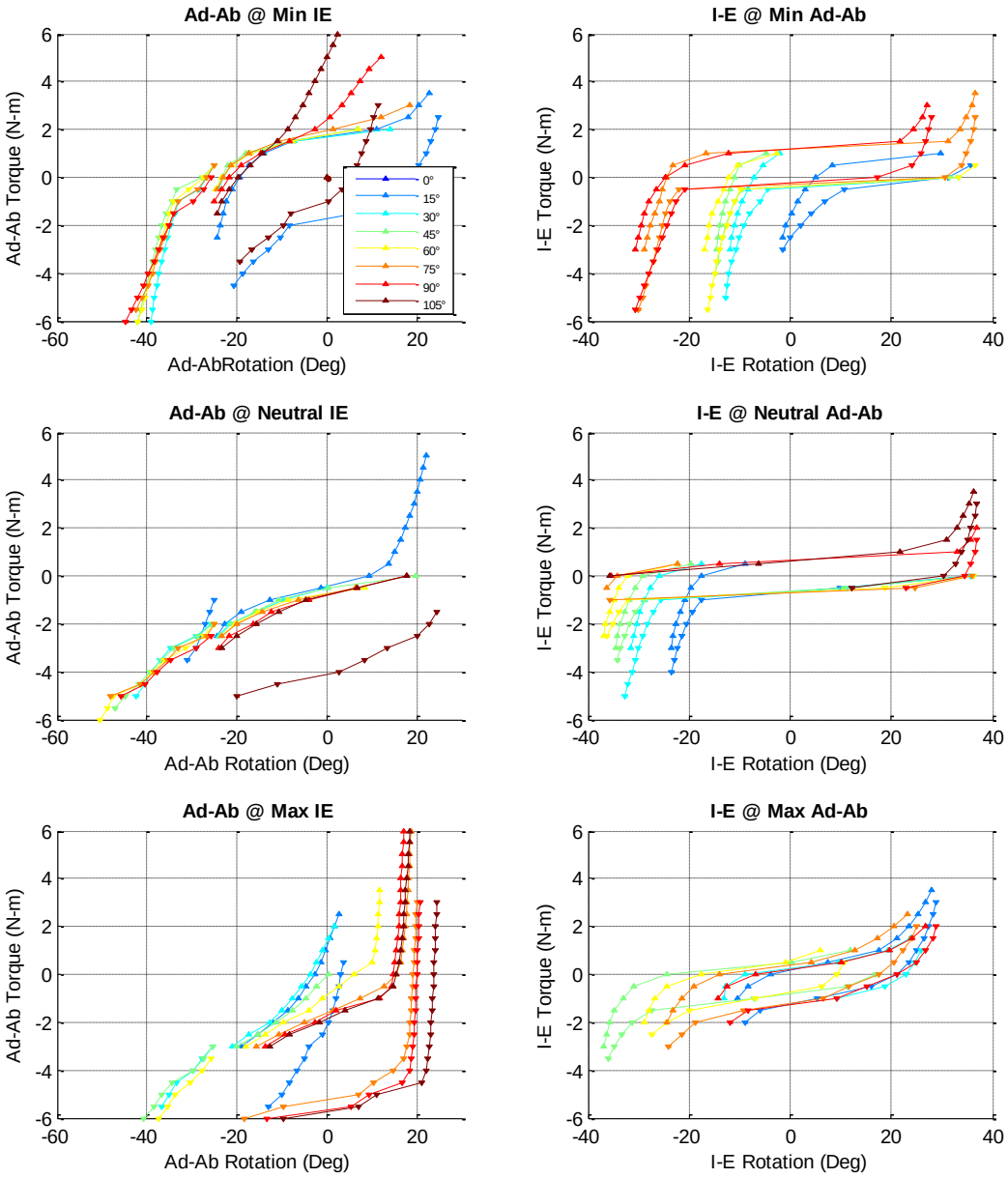

S171618R - Natural

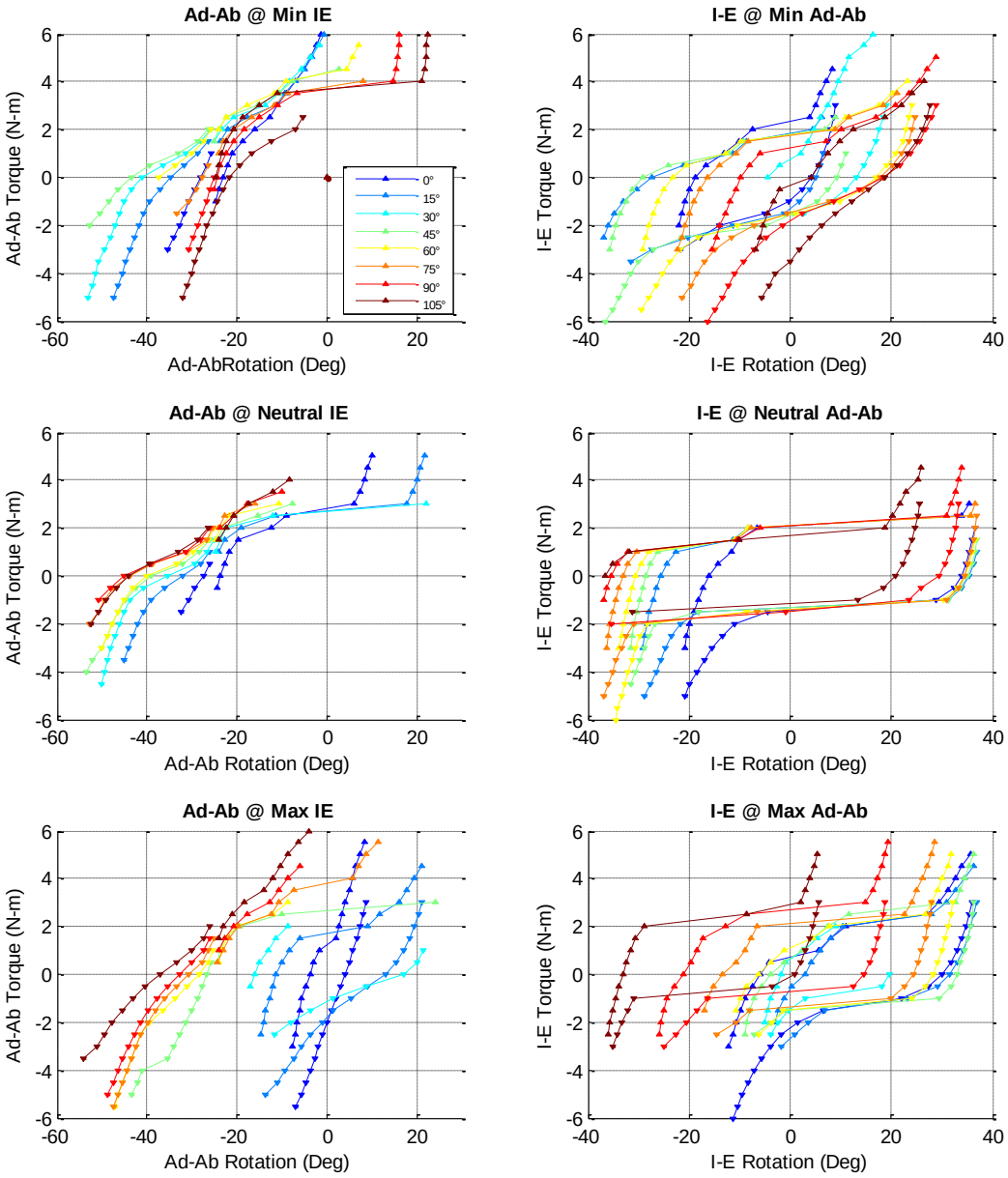

Appendix 1B: Full Primary Axis Laxity Curves for Posteriorly Implanted Specimens

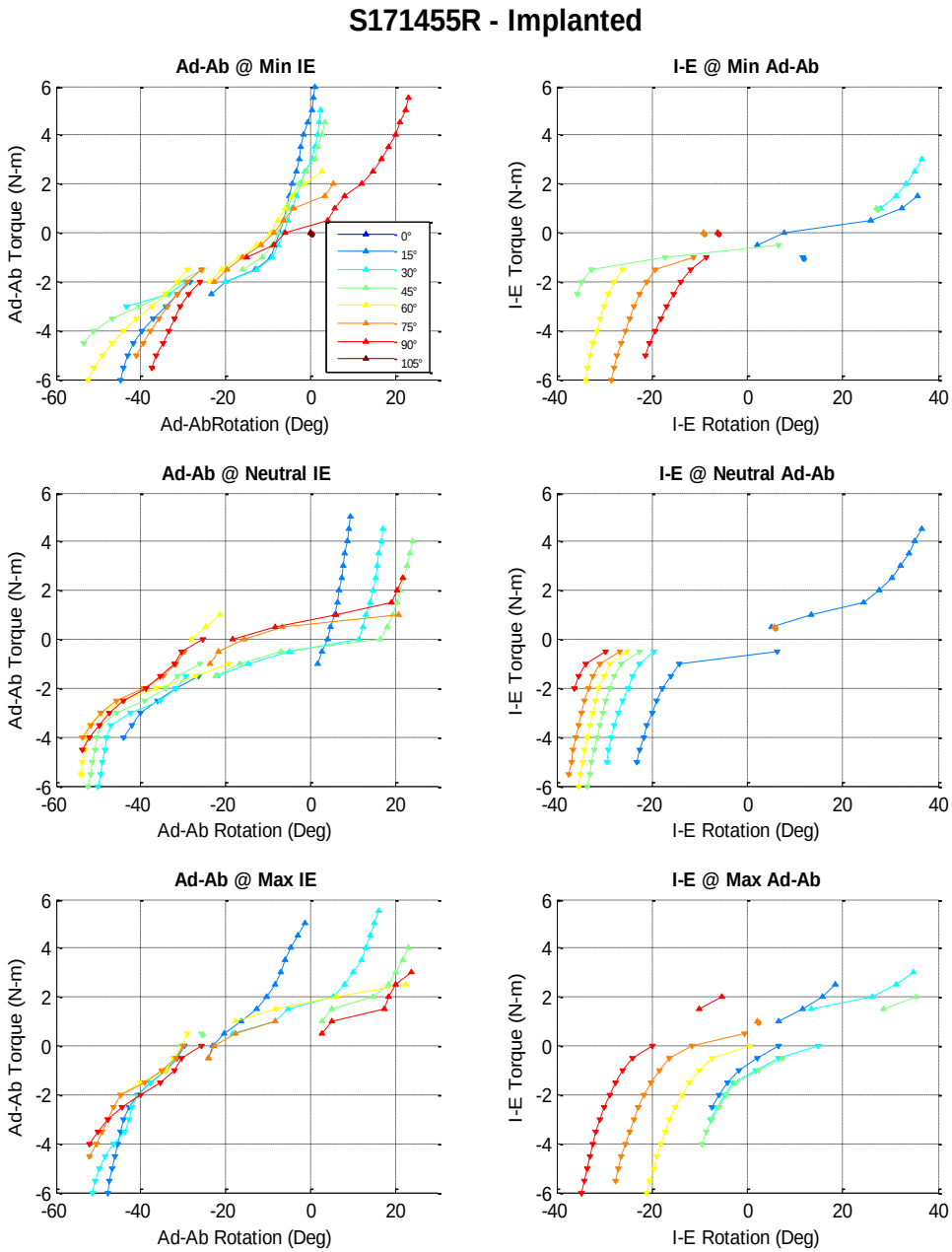

S171455L - Implanted

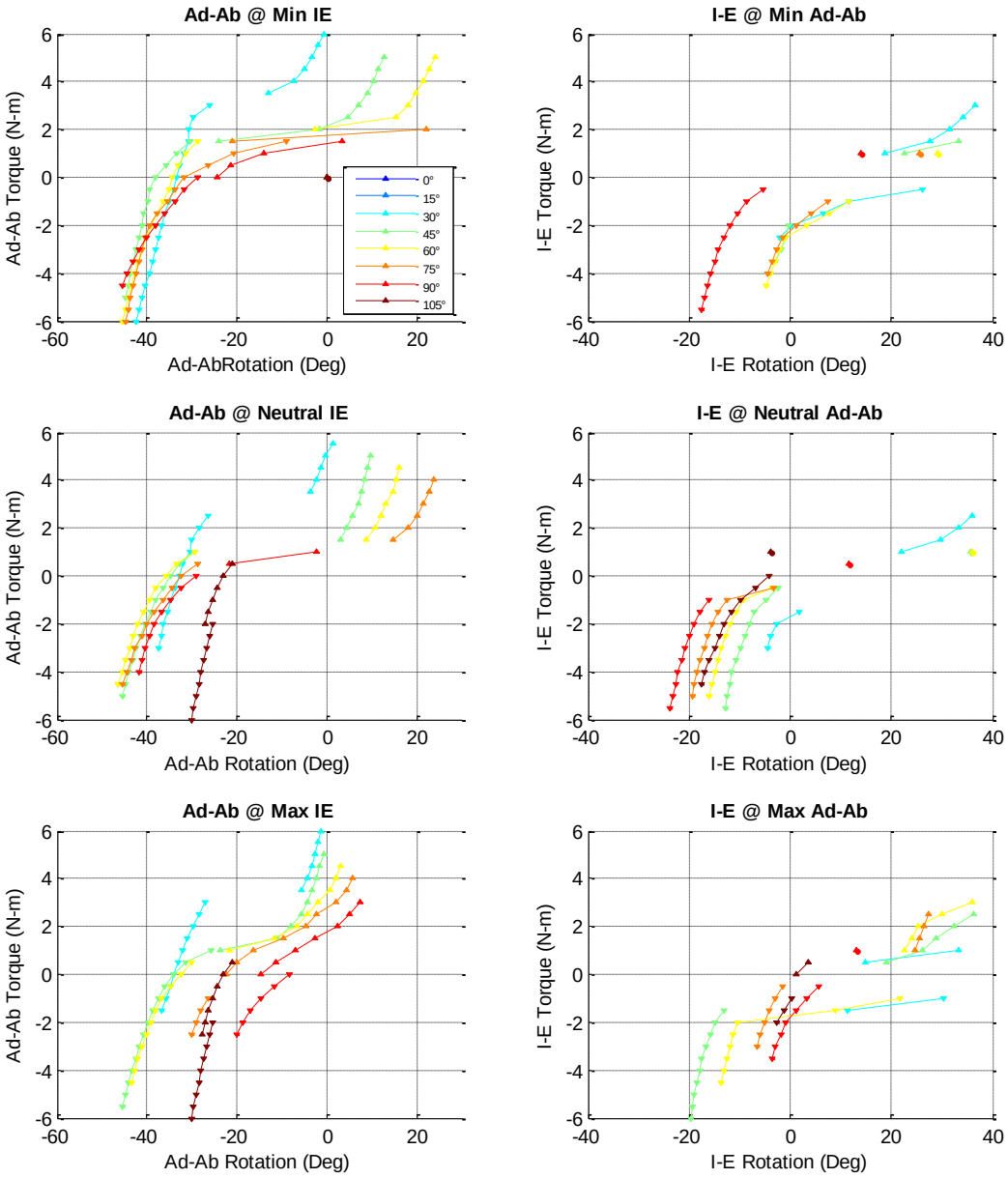

S171613R - Implanted

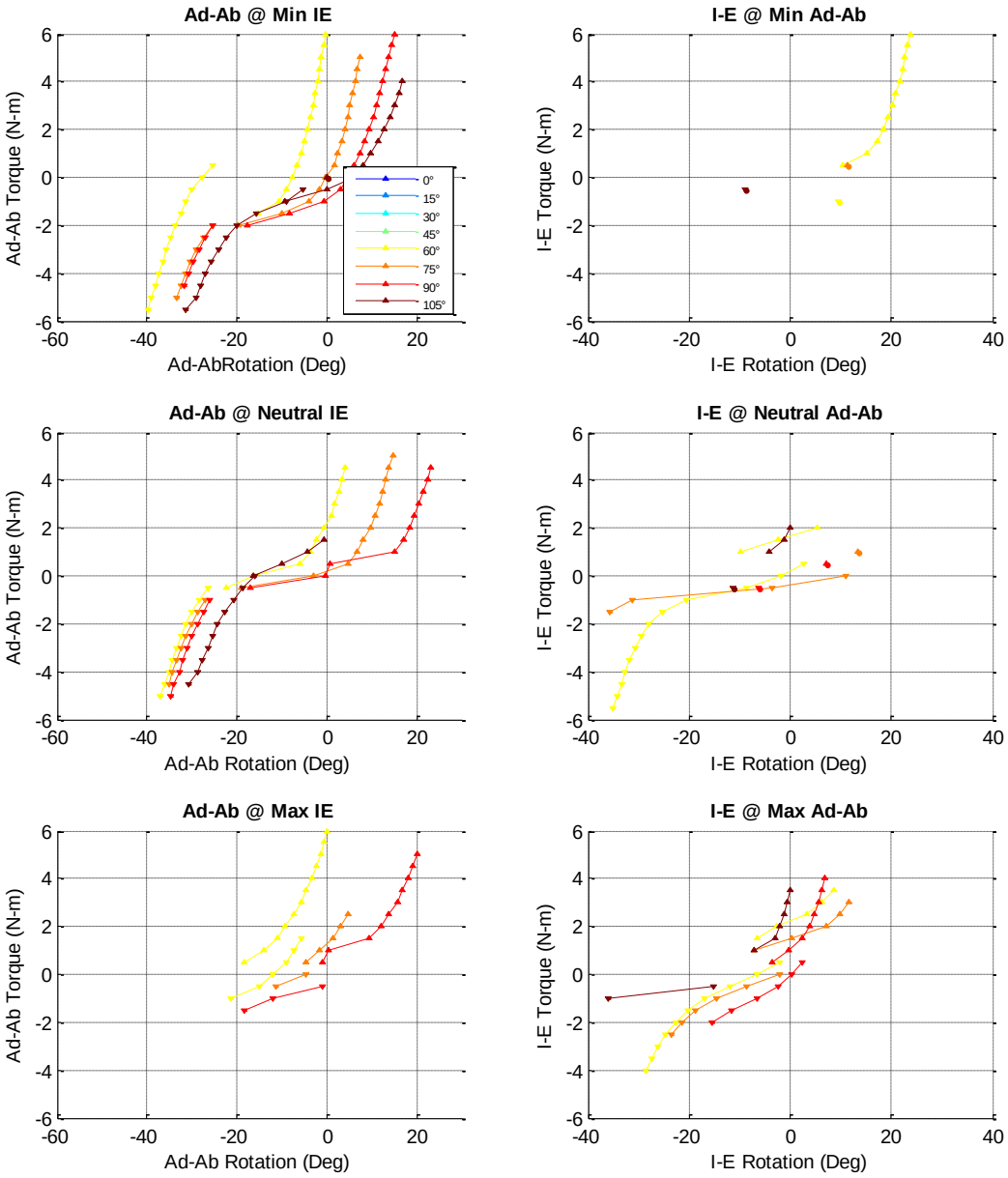

S171613L - Implanted

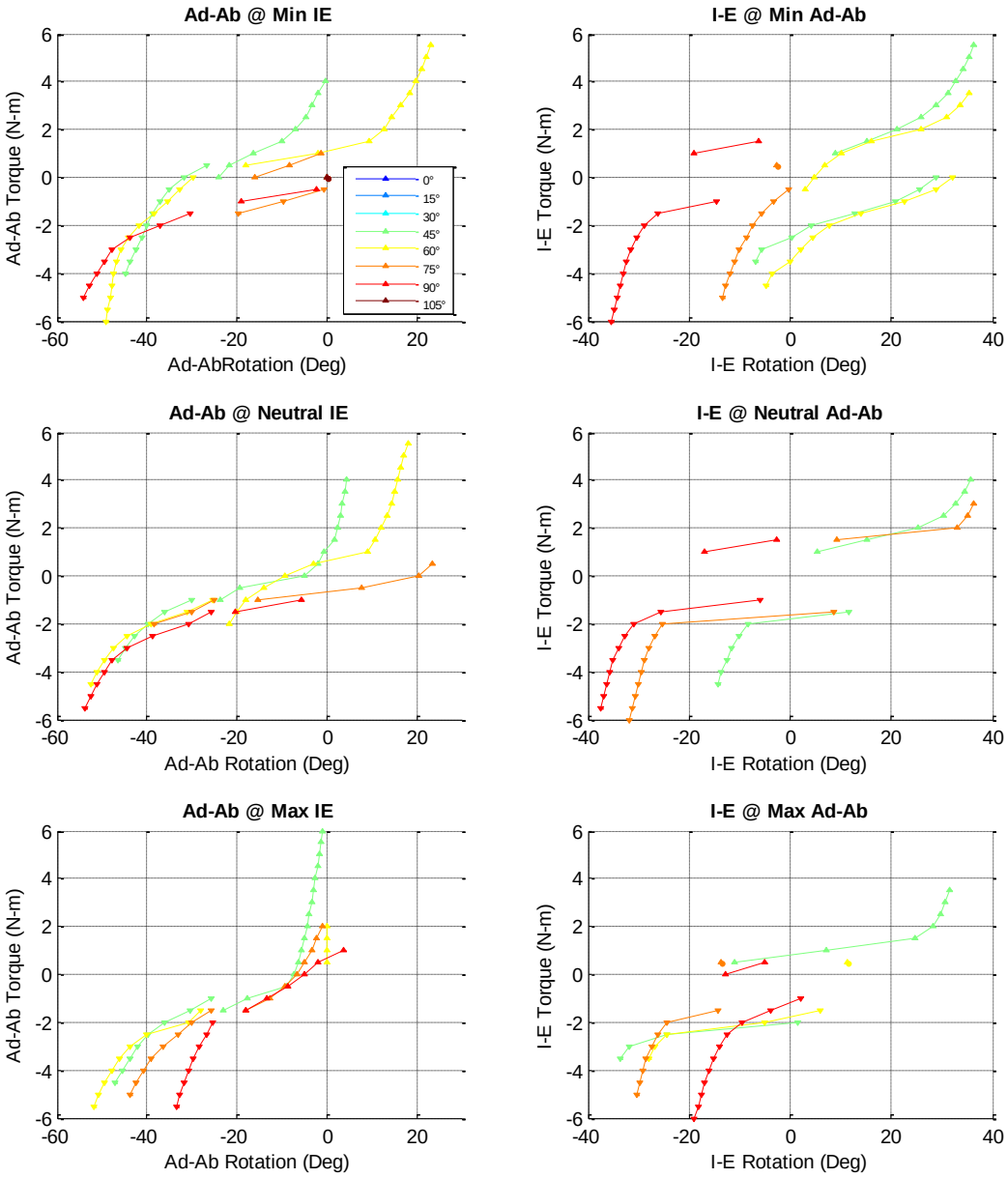

S171624R - Implanted

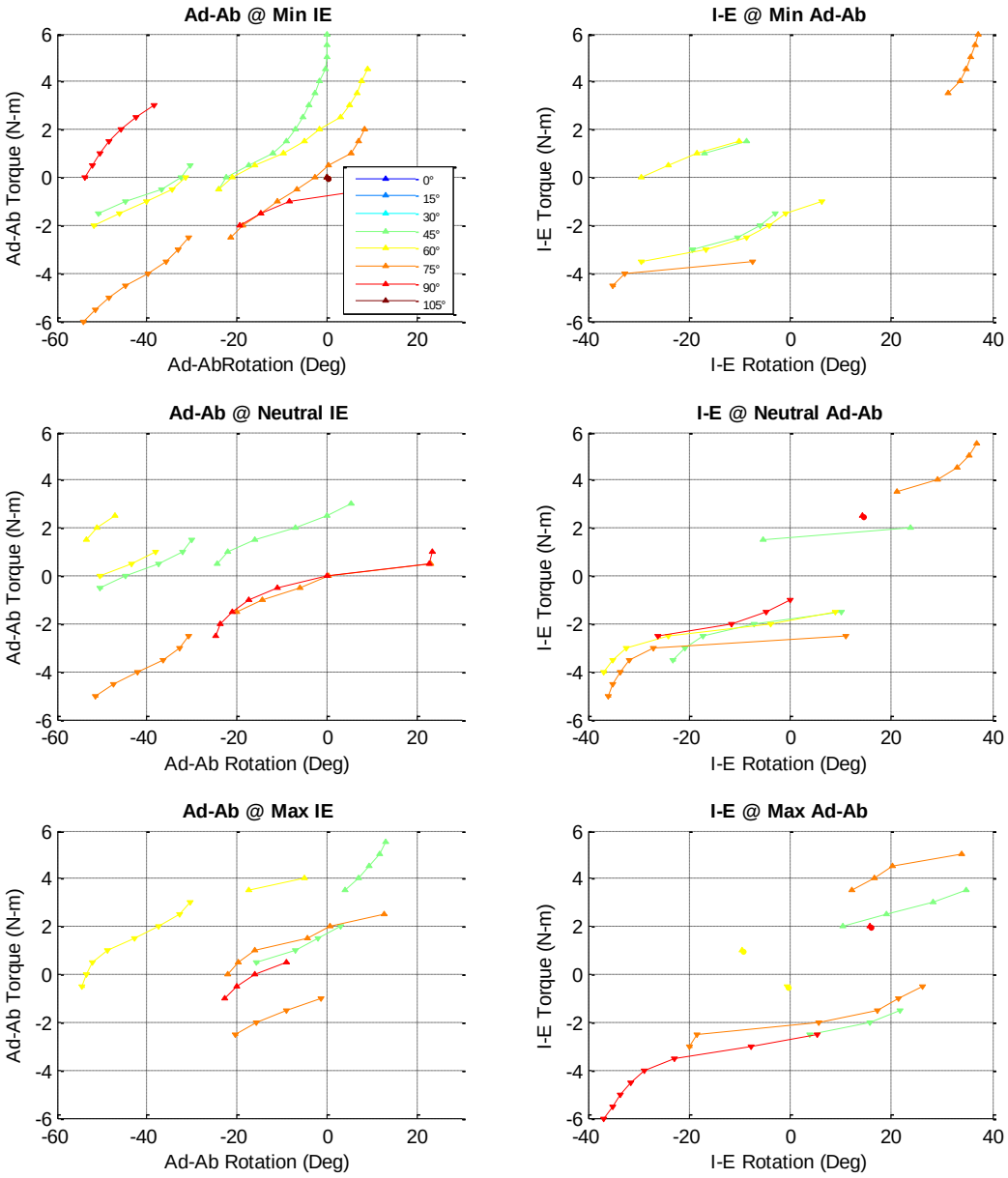

S171624L - Implanted

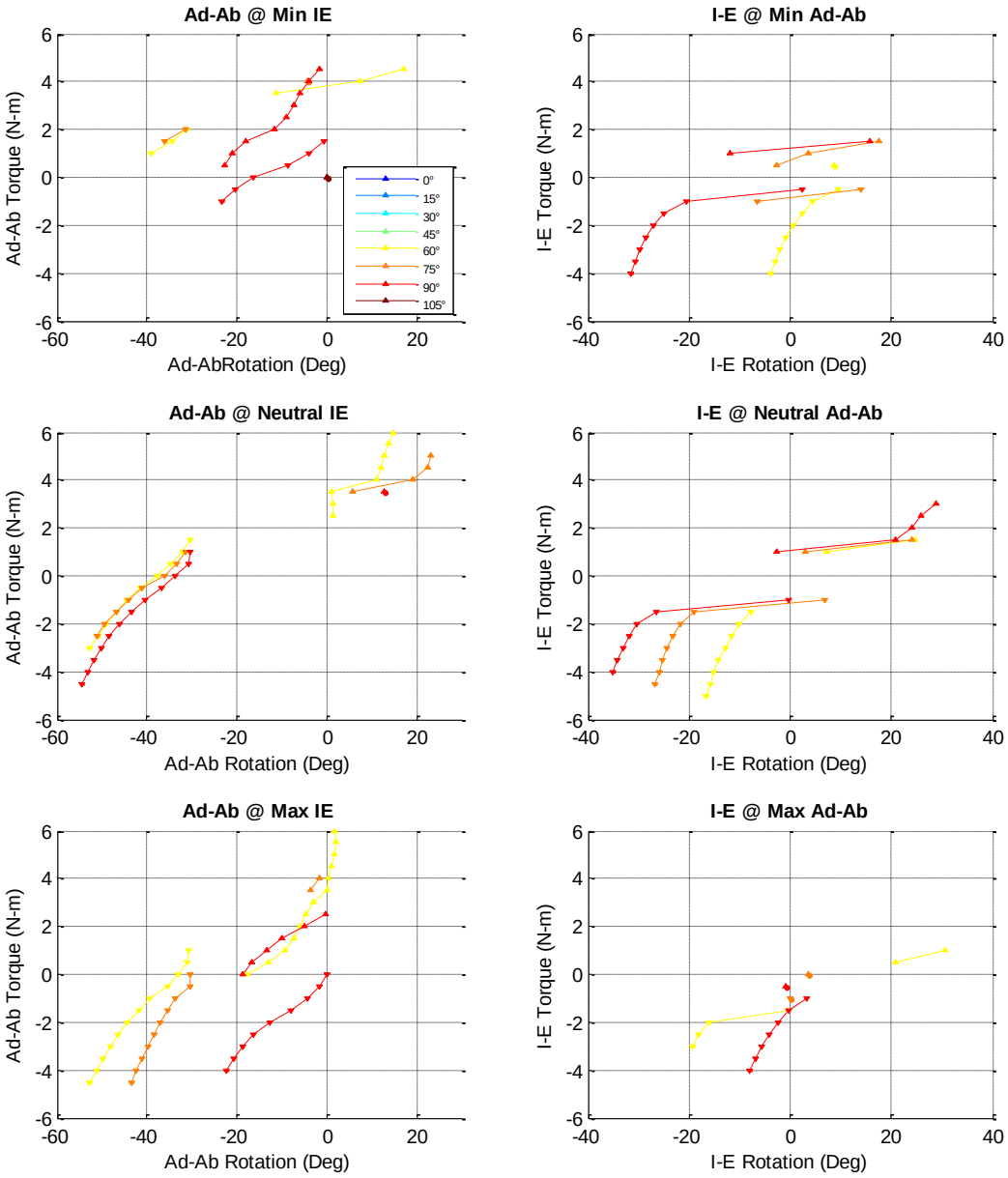

Appendix 1C 1-10: 4-Dimensional Laxity Curves for Natural Hips Ad/Ab Torque Response

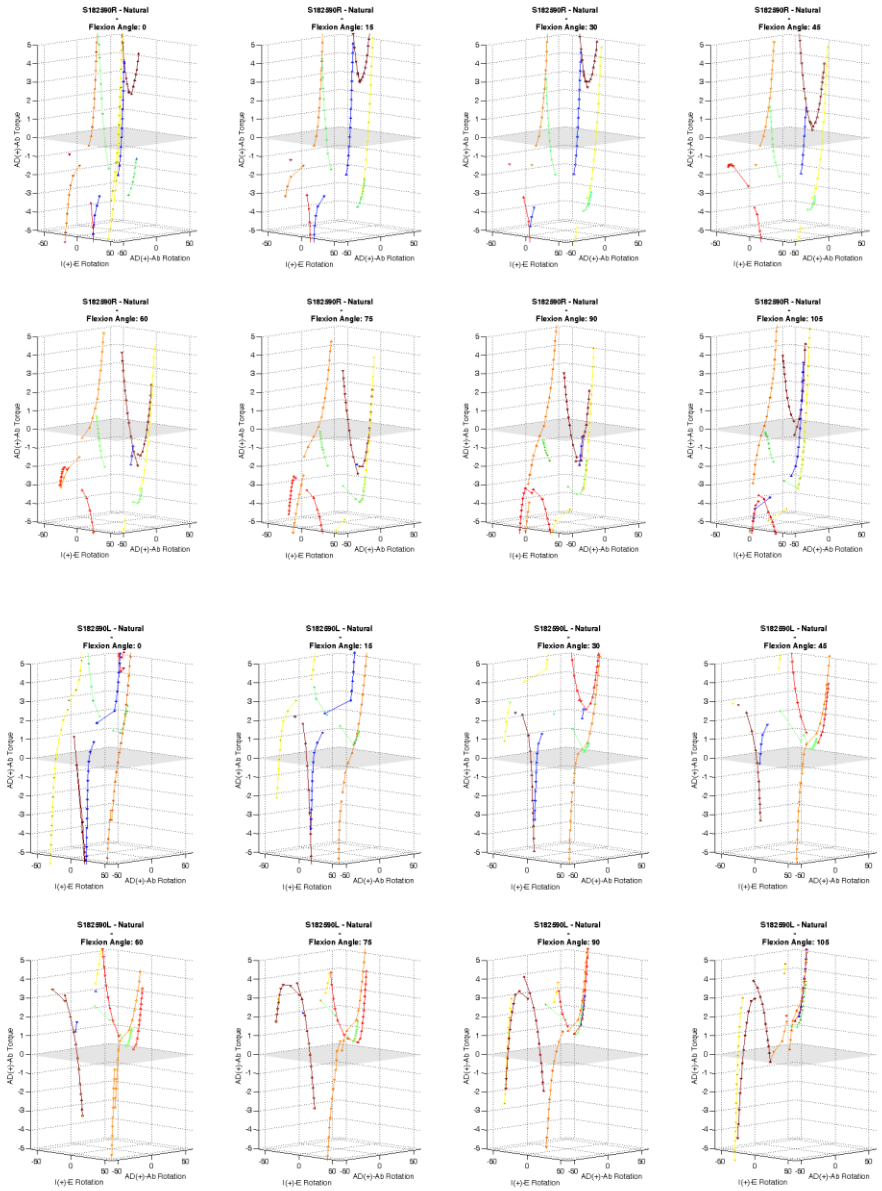

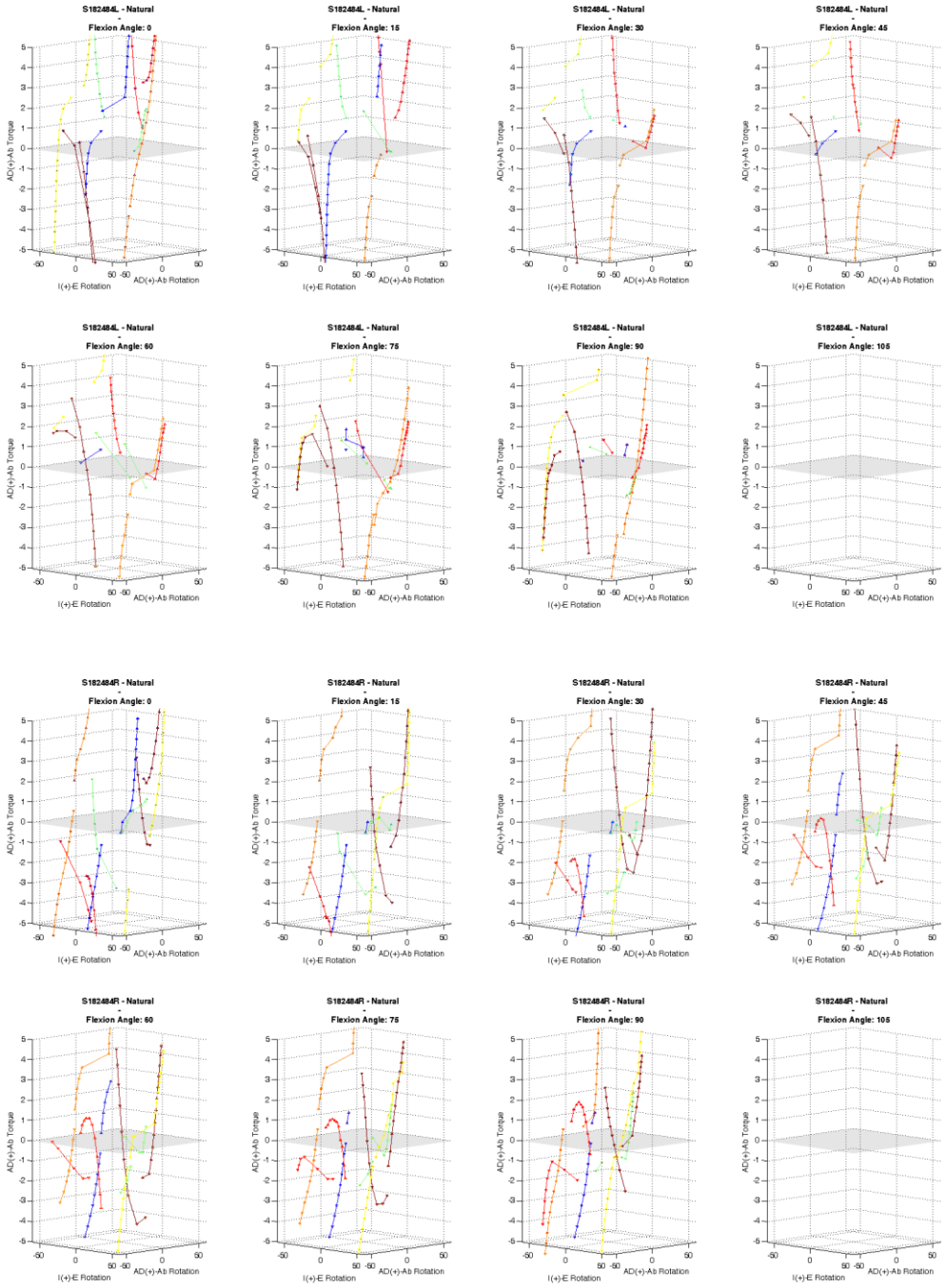
S182484L - Natural
Flexion Angle: 0
S182484L - Natural
Flexion Angle: 15
S182484L - Natural
Flexion Angle: 30
S182484L - Natural
Flexion Angle: 45
S182484L - Natural
Flexion Angle: 60
S182484L - Natural
Flexion Angle: 75
S182484L - Natural
Flexion Angle: 90
S182484L - Natural
Flexion Angle: 105
S182484R - Natural
Flexion Angle: 0
S182484R - Natural
Flexion Angle: 15
S182484R - Natural
Flexion Angle: 30
S182484R - Natural
Flexion Angle: 45
S182484R - Natural
Flexion Angle: 60
S182484R - Natural
Flexion Angle: 75
S182484R - Natural
Flexion Angle: 90
S182484R - Natural
Flexion Angle: 105
AD(+)-Ab Torque
I(+)-E Rotation
AD(+)-Ab Rotation

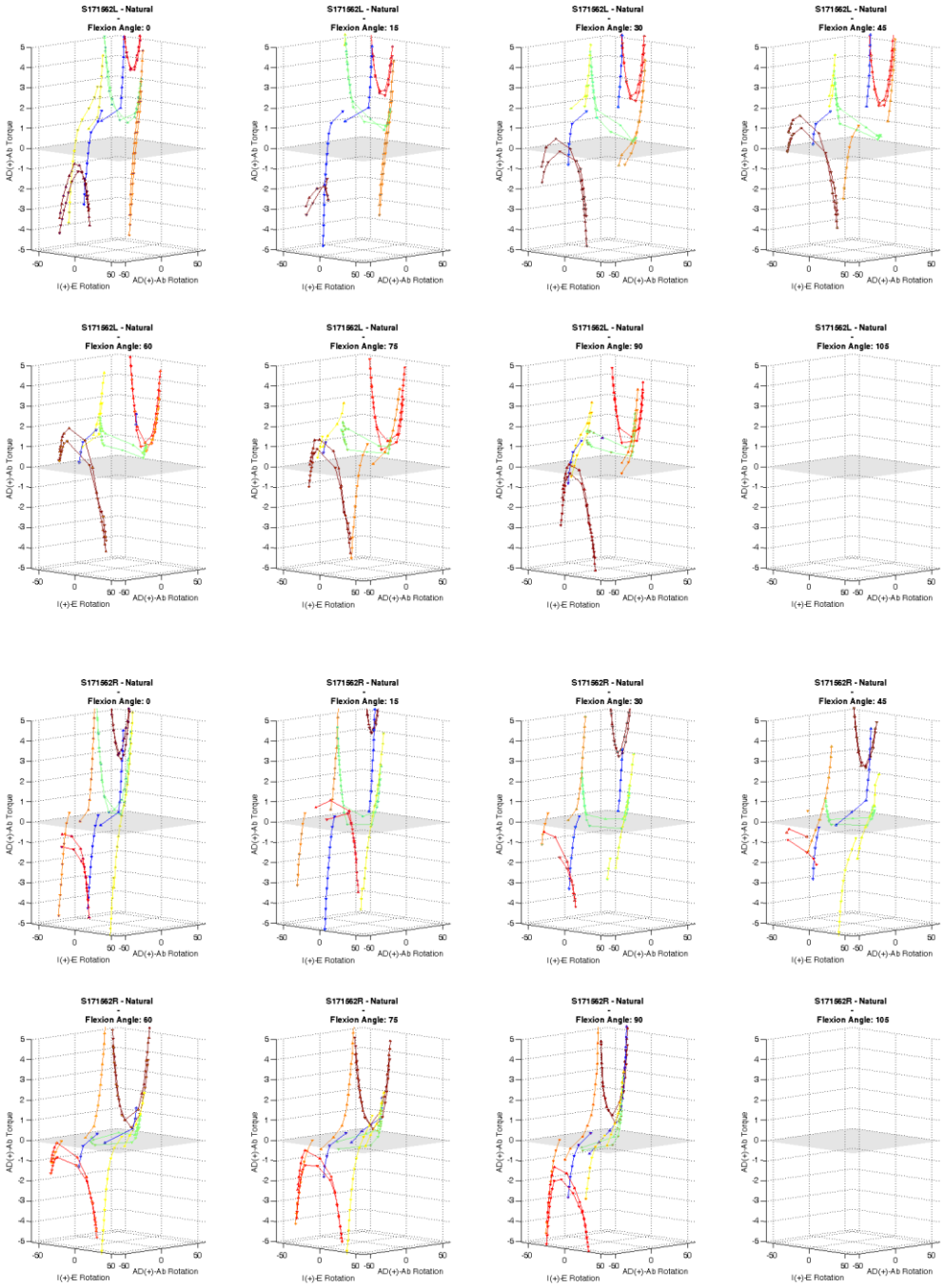
S171562L - Natural
Flexion Angle: 0
S171562L - Natural
Flexion Angle: 15
S171562L - Natural
Flexion Angle: 30
S171562L - Natural
Flexion Angle: 45
S171562L - Natural
Flexion Angle: 60
S171562L - Natural
Flexion Angle: 75
S171562L - Natural
Flexion Angle: 90
S171562L - Natural
Flexion Angle: 105
S171562R - Natural
Flexion Angle: 0
S171562R - Natural
Flexion Angle: 15
S171562R - Natural
Flexion Angle: 30
S171562R - Natural
Flexion Angle: 45
S171562R - Natural
Flexion Angle: 60
S171562R - Natural
Flexion Angle: 75
S171562R - Natural
Flexion Angle: 90
S171562R - Natural
Flexion Angle: 105
AD(+)-Ab Torque
I(+)-E Rotation
AD(+)-Ab Rotation

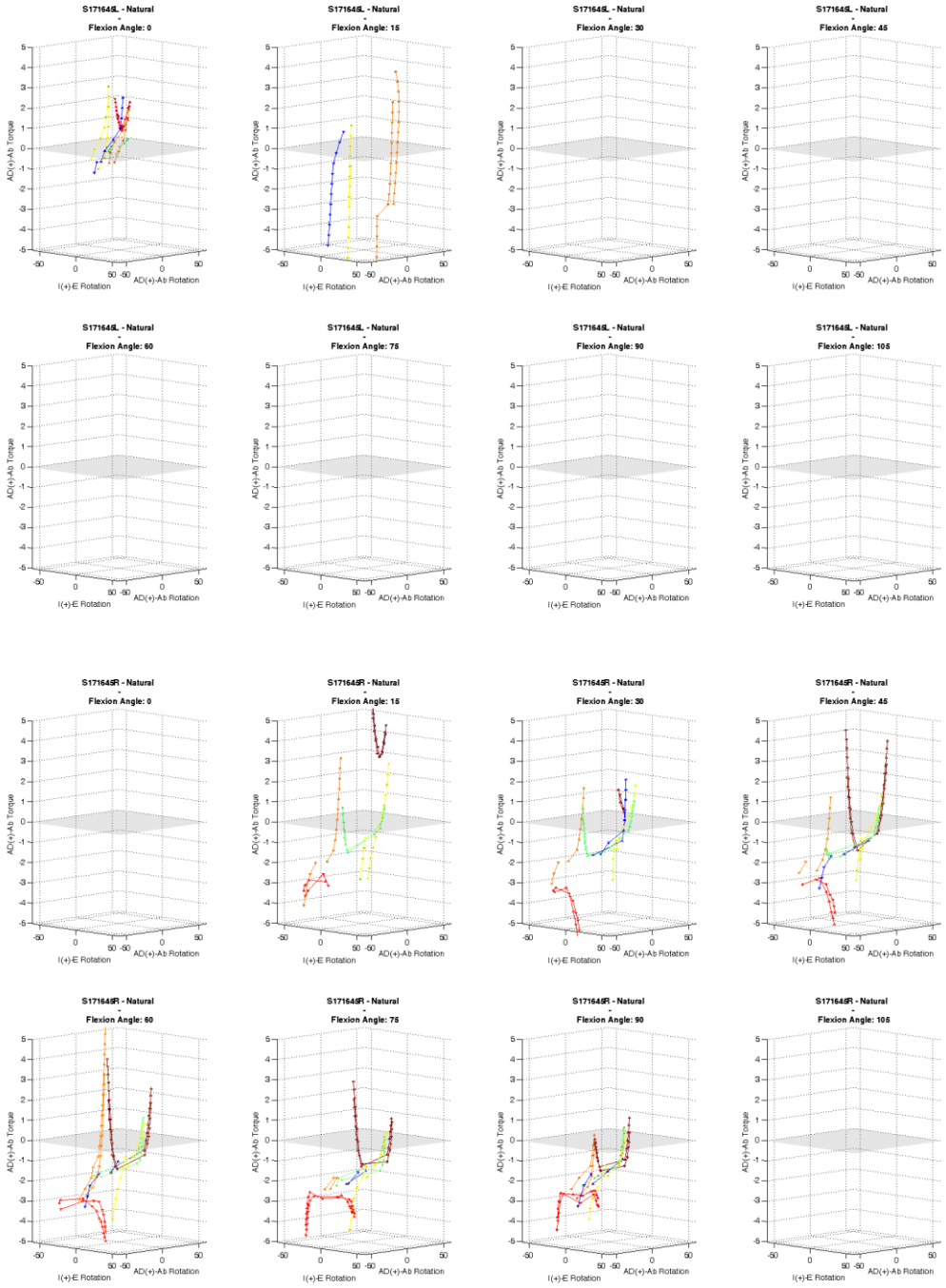
S171645L - Natural
Flexion Angle: 0
S171645L - Natural
Flexion Angle: 15
S171645L - Natural
Flexion Angle: 30
S171645L - Natural
Flexion Angle: 45
S171645L - Natural
Flexion Angle: 60
S171645L - Natural
Flexion Angle: 75
S171645L - Natural
Flexion Angle: 90
S171645L - Natural
Flexion Angle: 105
S171645R - Natural
Flexion Angle: 0
S171645R - Natural
Flexion Angle: 15
S171645R - Natural
Flexion Angle: 30
S171645R - Natural
Flexion Angle: 45
S171645R - Natural
Flexion Angle: 60
S171645R - Natural
Flexion Angle: 75
S171645R - Natural
Flexion Angle: 90
S171645R - Natural
Flexion Angle: 105
AD(+)-Ab Torque
I(+)-E Rotation
AD(+)-Ab Rotation

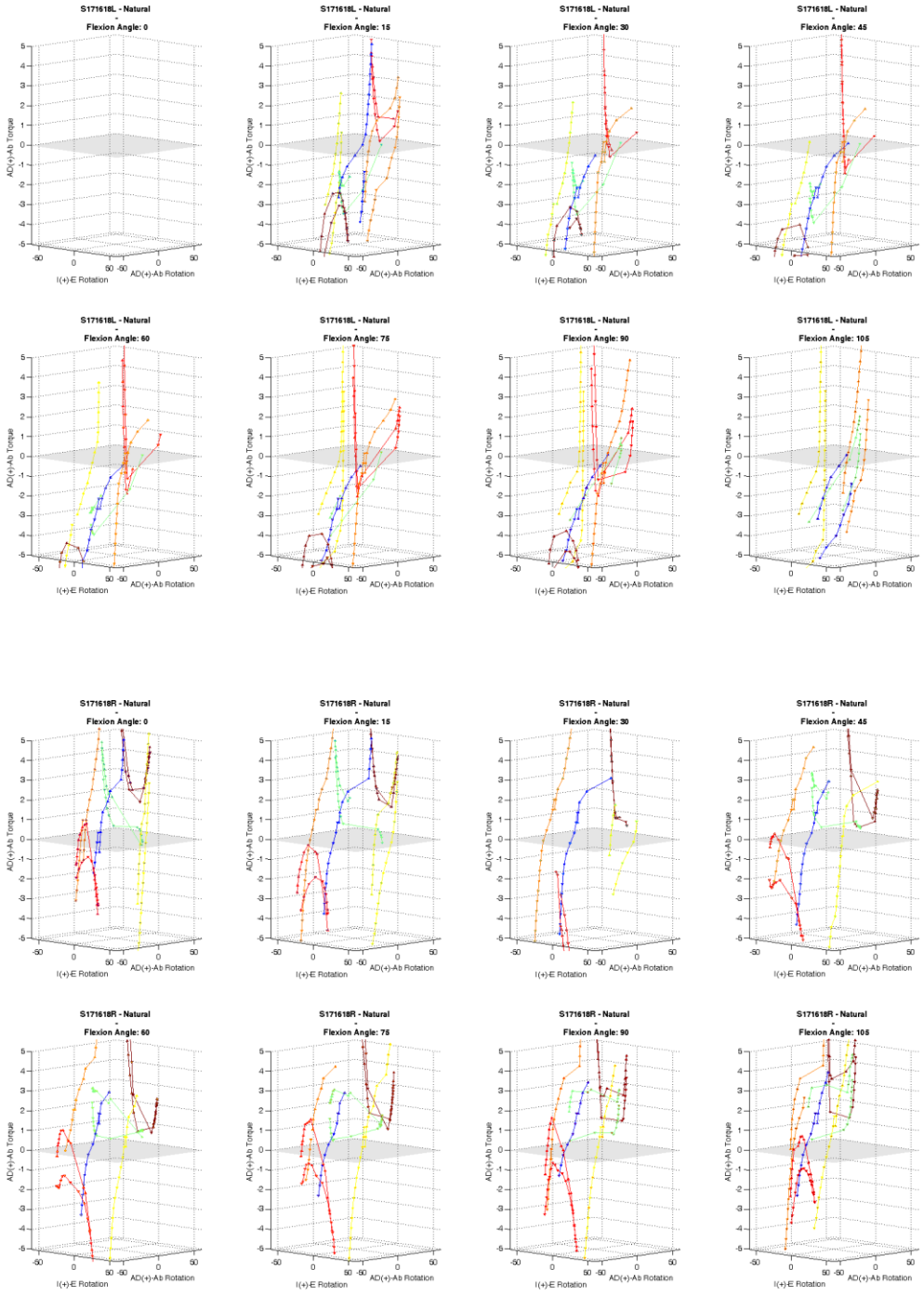
S171618L - Natural
Flexion Angle: 0
S171618L - Natural
Flexion Angle: 15
S171618L - Natural
Flexion Angle: 30
S171618L - Natural
Flexion Angle: 45
S171618L - Natural
Flexion Angle: 60
S171618L - Natural
Flexion Angle: 75
S171618L - Natural
Flexion Angle: 90
S171618L - Natural
Flexion Angle: 105
S171618R - Natural
Flexion Angle: 0
S171618R - Natural
Flexion Angle: 15
S171618R - Natural
Flexion Angle: 30
S171618R - Natural
Flexion Angle: 45
S171618R - Natural
Flexion Angle: 60
S171618R - Natural
Flexion Angle: 75
S171618R - Natural
Flexion Angle: 90
S171618R - Natural
Flexion Angle: 105
AD(+)-Ab Torque
I(+)-E Rotation
AD(+)-Ab Rotation

Appendix 1D 1-10: 4-Dimensional Laxity Curves for Natural Hips IE Torque Response

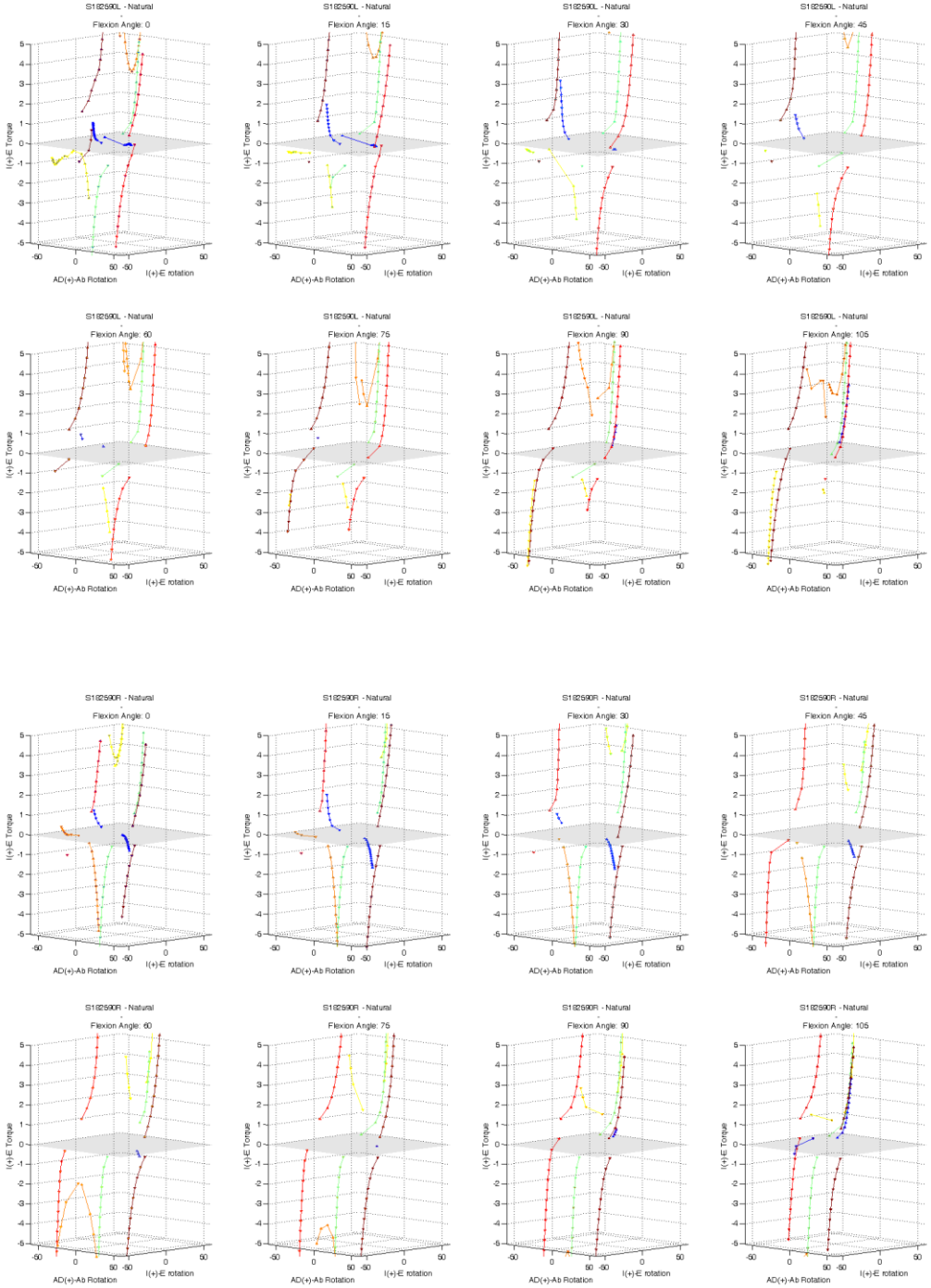

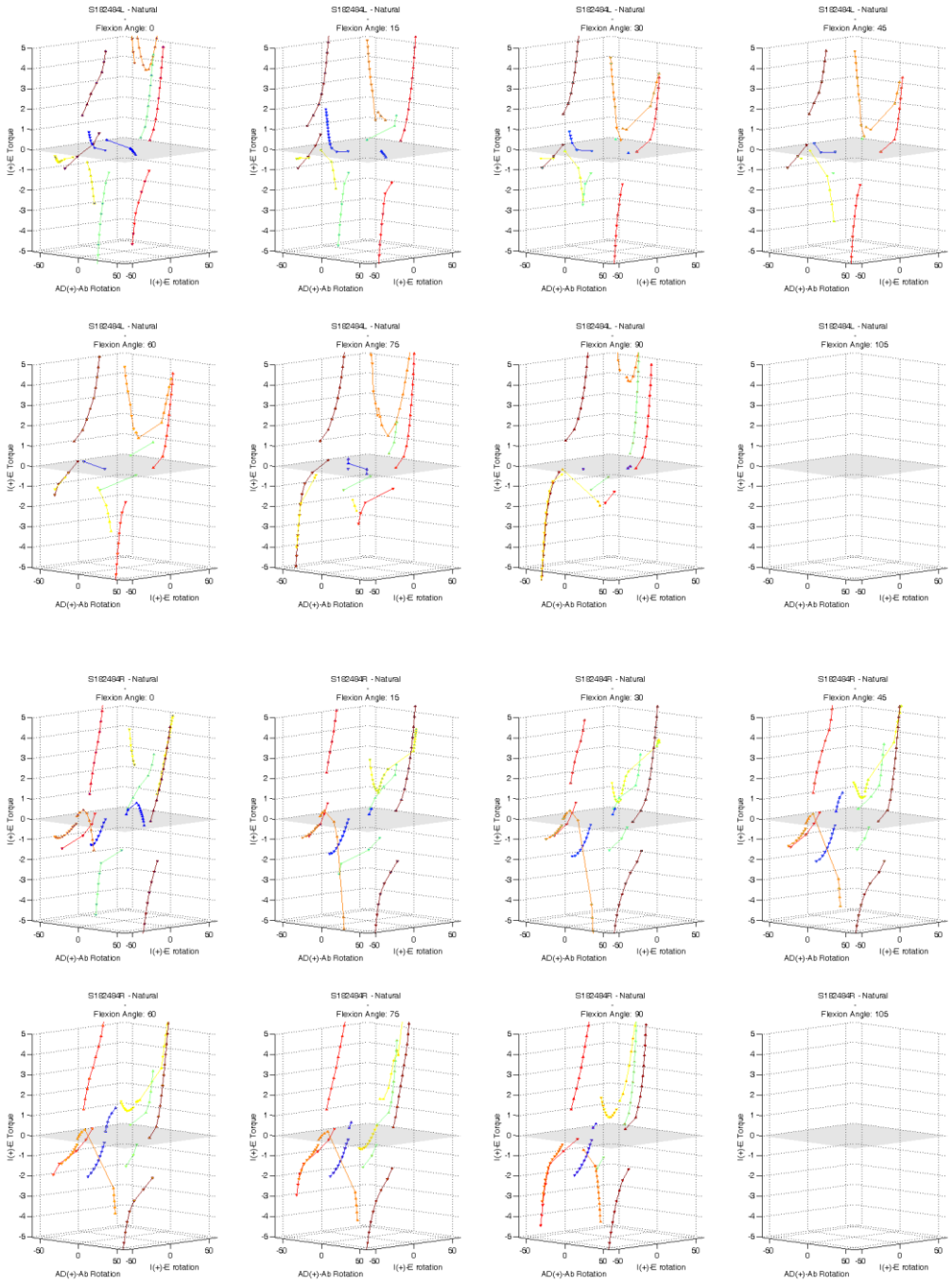
S182484L - Natural
Flexion Angle: 0
Flexion Angle: 15
Flexion Angle: 30
Flexion Angle: 45
Flexion Angle: 60
Flexion Angle: 75
Flexion Angle: 90
Flexion Angle: 105
S182484R - Natural
I(+)E Torque
AD(+)-Ab Rotation
I(+)E rotation

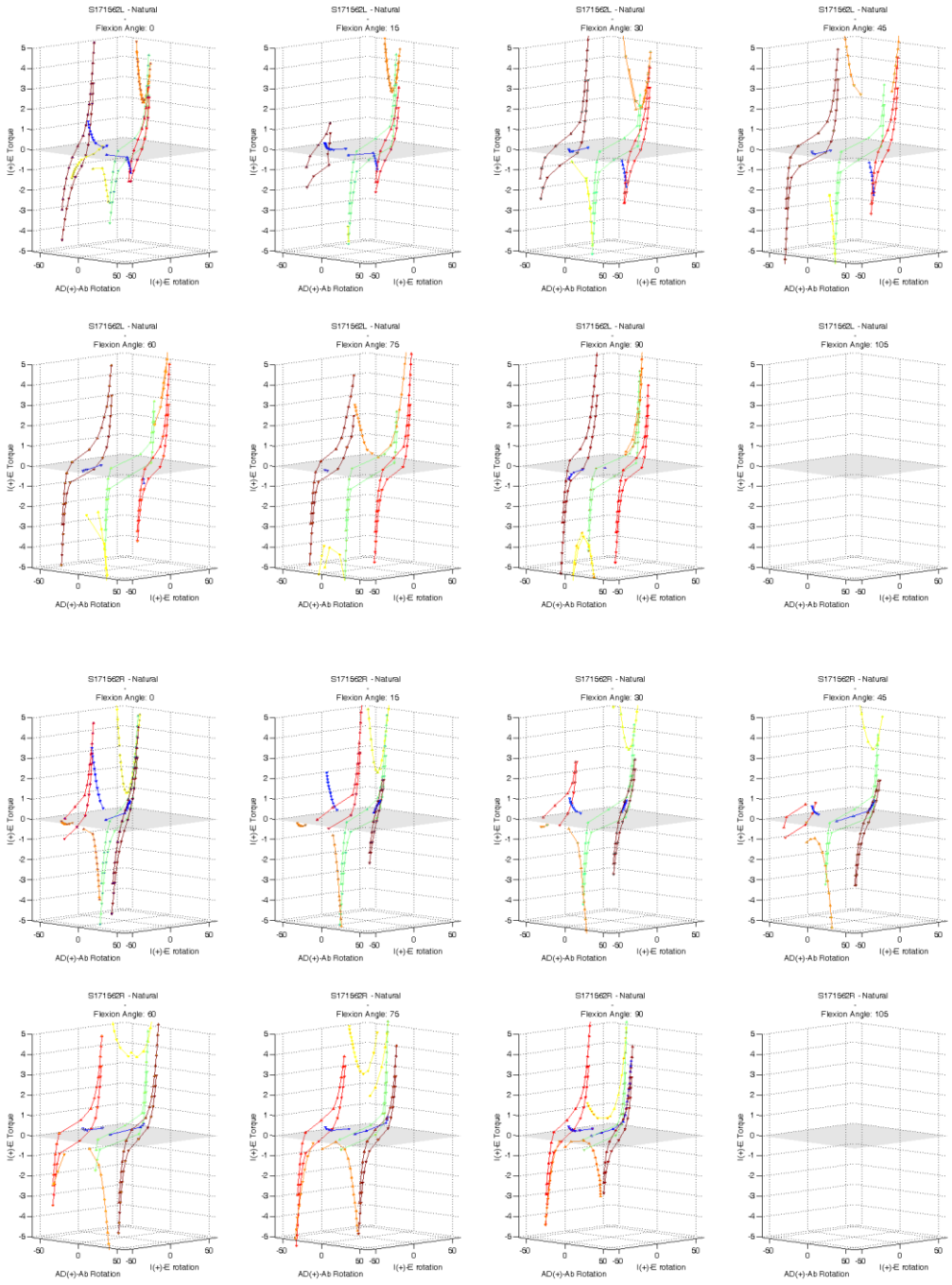
S171562L - Natural
Flexion Angle: 0
S171562L - Natural
Flexion Angle: 15
S171562L - Natural
Flexion Angle: 30
S171562L - Natural
Flexion Angle: 45
S171562L - Natural
Flexion Angle: 60
S171562L - Natural
Flexion Angle: 75
S171562L - Natural
Flexion Angle: 90
S171562L - Natural
Flexion Angle: 105
S171562R - Natural
Flexion Angle: 0
S171562R - Natural
Flexion Angle: 15
S171562R - Natural
Flexion Angle: 30
S171562R - Natural
Flexion Angle: 45
S171562R - Natural
Flexion Angle: 60
S171562R - Natural
Flexion Angle: 75
S171562R - Natural
Flexion Angle: 90
S171562R - Natural
Flexion Angle: 105
I(+)-E Torque
AD(+)-Ab Rotation
I(+)-E rotation

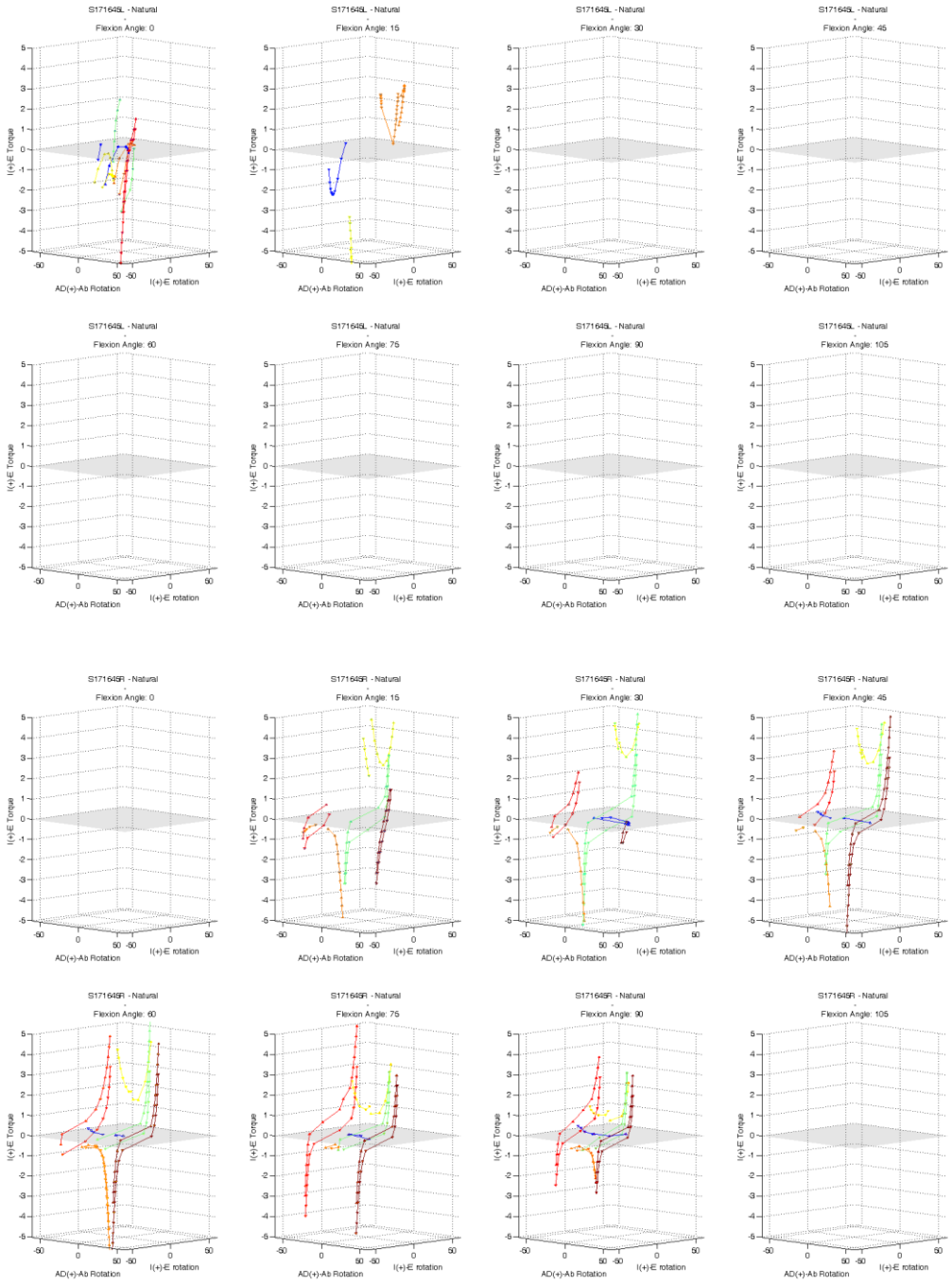
S171645L - Natural
Flexion Angle: 0
S171645L - Natural
Flexion Angle: 15
S171645L - Natural
Flexion Angle: 30
S171645L - Natural
Flexion Angle: 45
S171645L - Natural
Flexion Angle: 60
S171645L - Natural
Flexion Angle: 75
S171645L - Natural
Flexion Angle: 90
S171645L - Natural
Flexion Angle: 105
S171645R - Natural
Flexion Angle: 0
S171645R - Natural
Flexion Angle: 15
S171645R - Natural
Flexion Angle: 30
S171645R - Natural
Flexion Angle: 45
S171645R - Natural
Flexion Angle: 60
S171645R - Natural
Flexion Angle: 75
S171645R - Natural
Flexion Angle: 90
S171645R - Natural
Flexion Angle: 105
I(+)-E Torque
AD(+)-Ab Rotation
I(+)-E rotation

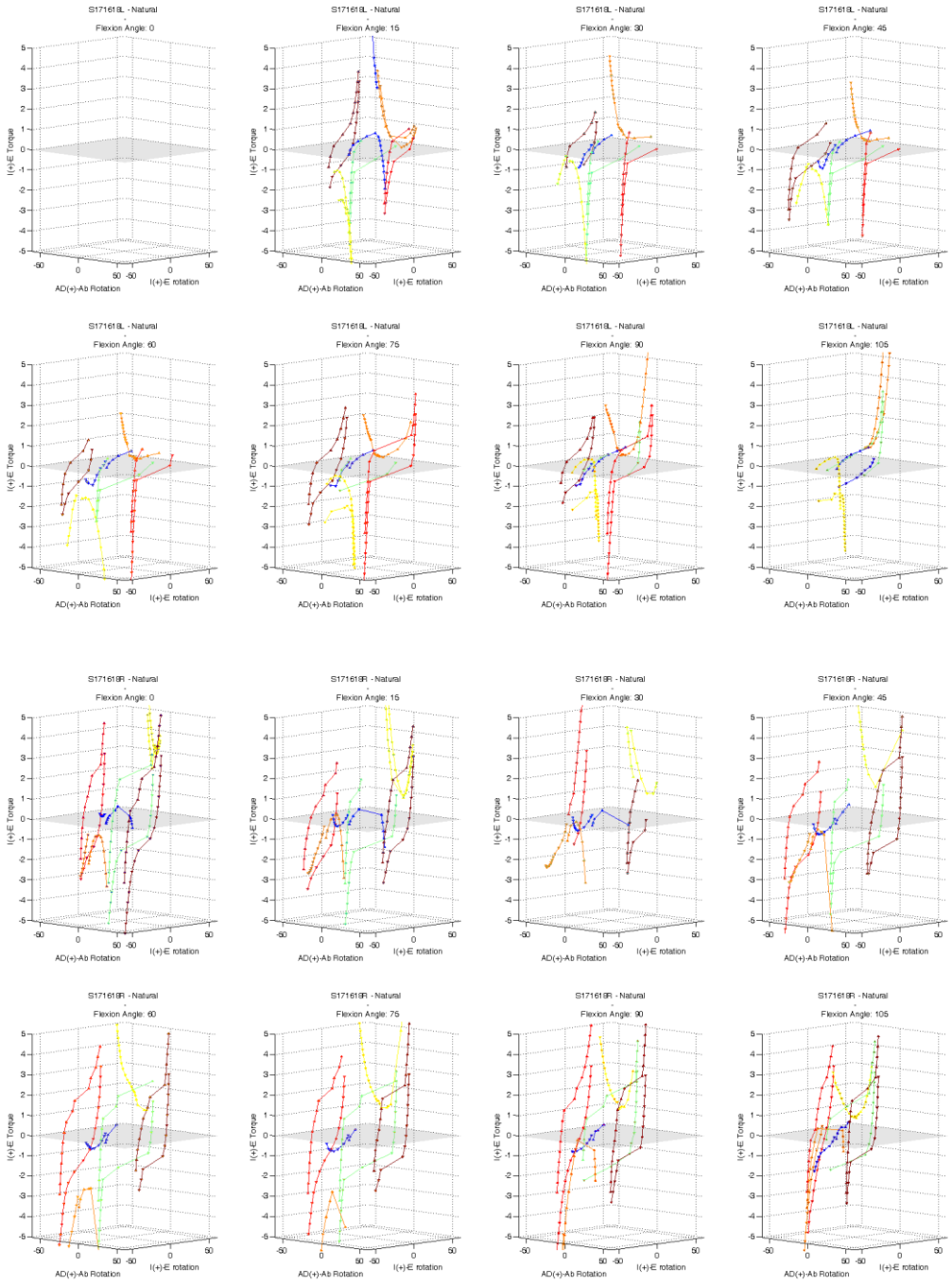
S171618L - Natural
Flexion Angle: 0
Flexion Angle: 15
Flexion Angle: 30
Flexion Angle: 45
Flexion Angle: 60
Flexion Angle: 75
Flexion Angle: 90
Flexion Angle: 105
S171618R - Natural
Flexion Angle: 0
Flexion Angle: 15
Flexion Angle: 30
Flexion Angle: 45
Flexion Angle: 60
Flexion Angle: 75
Flexion Angle: 90
Flexion Angle: 105
I(+)-E Torque
AD(+)-Ab Rotation
I(+)-E rotation

Appendix 1E 1-10: 3-Dimensional Laxity Curves for Natural Hips Flexion Torque Response

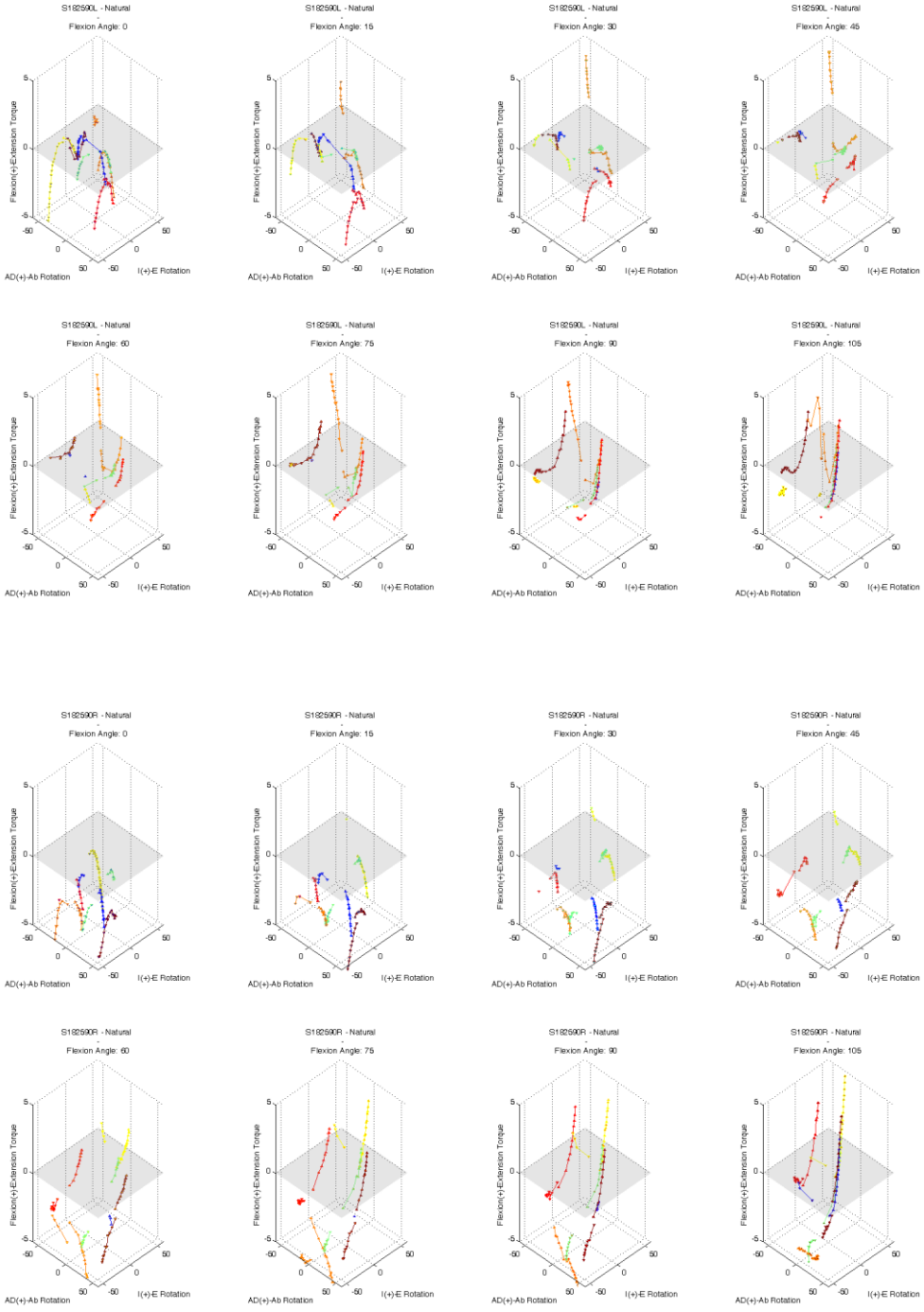

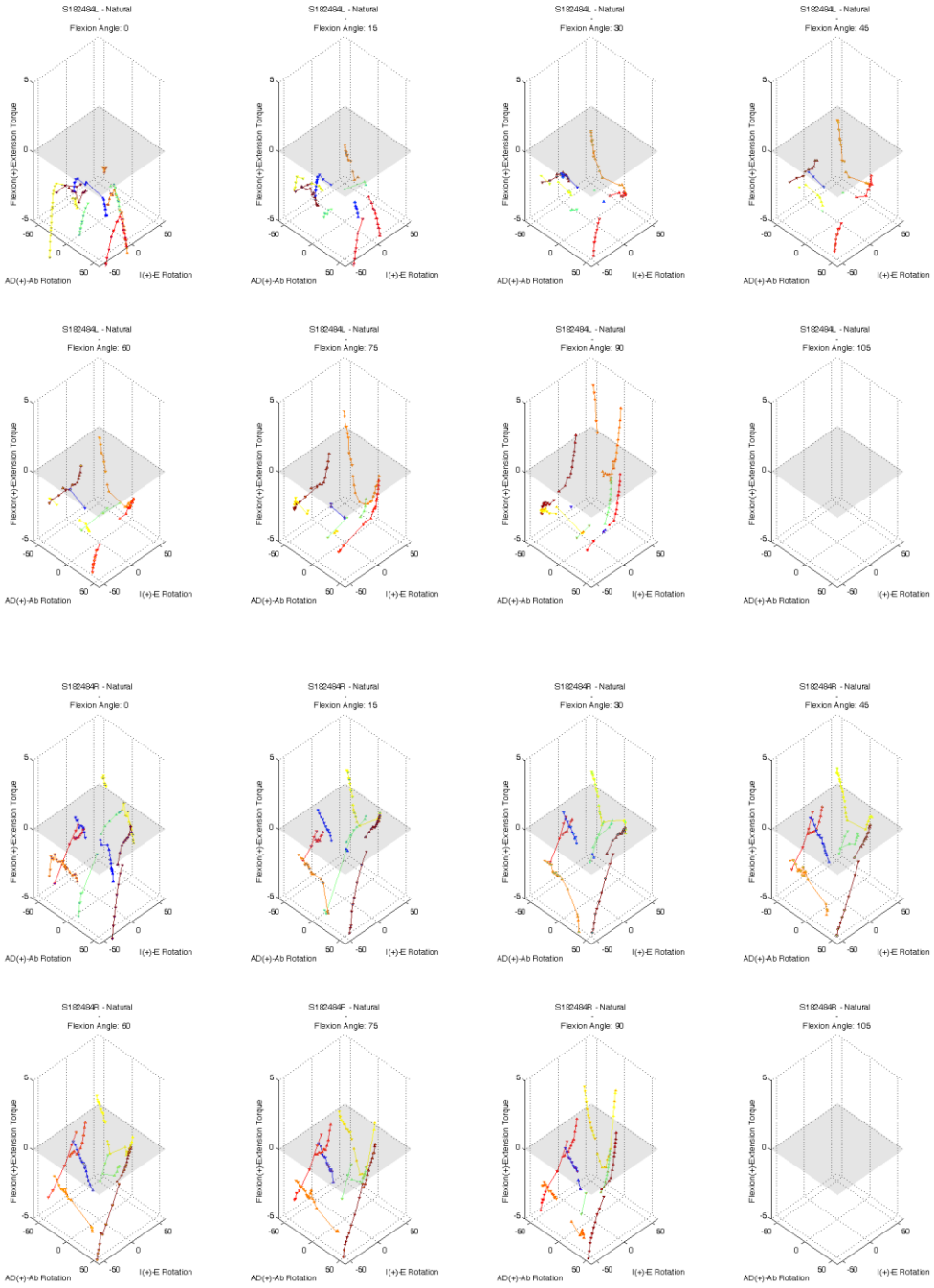
S182484L - Natural
Flexion Angle: 0
S182484L - Natural
Flexion Angle: 15
S182484L - Natural
Flexion Angle: 30
S182484L - Natural
Flexion Angle: 45
S182484L - Natural
Flexion Angle: 60
S182484L - Natural
Flexion Angle: 75
S182484L - Natural
Flexion Angle: 90
S182484L - Natural
Flexion Angle: 105
S182484R - Natural
Flexion Angle: 0
S182484R - Natural
Flexion Angle: 15
S182484R - Natural
Flexion Angle: 30
S182484R - Natural
Flexion Angle: 45
S182484R - Natural
Flexion Angle: 60
S182484R - Natural
Flexion Angle: 75
S182484R - Natural
Flexion Angle: 90
S182484R - Natural
Flexion Angle: 105
Flexion(+)-Extension Torque
AD(+)-Ab Rotation
I(+)-E Rotation

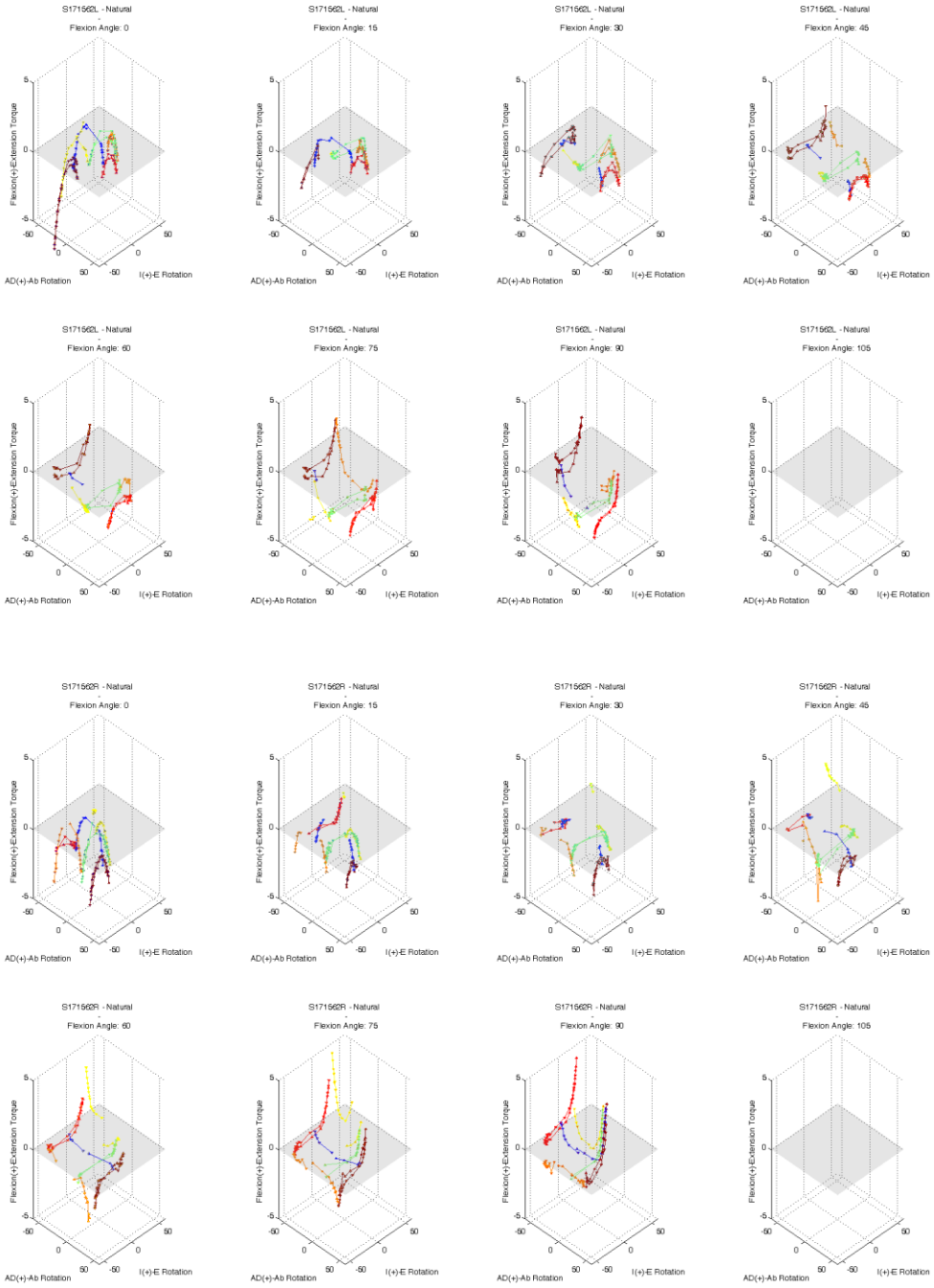
S171562L - Natural
Flexion Angle: 0
S171562L - Natural
Flexion Angle: 15
S171562L - Natural
Flexion Angle: 30
S171562L - Natural
Flexion Angle: 45
S171562L - Natural
Flexion Angle: 60
S171562L - Natural
Flexion Angle: 75
S171562L - Natural
Flexion Angle: 90
S171562L - Natural
Flexion Angle: 105
S171562R - Natural
Flexion Angle: 0
S171562R - Natural
Flexion Angle: 15
S171562R - Natural
Flexion Angle: 30
S171562R - Natural
Flexion Angle: 45
S171562R - Natural
Flexion Angle: 60
S171562R - Natural
Flexion Angle: 75
S171562R - Natural
Flexion Angle: 90
S171562R - Natural
Flexion Angle: 105
Flexion(+)-Extension Torque
AD(+)-Ab Rotation
I(+)-E Rotation

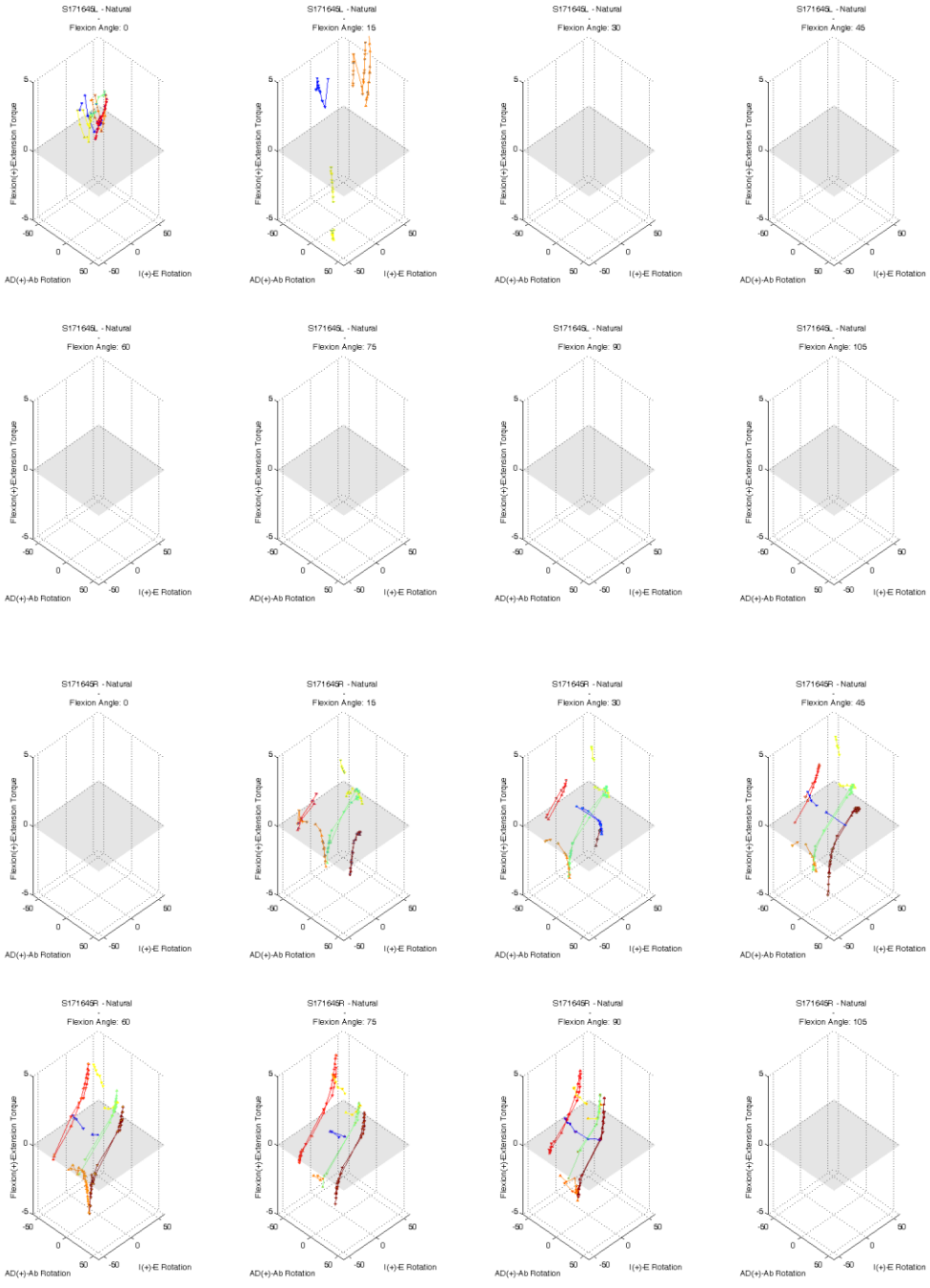
S171645L - Natural
Flexion Angle: 0
S171645L - Natural
Flexion Angle: 15
S171645L - Natural
Flexion Angle: 30
S171645L - Natural
Flexion Angle: 45
S171645L - Natural
Flexion Angle: 60
S171645L - Natural
Flexion Angle: 75
S171645L - Natural
Flexion Angle: 90
S171645L - Natural
Flexion Angle: 105
S171645R - Natural
Flexion Angle: 0
S171645R - Natural
Flexion Angle: 15
S171645R - Natural
Flexion Angle: 30
S171645R - Natural
Flexion Angle: 45
S171645R - Natural
Flexion Angle: 60
S171645R - Natural
Flexion Angle: 75
S171645R - Natural
Flexion Angle: 90
S171645R - Natural
Flexion Angle: 105
Flexion(+)-Extension Torque
AD(+)-Ab Rotation
I(+)-E Rotation

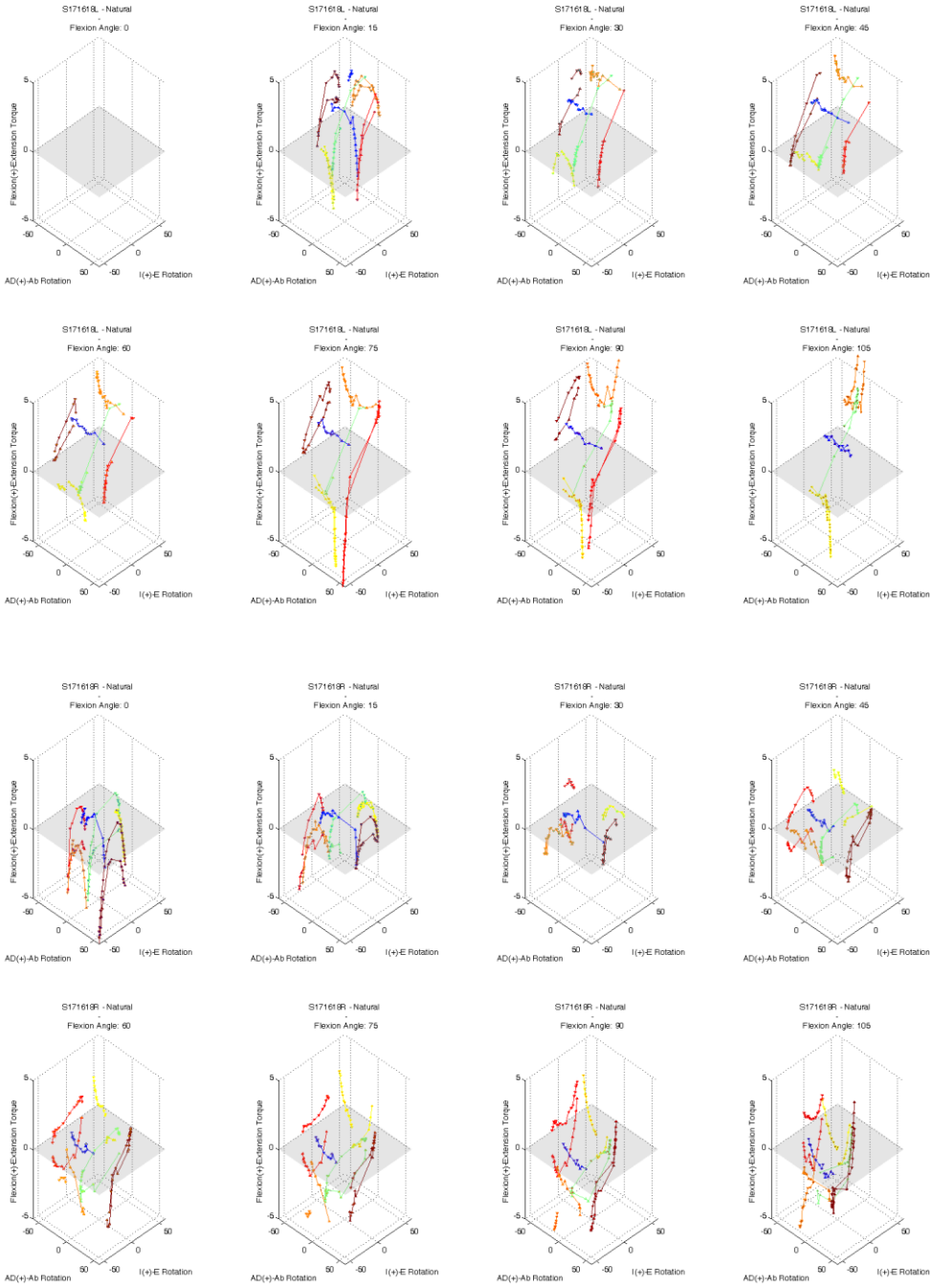
S171618L - Natural
Flexion Angle: 0
S171618L - Natural
Flexion Angle: 15
S171618L - Natural
Flexion Angle: 30
S171618L - Natural
Flexion Angle: 45
S171618L - Natural
Flexion Angle: 60
S171618L - Natural
Flexion Angle: 75
S171618L - Natural
Flexion Angle: 90
S171618L - Natural
Flexion Angle: 105
S171618R - Natural
Flexion Angle: 0
S171618R - Natural
Flexion Angle: 15
S171618R - Natural
Flexion Angle: 30
S171618R - Natural
Flexion Angle: 45
S171618R - Natural
Flexion Angle: 60
S171618R - Natural
Flexion Angle: 75
S171618R - Natural
Flexion Angle: 90
S171618R - Natural
Flexion Angle: 105
Flexion(+)-Extension Torque
AD(+)-Ab Rotation
I(+)-E Rotation

Appendix 1F 1-6: 3-Dimensional Laxity Curves or Implanted Hips Ad/ab Torque Response

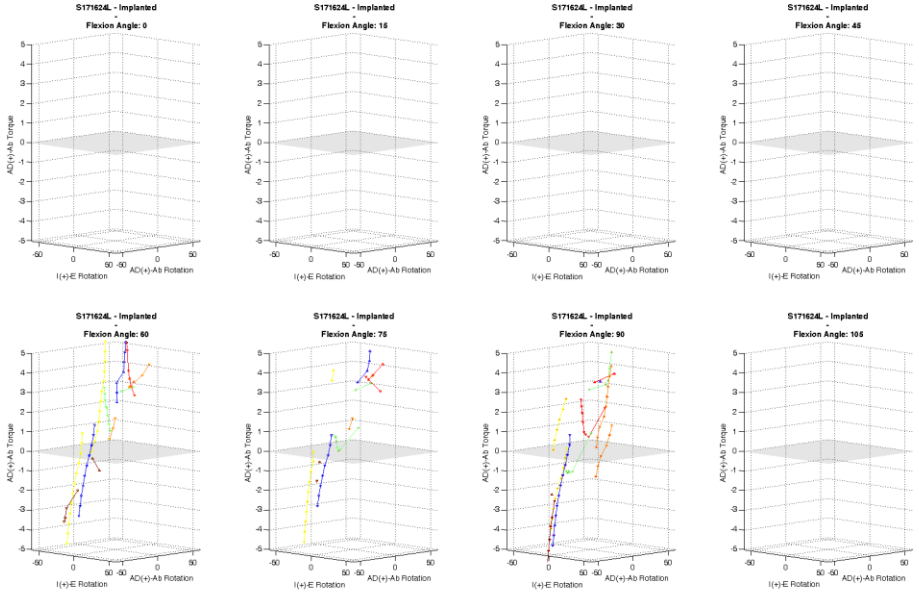

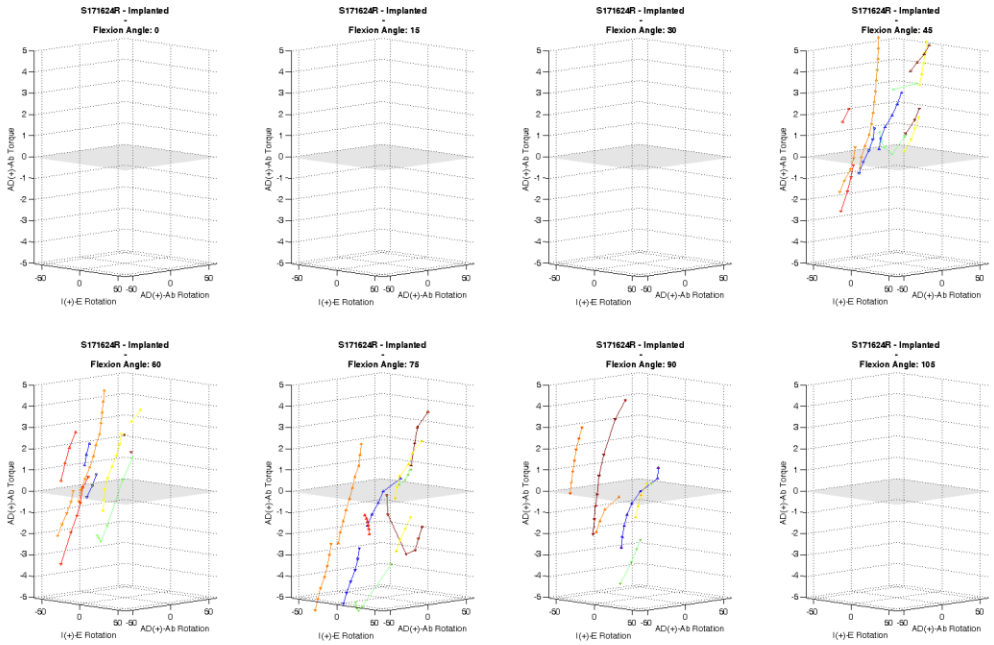

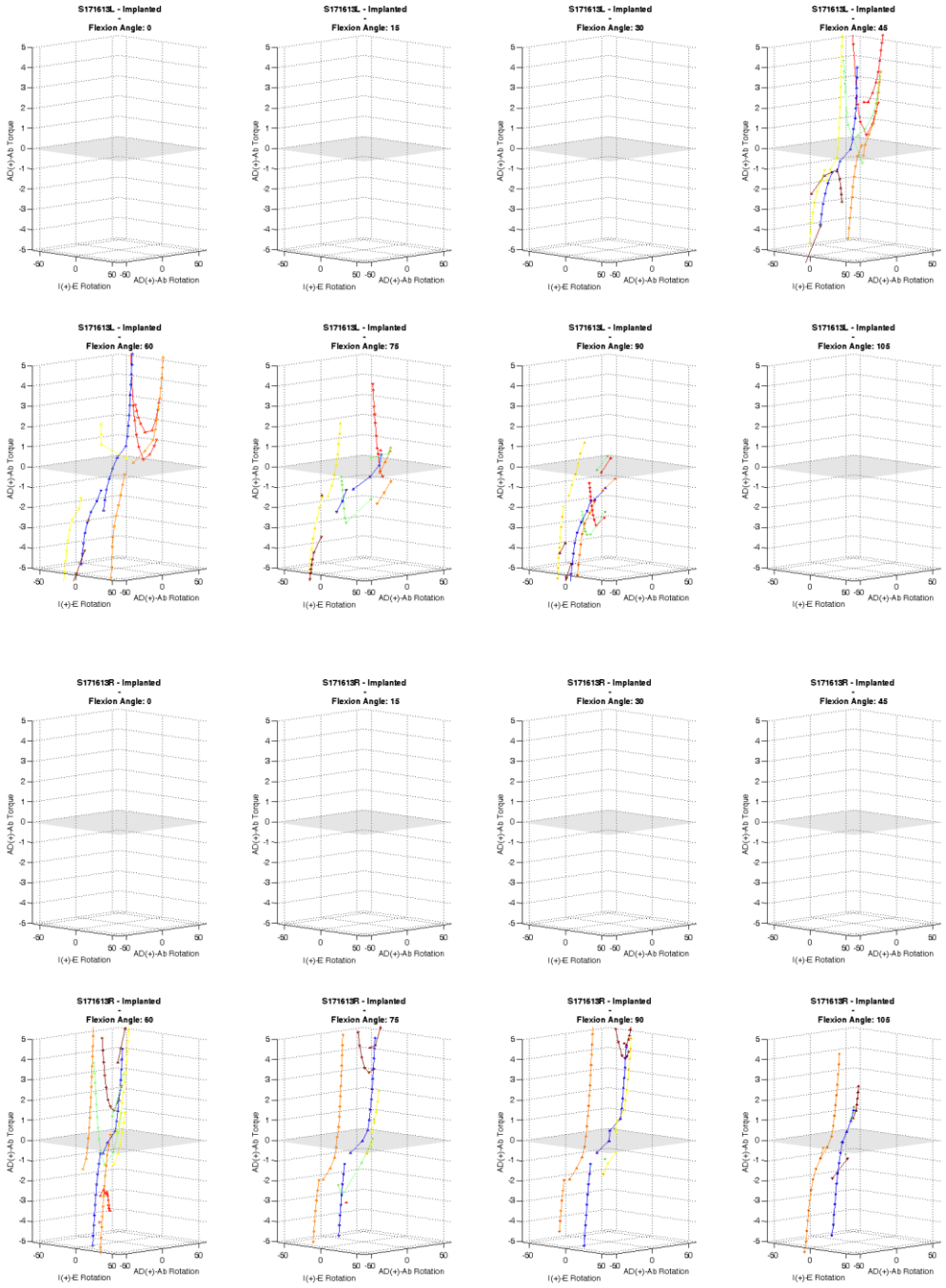
S171613L - Implanted - Flexion Angle: 0
S171613L - Implanted - Flexion Angle: 15
S171613L - Implanted - Flexion Angle: 30
S171613L - Implanted - Flexion Angle: 45
S171613L - Implanted - Flexion Angle: 60
S171613L - Implanted - Flexion Angle: 75
S171613L - Implanted - Flexion Angle: 90
S171613L - Implanted - Flexion Angle: 105
S171613R - Implanted - Flexion Angle: 0
S171613R - Implanted - Flexion Angle: 15
S171613R - Implanted - Flexion Angle: 30
S171613R - Implanted - Flexion Angle: 45
S171613R - Implanted - Flexion Angle: 60
S171613R - Implanted - Flexion Angle: 75
S171613R - Implanted - Flexion Angle: 90
S171613R - Implanted - Flexion Angle: 105
AD(+)-Ab Torque
I(+)-E Rotation
AD(+)-Ab Rotation

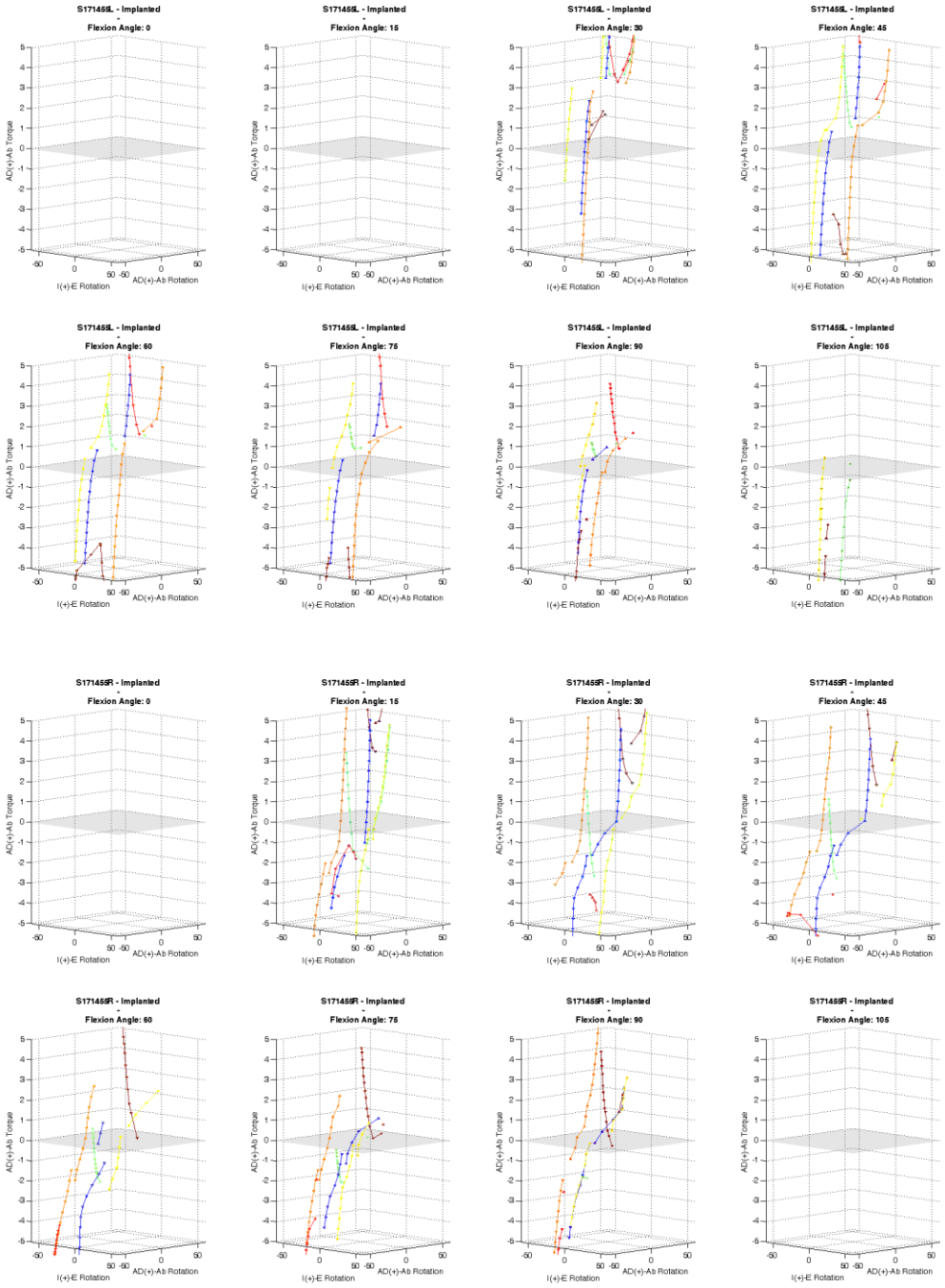
S171455L - Implanted - Flexion Angle: 0
S171455L - Implanted - Flexion Angle: 15
S171455L - Implanted - Flexion Angle: 30
S171455L - Implanted - Flexion Angle: 45
S171455L - Implanted - Flexion Angle: 60
S171455L - Implanted - Flexion Angle: 75
S171455L - Implanted - Flexion Angle: 90
S171455L - Implanted - Flexion Angle: 105
S171455R - Implanted - Flexion Angle: 0
S171455R - Implanted - Flexion Angle: 15
S171455R - Implanted - Flexion Angle: 30
S171455R - Implanted - Flexion Angle: 45
S171455R - Implanted - Flexion Angle: 60
S171455R - Implanted - Flexion Angle: 75
S171455R - Implanted - Flexion Angle: 90
S171455R - Implanted - Flexion Angle: 105
AD(+)-Ab Torque
I(+)-E Rotation
AD(+)-Ab Rotation

Appendix 1G 1-6: 4-Dimensional Laxity Curves for Implanted Hips IE Torque Response

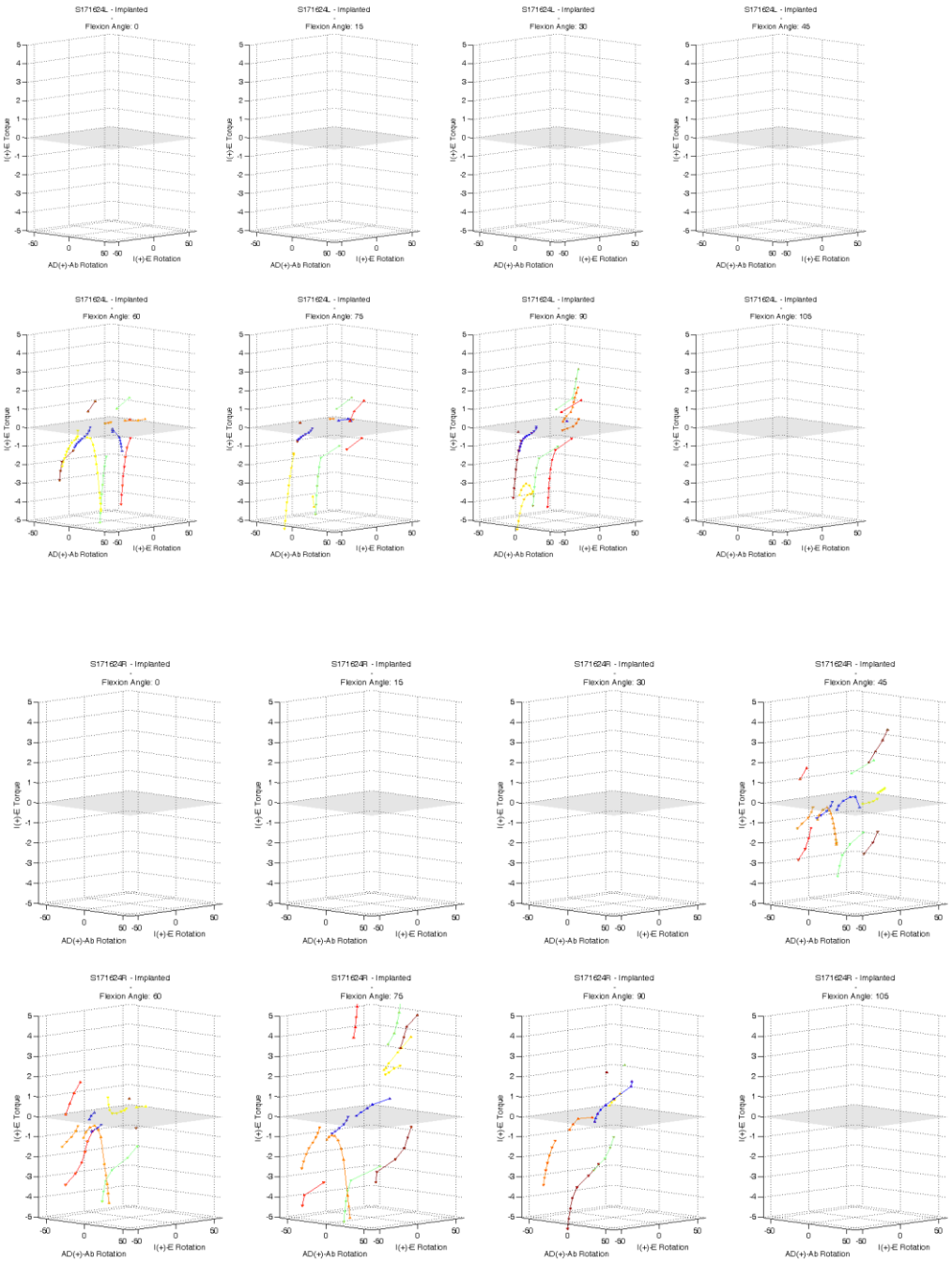

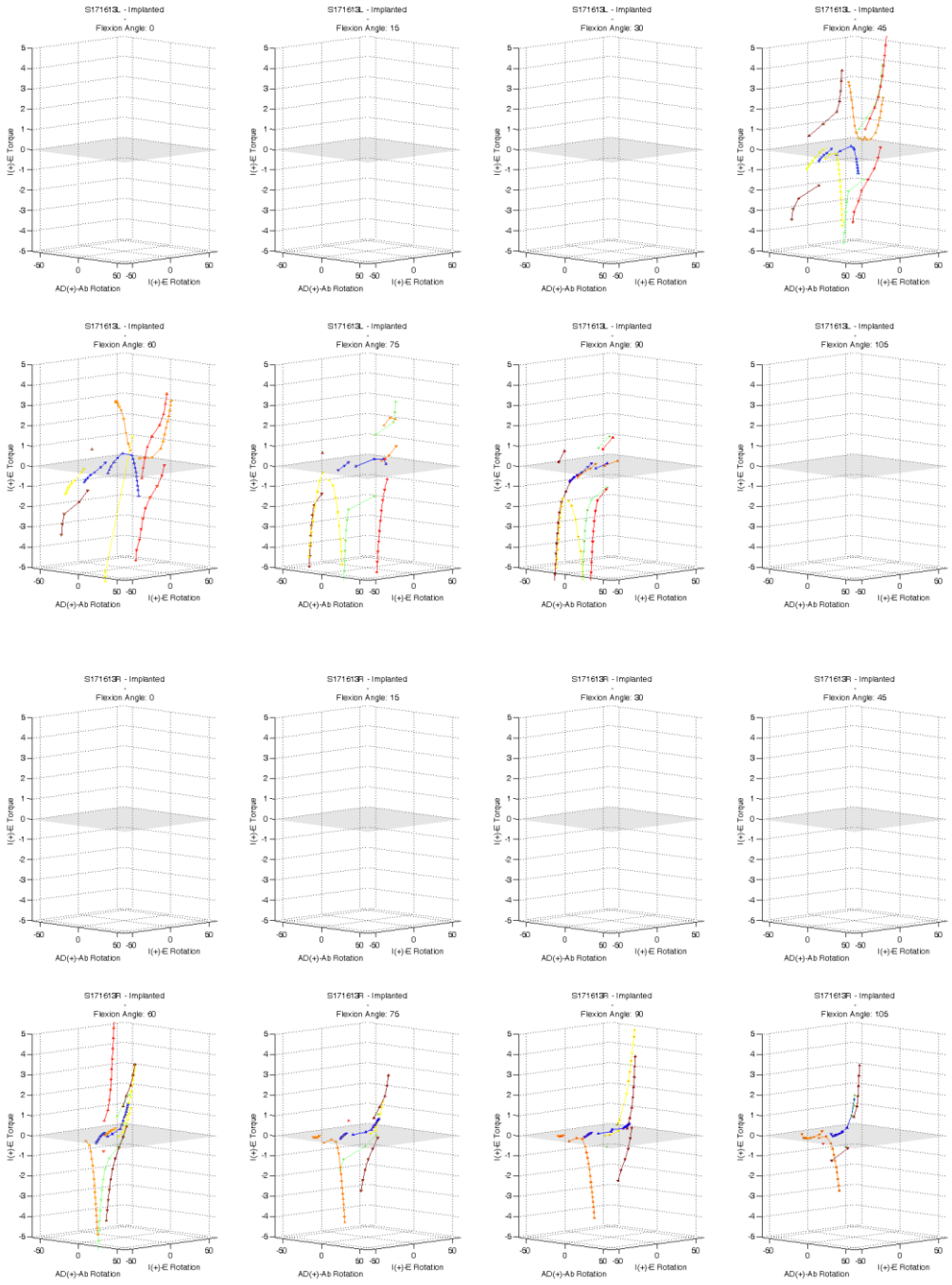
S171613L - Implanted
Flexion Angle: 0
S171613L - Implanted
Flexion Angle: 15
S171613L - Implanted
Flexion Angle: 30
S171613L - Implanted
Flexion Angle: 45
S171613L - Implanted
Flexion Angle: 60
S171613L - Implanted
Flexion Angle: 75
S171613L - Implanted
Flexion Angle: 90
S171613L - Implanted
Flexion Angle: 105
S171613R - Implanted
Flexion Angle: 0
S171613R - Implanted
Flexion Angle: 15
S171613R - Implanted
Flexion Angle: 30
S171613R - Implanted
Flexion Angle: 45
S171613R - Implanted
Flexion Angle: 60
S171613R - Implanted
Flexion Angle: 75
S171613R - Implanted
Flexion Angle: 90
S171613R - Implanted
Flexion Angle: 105
I(+)-E Torque
AD(+)-Ab Rotation
I(+)-E Rotation

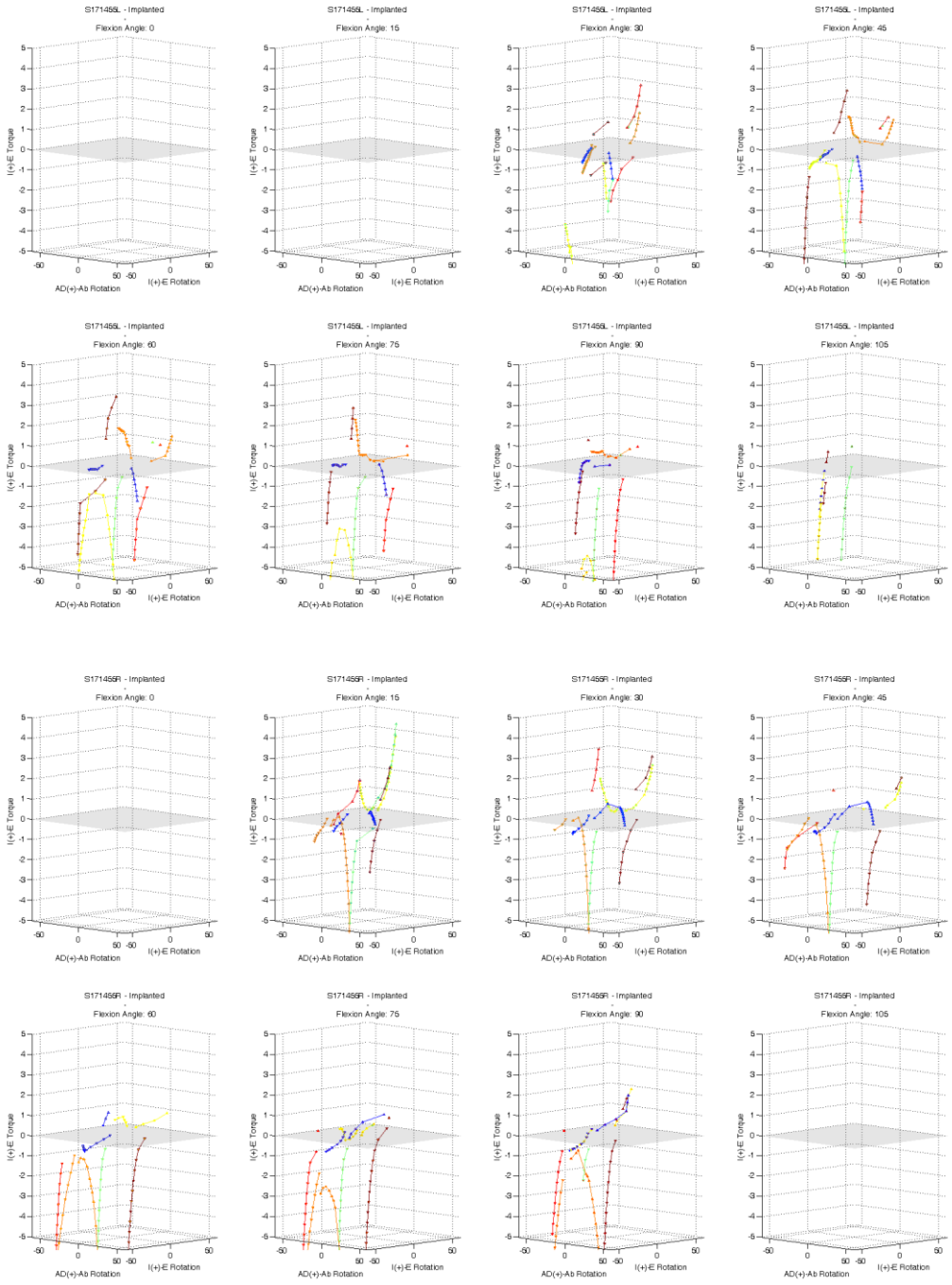
S171455L - Implanted
Flexion Angle: 0
S171455L - Implanted
Flexion Angle: 15
S171455L - Implanted
Flexion Angle: 30
S171455L - Implanted
Flexion Angle: 45
S171455L - Implanted
Flexion Angle: 60
S171455L - Implanted
Flexion Angle: 75
S171455L - Implanted
Flexion Angle: 90
S171455L - Implanted
Flexion Angle: 105
S171455R - Implanted
Flexion Angle: 0
S171455R - Implanted
Flexion Angle: 15
S171455R - Implanted
Flexion Angle: 30
S171455R - Implanted
Flexion Angle: 45
S171455R - Implanted
Flexion Angle: 60
S171455R - Implanted
Flexion Angle: 75
S171455R - Implanted
Flexion Angle: 90
S171455R - Implanted
Flexion Angle: 105
I(+)-E Torque
AD(+)-Ab Rotation
I(+)-E Rotation

Appendix 1H 1-6: 3-Dimensional Laxity Curves for Implanted Hips Flexion Torque Response

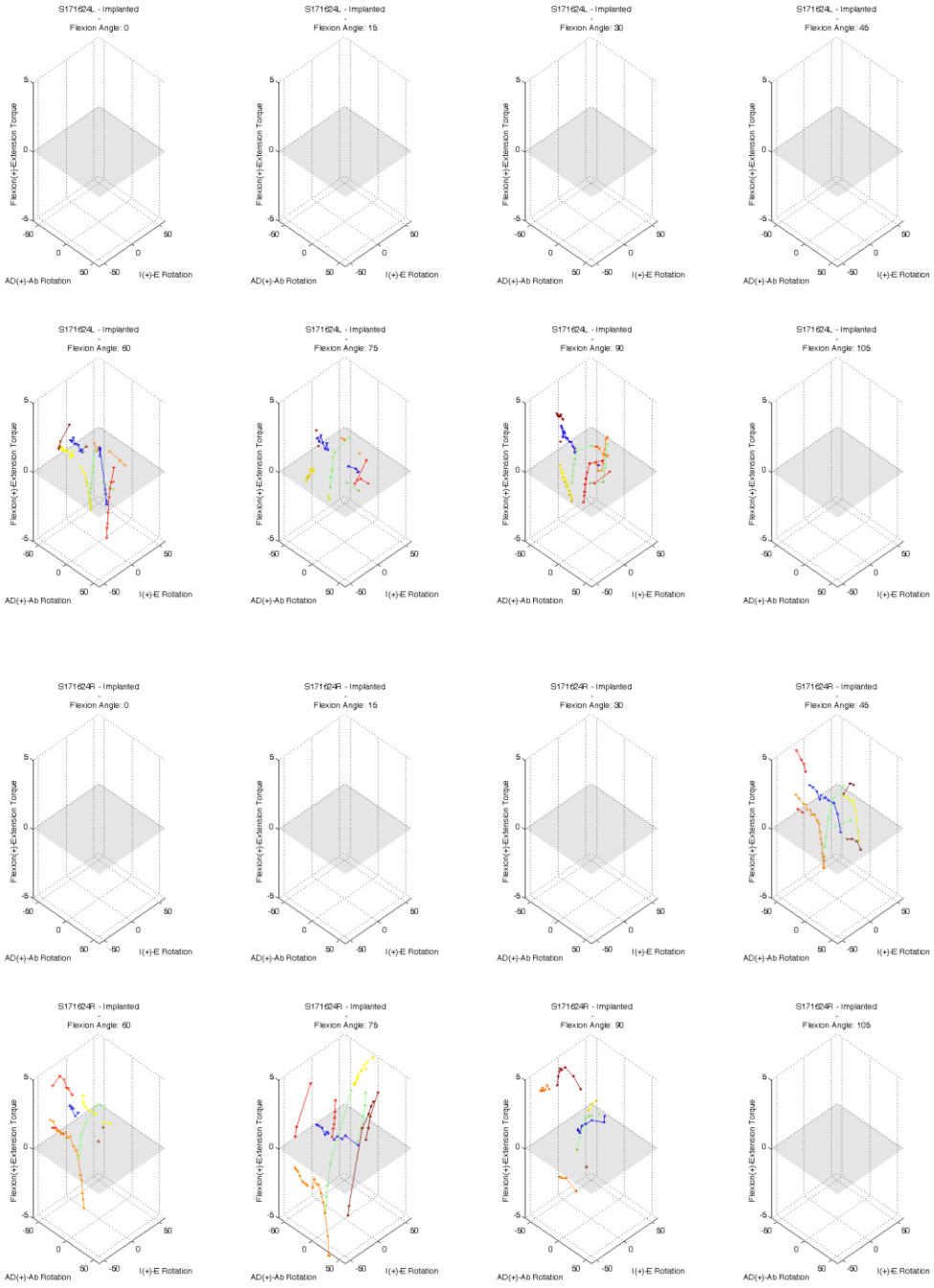

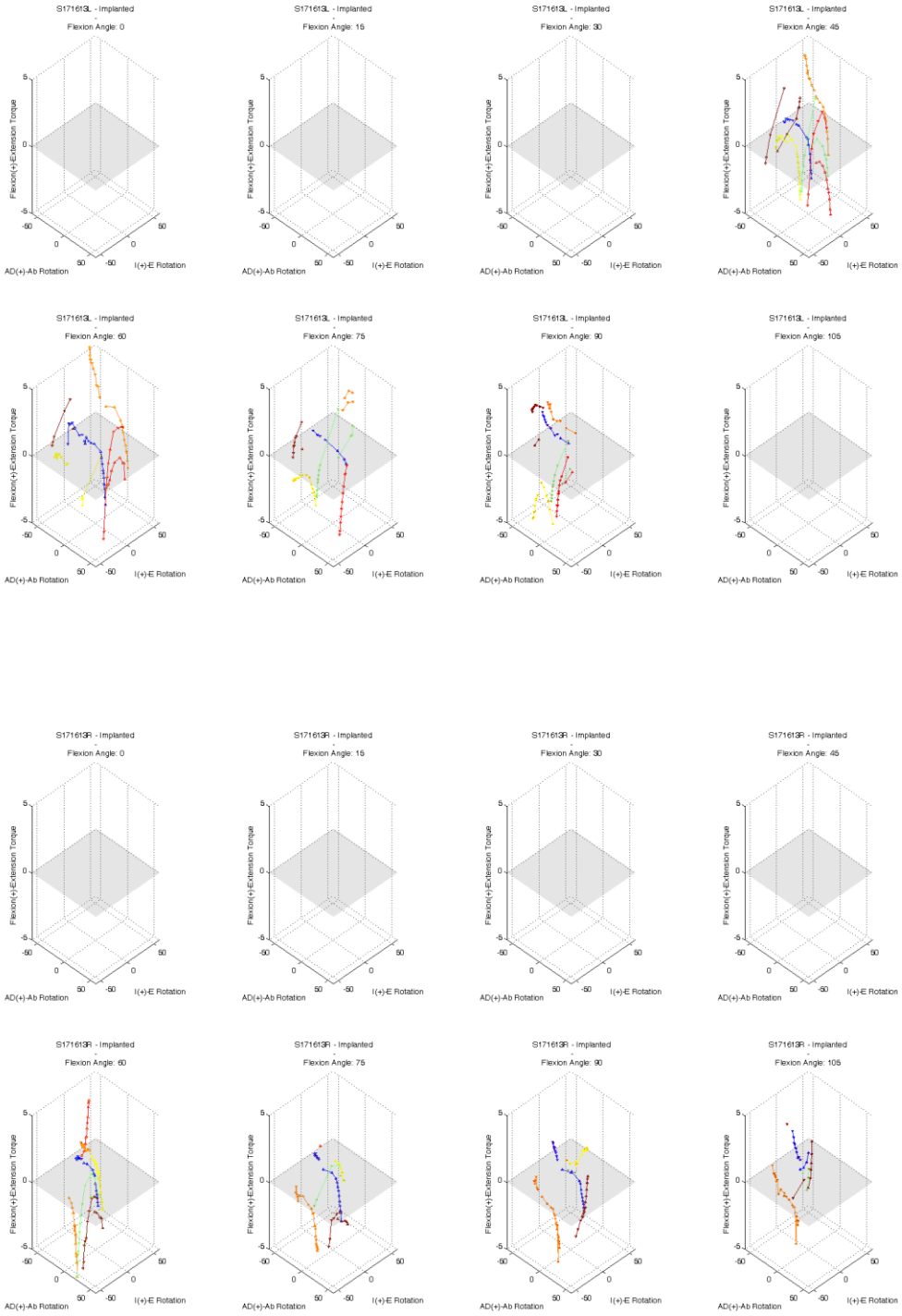
S171613L - Implanted
Flexion Angle: 0
S171613L - Implanted
Flexion Angle: 15
S171613L - Implanted
Flexion Angle: 30
S171613L - Implanted
Flexion Angle: 45
S171613L - Implanted
Flexion Angle: 60
S171613L - Implanted
Flexion Angle: 75
S171613L - Implanted
Flexion Angle: 90
S171613L - Implanted
Flexion Angle: 105
S171613R - Implanted
Flexion Angle: 0
S171613R - Implanted
Flexion Angle: 15
S171613R - Implanted
Flexion Angle: 30
S171613R - Implanted
Flexion Angle: 45
S171613R - Implanted
Flexion Angle: 60
S171613R - Implanted
Flexion Angle: 75
S171613R - Implanted
Flexion Angle: 90
S171613R - Implanted
Flexion Angle: 105
Flexion(+)-Extension Torque
AD(+)-Ab Rotation
I(+)-E Rotation

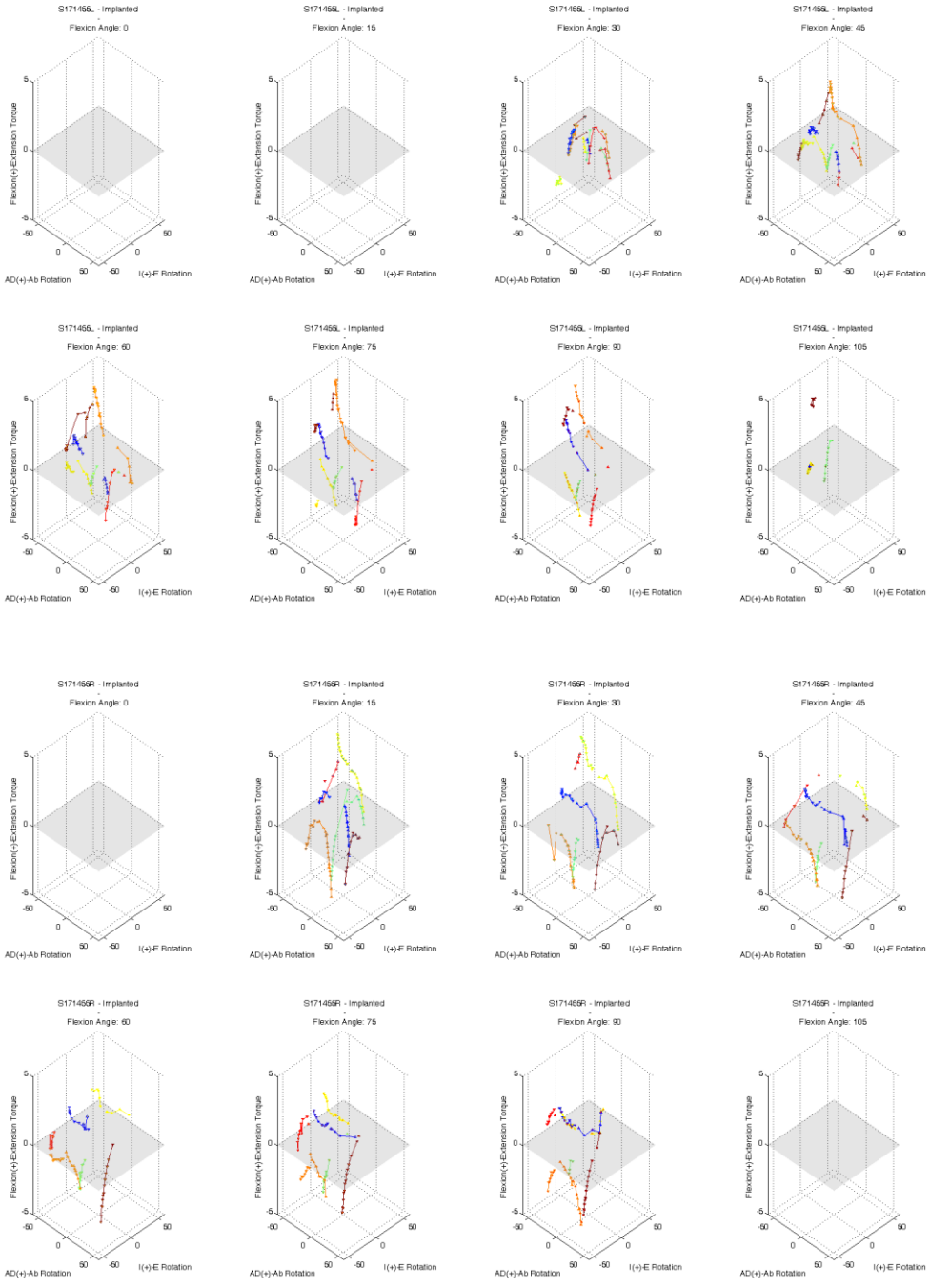
S171455L - Implanted
Flexion Angle: 0
S171455L - Implanted
Flexion Angle: 15
S171455L - Implanted
Flexion Angle: 30
S171455L - Implanted
Flexion Angle: 45
S171455L - Implanted
Flexion Angle: 60
S171455L - Implanted
Flexion Angle: 75
S171455L - Implanted
Flexion Angle: 90
S171455L - Implanted
Flexion Angle: 105
S171455R - Implanted
Flexion Angle: 0
S171455R - Implanted
Flexion Angle: 15
S171455R - Implanted
Flexion Angle: 30
S171455R - Implanted
Flexion Angle: 45
S171455R - Implanted
Flexion Angle: 60
S171455R - Implanted
Flexion Angle: 75
S171455R - Implanted
Flexion Angle: 90
S171455R - Implanted
Flexion Angle: 105
Flexion(+)-Extension Torque
AD(+)-Ab Rotation
I(+)-E Rotation